CHARACTERIZATION AND DYNAMIC ANALYSIS OF LONG-CAVITY MULTI-SECTION GAIN-LEVERED QUANTUM-DOT LASERS

THESIS

John R. Schmidt, Second Lieutenant, USAF

AFIT-ENG-13-M-45

DEPARTMENT OF THE AIR FORCE
AIR UNIVERSITY

AIR FORCE INSTITUTE OF TECHNOLOGY

Wright-Patterson Air Force Base, Ohio

AFIT-ENG-13-M-45

CHARACTERIZATION AND DYNAMIC ANALYSIS OF LONG-CAVITY MULTI-SECTION GAIN-LEVERED QUANTUM-DOT LASERS

THESIS

Presented to the Faculty

Department of Electrical and Computer Engineering

Graduate School of Engineering and Management

Air Force Institute of Technology

Air University

Air Education and Training Command

In Partial Fulfillment of the Requirements for the

Degree of Master of Science in Electrical Engineering

John R. Schmidt, BSE

Second Lieutenant, USAF

March 2013

AFIT-ENG-13-M-45

CHARACTERIZATION AND DYNAMIC ANALYSIS OF LONG-CAVITY MULTI-SECTION GAIN-LEVERED QUANTUM-DOT LASERS

John R. Schmidt, BSE
Second Lieutenant, USAF

Approved:

Michael C. Pochet, Maj, Ph.D. (Chairman) — 3/5/2013 Date

Nicholas G. Usechak, Ph.D. (Member) — 03/04/2013 Date

Derrick Langley, Capt, Ph.D. (Member) — 03/04/2013 Date

Abstract

This research investigates the impact of different device architectures on the frequency response of long-cavity multi-section quantum-dot lasers. This work focused on a novel 8.3-mm multi-section quantum-dot device which possessed the flexibility to be configured either as a single- or multi-section device having gain-to-modulation section ratios of 14:2 and 15:1. The long-cavity device design facilitated the testing of increased gain-to-modulation section length ratios previously unexplored in the context of the gain-lever effect. The investigation of the gain-lever effect showed improvements to both the modulation efficiency and modulation bandwidth of the device under test. The modulation efficiency and modulation bandwidth were found to vary as the modulation section length was increased, leading to the conclusion of an ideal gain-to-modulation section ratio. In addition to providing a means to investigate the gain-lever effect, the long-cavity quantum-dot device exhibited passive mode locking in the multi-section and single-section configurations. While the predictable gain-lever effects were observed, long-cavity and mode-locking effects were also present in the response; these effects presented unexpected characteristics that are not captured by current published models.

To my brother

Jacob Schmidt
Nov 1986 – Oct 2012
Rest in peace

Acknowledgments

First and foremost I would like to thank my advisor, Maj. Michael Pochet, for providing the perfect balance of guidance and freedom throughout this process. His approach created a positive environment and was instrumental to my success at AFIT. I am indebted to Dr. Nicholas Usechak for patiently answering my countless questions about laser physics and allowing me to perform my research in his *state-of-the-art* optics laboratory (note the use of hyphens). I would have been lost without his innate ability to explain complex concepts in a concise, straightforward manner. Also, I would like to thank Capt. Derrick Langley for being a part of my committee and providing me with meaningful feedback which helped shape my thesis.

In addition, I express my gratitude to my parents and two brothers who were supportive and even pretended to be interested about quantum-dot lasers no matter how many times I bombarded them with the details of my research. I would be remiss if I didn't thank my friends: Evan Harvey, Anthony Runco, Brent Danner, Julio Armijos and Ben Toler who helped keep the atmosphere enjoyable even when faced with looming deadlines.

John R. Schmidt

Table of Contents

List of Figures

Page

CHARACTERIZATION AND DYNAMIC ANALYSIS OF LONG-CAVITY MULTI-SECTION GAIN-LEVERED QUANTUM-DOT LASERS

1. Introduction

The world today is inundated with electronic communication devices that dominate major aspects of peoples' professional and personal lives. As the military and the public continue to increase their reliance on these devices, the existing communication infrastructure will be taxed, leading to potential bottlenecks within the current communication architecture. In extreme cases the network will be congested, leading to delays and disruptions in communication flow. It is estimated that by 2025 communication network traffic will be 200 times greater than it is today [1]. With the sheer volume of data that are expected to be transmitted over the existing systems, it is clear that communication systems will benefit from optical transmitters capable of handling higher bandwidths. Transmitters with increased bandwidths will enable simplified communication hubs capable of handling increased data rates, rather than merely linearly expanding the number of wavelength division multiplexed (WDM) channels over a single fiber optic link.

This research is focused on optimizing optical transmitter design to increase the information carrying ability in optical communication systems. The specific nature of this work is concentrated on improving the 3-dB modulation bandwidth of directly modulated semiconductor lasers electrically biased/pumped in a multi-section nature, using an approach commonly referred to as the gain-lever effect.

1.1 Background

Optical communication systems are the most efficient and capable means of transmitting information at high data rates over significant distances (greater than 100 meters). The primary advantages of fiber-optic communication links include the following: extremely high bandwidths (~200 THz); extremely low transmission loss; and immunity to electromagnetic interference. Optical communication systems, as illustrated in Figure 1, consist of three main components: a transmitter, transmission media (optical fiber), and a receiver. The transmitter is responsible for imprinting an electrical data signal onto an optical carrier which is coupled to an optical fiber suitable for long-haul transmission distances. This fiber is used as the transmitting medium from point-to-point. The receiver converts the light signal back to the originally transmitted electrical impulses.

As of 2002 submarine fiber-optic communication links, spanning cumulatively over 250,000 kilometers, have been in operation connecting communication systems all over the world [2]. Worldwide communication is dependent on optical communication systems as is shown in Figure 1; therefore, it is imperative that transmitter technology continues to evolve in order to meet future bandwidth demands while also simplifying transmitter module design.

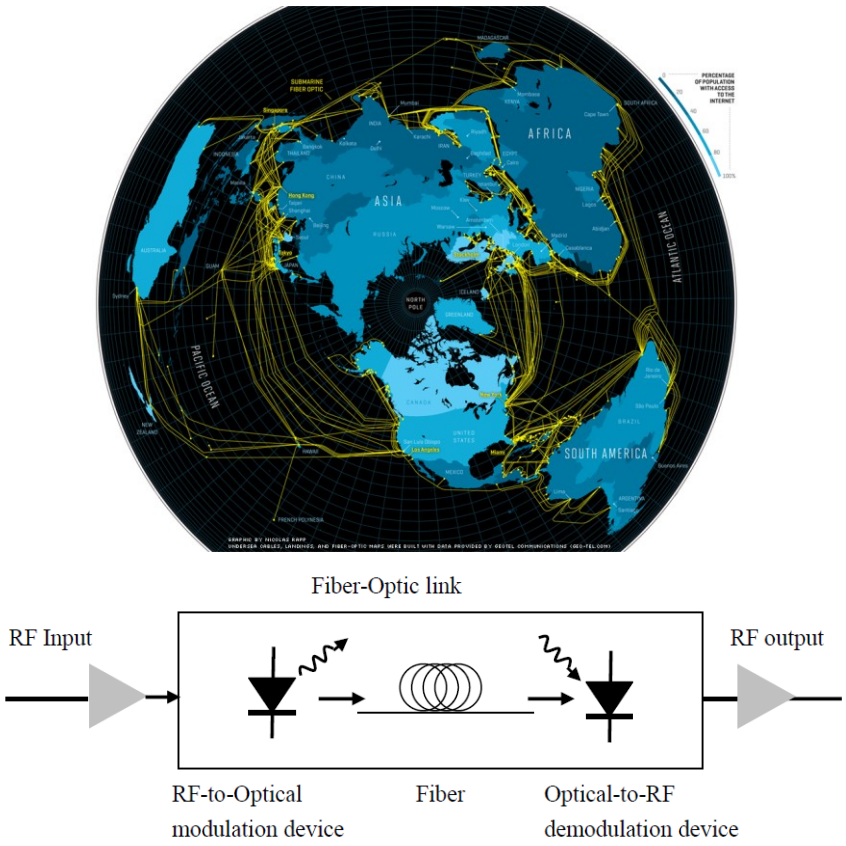

Figure 1: (top) Mapping of undersea fiber network links [3]. (bottom) Basic components of a fiber optic link.

Modulation is the process in which information, in the form of baseband electrical waveforms, is superimposed onto a carrier frequency to take advantage of the low loss transmission properties of the carrier signal. The integration of semiconductor laser's into optical transmitters is divided into two main categories: direct modulation and external modulation. The direct modulation of semiconductor lasers is the simplest and most compact approach to pass data onto an optical fiber; however, drawbacks such as wavelength chirp and inherent relaxation oscillation frequency limits impede the high-speed and long-distance capabilities of such systems [4]. In external modulation, the optical source is operated continuously and its output light is modulated using an optical

external modulator. Although more complicated in design, the zero-chirp operation and higher bandwidth capabilities (~40 Gbps) of external modulators has motivated their large-scale use in fiber-optic systems [5]. Figure 2 illustrates the difference between the direct (left) and external (right) modulation schemes.

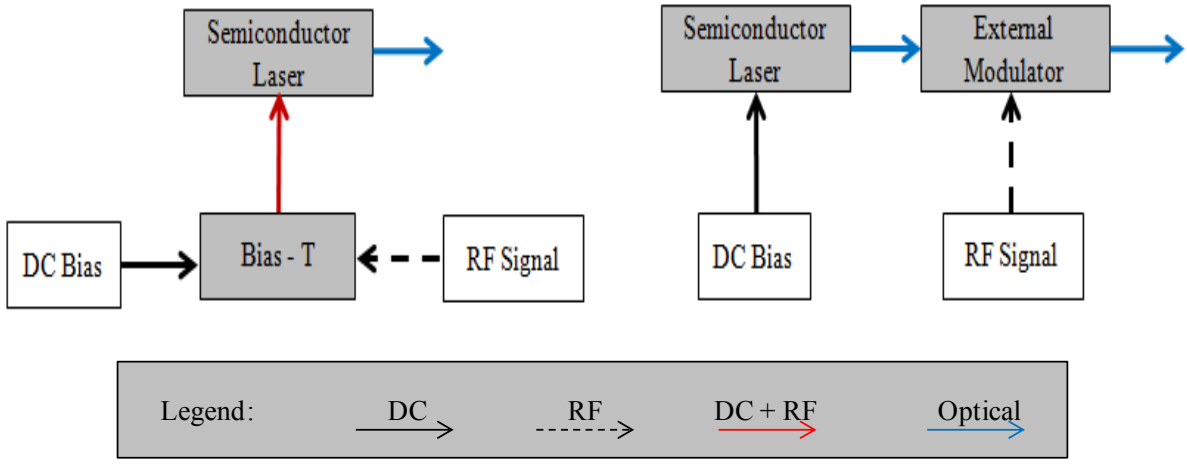

Figure 2: Block diagram of direct modulation (left), external modulation (right).

Several types of semiconductor lasers have been investigated and are in operation in optical communication systems today. The varied types of semiconductor lasers can be categorized based on their active region geometry (bulk, quantum-well, and quantum-dot) and feedback mechanism (for example Fabry–Perot and distributed-feedback designs), with each possessing advantages and disadvantages that will be discussed in detail in Chapter 2.

This research focuses on characterizing the modulation properties of a long cavity (8.3 mm) multi-section quantum-dot laser. The multi-section quantum-dot laser is a device that utilizes a unique modulation scheme to increase the information carrying capability (S21 modulation response) and modulation efficiency of the optical carrier. The multi-section quantum-dot laser is illustrated in Figure 3, whereby the device

possesses a continuous optical/gain region that is broken into 16 electrically isolated sections. In this work, the impact of different electrical biasing/modulation architectures on the modulation response of multi-section quantum-dot gain-levered lasers will be investigated experimentally.

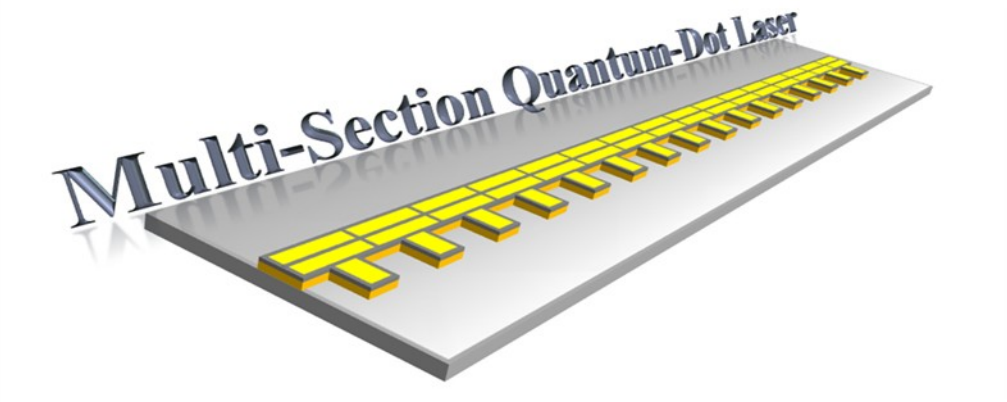

Figure 3: Illustration of a 16 section quantum-dot laser.

The gain-lever effect is a method designed to improve the modulation efficiency of semiconductor lasers. Improvements to the modulation efficiency enable increased modulation depth given a fixed input modulation signal. Overall, in a communications link, increased modulation efficiency improves detection and demodulation schemes. A two-section laser is used to exploit the gain-lever effect, whereby the two sections are biased asymmetrically based on the gain profile of the semiconductor lasers. Normally, the smaller of the two sections will be biased to provide a low gain, but high differential gain. The larger section is biased to a high level where it achieves high overall gain and low differential gain. The combination of the gain in the two sections is clamped, or held constant, once the laser is operating above threshold. To utilize the gain-lever effect, a modulating signal is placed on the section with the higher differential gain. As the

modulating signal increases/decreases the overall gain of the modulated section, the other section must reduce/increase its gain in order to keep the gain clamped at threshold [6].

The gain-lever effect is evaluated/explored using frequency response data for several different device configurations. Reconfigurations are accomplished by modifying the wire bonds used to connect individual device sections. The data will be analyzed to determine the most suitable biasing parameters that yield the largest improvement in modulation response and efficiency. Additionally, the data will be examined to establish a limit to the benefits attained by decreasing the modulation-section length with respect to the gain-section length.

1.2 Motivation

The study of the modulation response of lasers is not a new topic, nor is the gain-lever effect which was initially conceived in 1989 [7]. However, the gain-lever effect in quantum-dot devices having a large cavity length has not been extensively studied. This deficiency is primarily due to the availability of the devices themselves. Multi-section quantum-dot lasers of this type are not readily available in the current commercial market. These lasers are possessed only by a few academic institutions because of the complicated process required for semiconductor crystal growth and device fabrication. The rarity of these devices, and multi-section lasers in general, has limited research in this field in comparison with other laser designs that are easier to fabricate or acquire, such as quantum-well lasers. A better understanding of an optimal quantum-dot laser can be realized by studying how changing the length of the laser's sections affects the modulation characteristics. The study of the gain-lever effect in the 16-section, 8.3-mm

quantum-dot laser under study here is unique in that it allows the following: the size of the modulation section to be varied in length given the addition/removal of wire bonds on the device, and the study of an extreme gain-lever case, where the ratio of gain sections-to-modulation sections is 15:1 which contrasts the typical 3:1 ratio [8], or 4:1 ratio [9] typically investigated in the literature due to fabrication limitations.

1.3 Methodology

Characterization of the laser was carried out in the Ultrafast Photonic Devices and Research laboratory operated by AFRL/RYDH, at Wright–Patterson Air Force Base. Initially the laser was experimentally tested to determine its operating parameters, such as threshold current and optical power vs. current characteristics. Because this device is an unpackaged laser it was first mounted to a thermoelectric cooler to enable continuous/stable operation at room temperature. Due to the small footprint of the laser, small-pitch high-frequency RF probes were used to electrically bias the laser. Modulation response measurements are used to compare the experimental data to values theoretically predicted. This allowed the proper biasing points to be determined for the modulation experiments. A network analyzer was used to modulate one section of the quantum-dot laser with an RF signal to examine the modulation efficiency of the device. To bias the modulated section, a bias tee was inserted into the setup to allow a DC current source to provide a bias without affecting the RF signal. The remaining section was biased by an additional DC current source. The network analyzer was used to sweep the applied frequency. Various frequency sweeps were made that show how the laser responds to

different modulation levels. The typical configuration used to measure the modulation response is shown below in Figure 4.

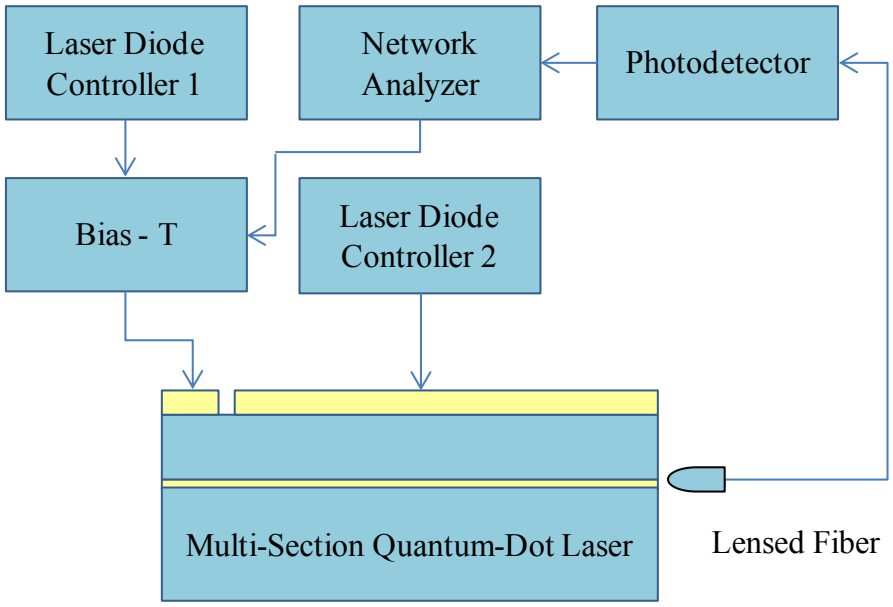

Figure 4: Modulation response test setup.

1.4 Organization of Thesis

This thesis begins by presenting a literature review of semiconductor laser related topics, to include mode-locking, the gain-lever effect, and semiconductor gain region characteristics in Chapter 2. Chapter 3 addresses the methodology that is used to experimentally investigate the phenomenon of the gain-lever effect. Chapter 4 concentrates on presenting and interpreting the results and providing further analysis. Finally, Chapter 5 presents a synopsis and conclusion gained from the results. Additionally, this chapter offers guidance on possible future work that will advance this research.

2. Literature Review

This chapter presents the current state of research in the area of quantum-dot lasers and their use in optical communication systems. The literature review provides a foundation for the research examined in this thesis through laboratory experiments and mathematical models. This chapter begins with a brief overview of optical communication systems. Laser designs with different active regions and feedback mechanisms are compared to demonstrate the benefits of the quantum-dot device designs. Additionally, long optical cavity effects are discussed. Finally, the characteristics of quantum-dot lasers are discussed with a focus on changes observed in the microwave modulation response of multi-section lasers operated using the gain-lever effect.

2.1 Optical Communication Systems and Laser Designs

This section aims to provide a basic background of semiconductor lasers, specifically describing active region types and optical feedback mechanisms of semiconductor laser designs.

Optical communication systems have been integrated into all of the transoceanic communication networks on which the world relies [2]. This integration is a direct result of the high data rates achievable by semiconductor lasers and the low attenuation levels characteristic of optical components. Researchers and engineers are continually investigating new techniques and technologies to increase the data-carrying capacities of these optical systems. Transmitters, which rely on lasers to convert electrical impulses into optical signals, are studied to determine the best device configuration and modulation scheme to maximize the performance of the network. Different types of

semiconductor lasers can be used in transmitters, all with unique geometries, fabrication properties, and materials associated with them.

Distributive feedback (DFB) lasers are commonly used in optical communication systems because of their reliability and single-mode operation. These two characteristics led to their implementation in all transoceanic lightwave systems [2]. From the system's perspective, single-mode operation is requisite for long-haul communications to alleviate the impacts of optical dispersion which limit the maximum achievable bit-rate and/or transmission distance. Multi-mode fibers are insufficient because they suffer from considerable pulse broadening (≈10 nS/km) due to intermodal dispersion. With single-mode operation there is no intermodal dispersion but group velocity dispersion and material dispersion are still present. Optical pulses are broadened because the different spectral components of the pulse arrive at different times at the output due to the wavelength dependency of both the group velocity and the index of refraction of the fiber [2].

The design of the distributed feedback laser relies on a grating that is etched into the active region of a double heterostructure semiconductor. The grating results in a periodic change in the refractive index, resulting in one dimensional interference pattern. The different indices cause Bragg diffraction, providing optical feedback that yields lasing over only a single longitudinal mode. This is in contrast to Fabry–Perot cavities (two discrete mirrors) that result in lasing over multiple longitudinal modes supported by the cavity. Figure 5 shows the laser spectrum of a Fabry–Perot laser on the left and a distributed feedback type laser on the right [10].

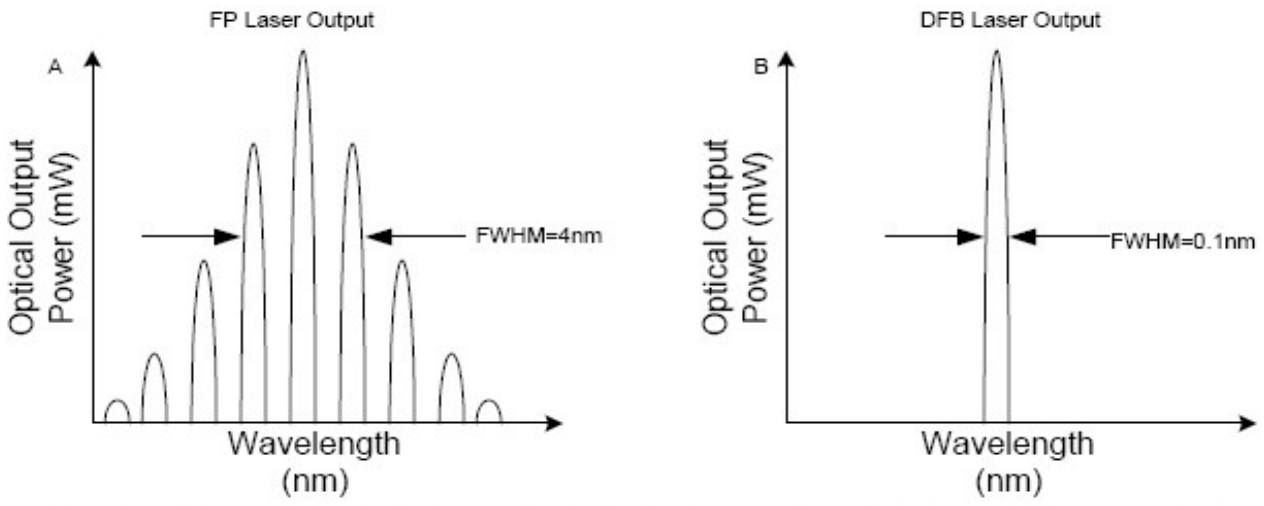

Figure 5: Comparison of a Fabry–Perot laser and a distributed feedback laser [10].

A double heterostructure device consists of two materials with large bandgaps that surround a material with a smaller bandgap, thereby aiding in the confinement of carriers (electrons and holes) to the active region of the laser. The variation in the index of refraction of the layered materials also results in the optical confinement of the resonant field, resulting in improved efficiency of the diode laser. The quantum-well, is similar to a double heterostructure device, however the active region is much smaller, to the point that it approaches the deBroglie wavelength. In Figure 6 the design of a bulk double heterostructure active region is shown on the left with a quantum-well active region depicted on the right. The structures maintain similar layer configurations, but the quantum-well laser relies on an active region ten times smaller than a bulk laser [11].

The quantum-well structure leads to improved efficiency in the physical nature of the electrical pumping and photon generation processes described in the next section. As advancements in fabrication processes progressed, the quantum-well led to the

production of the quantum-wire and quantum-dot structured active regions, with each having improved efficiency over the previous.

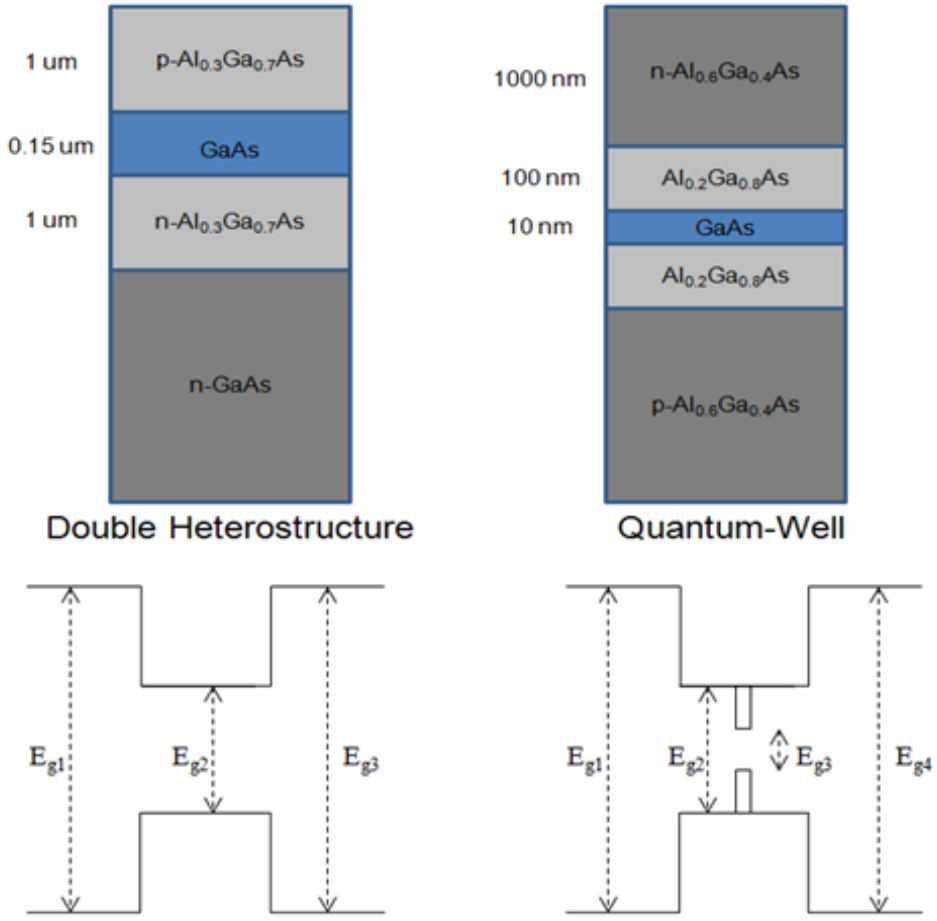

Figure 6: Physical structure (top) and bandgap structure (bottom) of double heterostructure and quantum-well devices [11].

Quantum-well based lasers have been thoroughly studied due to their commercial availability, whereas quantum-dot lasers are less mature in integration. The lack of thorough experimental understanding of quantum-dot lasers is linked to the fact that they are more difficult to fabricate (epitaxially grow) when compared to quantum-well laser diodes.

2.2 Laser Device Physics

Semiconductor lasers rely on electron hole recombination to emit light. A typical configuration for lasers is created by forming a p-n junction made from a direct-bandgap semiconductor material. This junction is forward biased in order to produce excess electrons in the conduction band and excess holes in the valence band [12]. This condition leads to what is referred to as a population inversion. Given a suitable level of electrical pumping, the population inversion state results in the radiative and non-radiative decay of excited electrons across the semiconductor bandgap (recombination) with available holes in the valence band. The radiative decay process results in the emission of light in the form of a photon, as shown in Figure 7(a). In the case where an optical feedback mechanism exists (ex. DFB or Fabry–Perot), the photons begin to couple together. At this point the photons no longer propagate in random directions but join the existing photons, as shown in Figure 7(b), matching their energy and direction of propagation thereby creating coherent light [2]. This is the basis for stimulated emission which is present in all lasers.

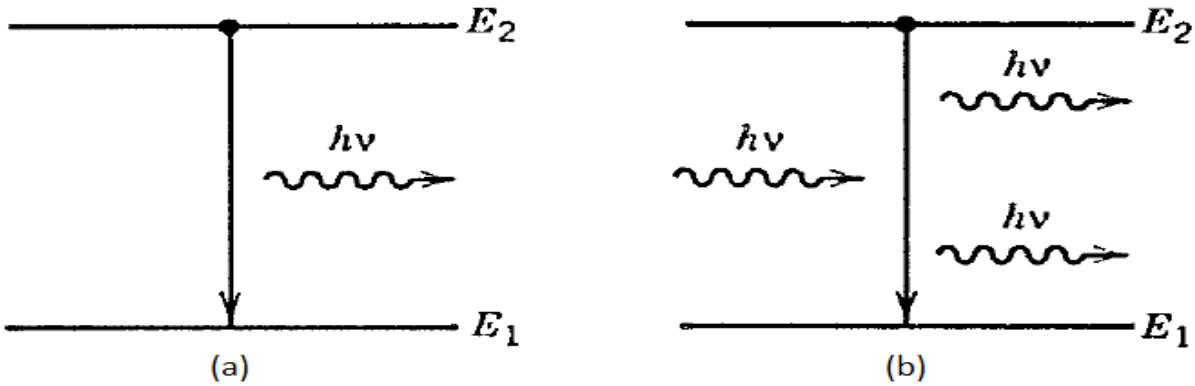

Figure 7: Two types of emission (a) spontaneous emission, (b) stimulated emission [2].

One can consider the physics and the parameters that make up the device's gain coefficient to determine the benefits of quantum structured over bulk semiconductor lasers, shown in Equation (1) [12].

$$\gamma_o(v) = \frac{\lambda^2}{8\pi\tau_r}\varrho(v)f_g(v) \qquad (1)$$

Wavelength, λ, is related to the bandgap, photon energy and quasi-Fermi levels by $E_g \leq hv \leq E_{fc} - E_{fv}$. The radiative recombination lifetime τ_r governs the rate of photon absorption and emission [12]. The next two terms are the optical joint density of states, $\varrho(v)$, and the Fermi inversion factor $f_g(v)$. When the semiconductor is electrically biased (pumped) until there is population inversion, the Fermi inversion factor will be positive and there will be gain in the laser [12]. The density of states differs depending on the structure of the device. Figure 8 below shows the ideal density of states for the bulk, quantum-well, quantum-wire, and quantum-dot lasers.

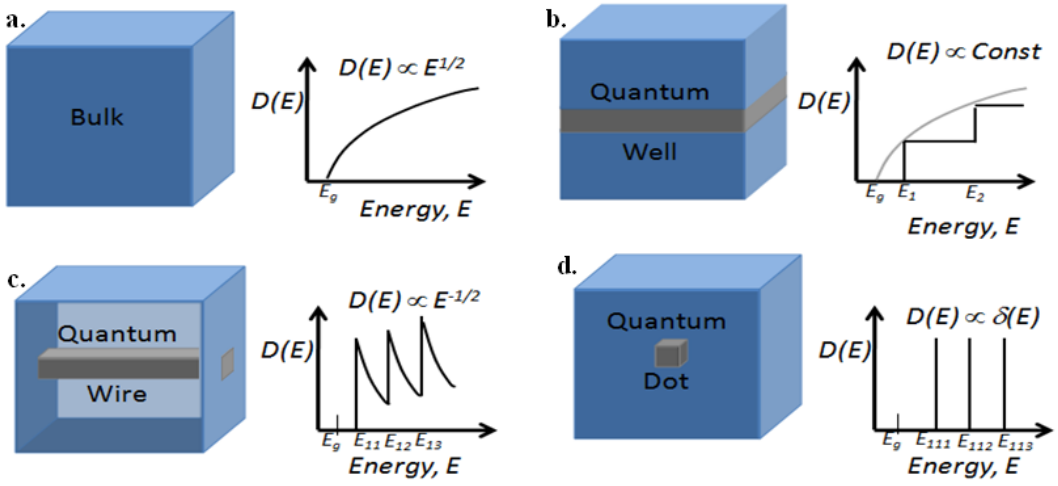

Figure 8: Density of states for the bulk (a), quantum-well (b), quantum-wire (c), and quantum-dot (d) devices.

Bulk semiconductors have a continuous density of states, whereas quantum devices have discrete energy levels. The quantum-well exhibits one-dimensional confinement, resulting in the stair-step nature of its density of states. This confinement is shown pictorially in the Figure 8(b). In the *x* direction the active region is so thin that the energy levels are quantized, but in the *y* and *z* directions the carriers have freedom to move about the material. Quantum-wire devices are quantized in two dimensions and finally quantum-dot devices provide three-dimensional confinement. This confinement gives the quantum-dot laser a density of states that is approximately a delta function; it is directly responsible for many of the optical characteristics that make the quantum-dot device more desirable than the other structures [12].

In Equation (1) we can see how the density of states, illustrated in Figure 8, can impact the overall shape of the gain profile. The bulk semiconductor laser will have a much broader profile when compared to the quantum-well, and this trend continues as the confinement is increased. This increase in the quantum confinement of the active region is responsible for improving laser performance by reducing both the threshold current and the spectral linewidth. A quantum-dot device should have a gain profile that ideally resembles a delta function. In reality, a delta function is not achievable due to fluctuations in the quantum-dot size as a result of the manufacturing processes. A quantum-dot laser is constructed on such a small scale that tiny imperfections create measureable differences in laser performance [13].

Quantum-dot devices have been rigorously investigated because of their high differential gain at low biasing levels. This differential gain is dependent on the slope of the gain profile and is specific to a type of active region geometry. An initial study

investigating this behavior is illustrated in Figure 9 where Box, Wire, and Film, refer to quantum-dot, quantum-wire, and quantum-well active regions. The slope of the gain spectrum becomes steeper as the active region confinement increases [14]. The logarithmic axes shown in the figure tend to visually downplay the significance of the differences between the devices.

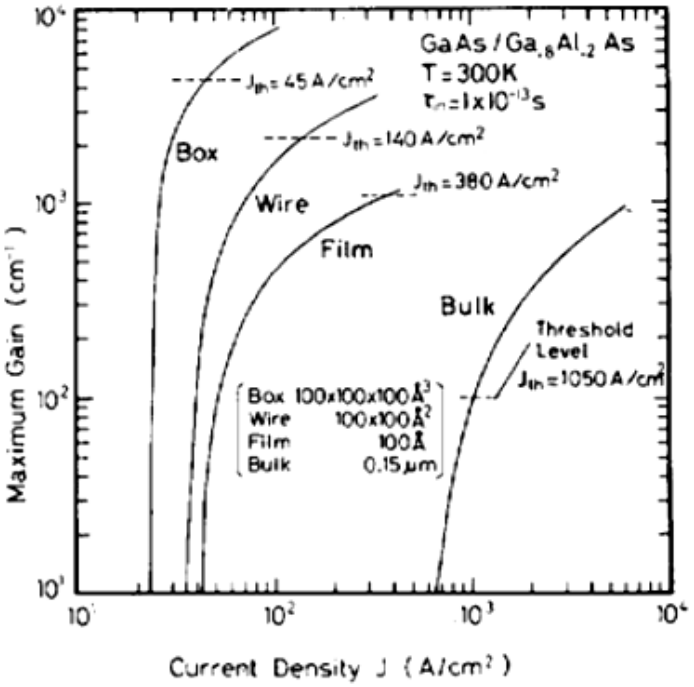

Figure 9: Maximum gain as a function of current density [14].

2.2.1 Threshold Current

As confinement increases it takes fewer carriers to bias a laser above threshold. In theory an active region could be made small enough that the current threshold would approach zero. Low threshold lasers would benefit in applications where efficiency is required, such as small on-chip designs that have limited power distribution. The only potential drawback to a laser having an ultra-low threshold is that as the current threshold is lowered, the maximum optical output power is also limited. Recently an electrically

pumped quantum-dot photonic crystal nanocavity laser reported a threshold current of 181 nA when cooled to 50K and 287 nA at a temperature of 150K [15]. The results of that test are shown in Figure 10.

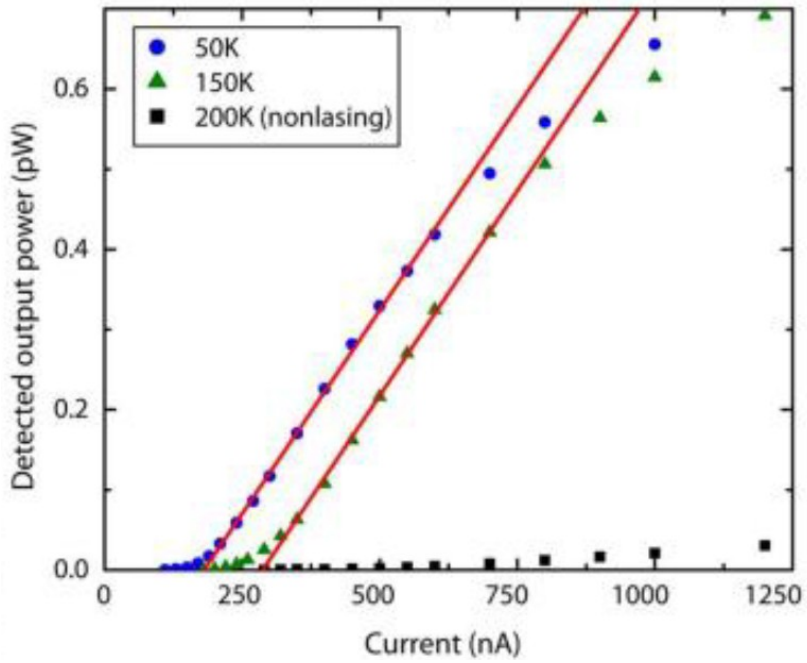

Figure 10: Detected output power of the laser as a function of pump current taken at 50K (blue points), 150K (green points) and 200K (black points - nonlasing). The red lines are linear fits to the above threshold characteristics to determine the laser threshold [15].

This effect can be described by the direct proportionality between the carrier concentration and the volume of the active region and is shown using Equation (2) [12]:

$$J_t = \frac{\alpha_r + \alpha}{\alpha} J_T \tag{2}$$

where the transparency current density J_T is the level of injected carrier concentration that results in neither gain nor loss. Two attenuation terms are present in Equation (2). The resonator loss coefficient, α_r, is inversely proportional to the gain medium length and a function of the reflectivity of the cavity. The other term, α, is the temperature dependent

attenuation factor [12]. The following substitution for transparency current density may be used to put Equation (3) in a form that is easily interpreted.

$$J_T = \frac{el}{\eta_i \tau_r} \Delta n_T \tag{3}$$

This makes Equation (3) become:

$$J_t = \frac{\alpha_r + \alpha}{\alpha} \frac{el}{\eta_i \tau_r} \Delta n_T \tag{4}$$

To simplify the interpretation of this relationship we can make the assumption that $\alpha_r \lll \alpha$, which reduces $\frac{\alpha_r + \alpha}{\alpha} \approx 1$. This approximation leads to:

$$J_t = \frac{el}{\eta_i \tau_r} \Delta n_T \tag{5}$$

The final form of the relation is reached by converting from a current threshold density to a current threshold.

$$I_t = \frac{eV}{\eta_i \tau_r} \Delta n_T \tag{6}$$

Equation (6) represents the threshold current as a function of the volume of the active region, V, and the carrier concentration. As the active region is confined in an increasing number of directions the volume is decreased, the threshold current decreases because the area is directly proportional to the threshold current. The quantum-dot laser, having the smallest active region volume of the quantum devices, has the lowest threshold current. The narrow gain profile and low threshold current make quantum-dot lasers an attractive candidate for use in transmitters.

2.2.2 Optical Spectrum

As the confinement is increased, changes to the density of states of the active region result in the narrowing of the photoluminescence spectrum; this narrowing reduces a key characteristic parameter of a laser referred to as the linewidth (similar to the bandwidth of an RF signal). The wavelength of the optical signals can be widely tuned by varying the shape and composition of the quantum-dot material via bandgap and quantized energy state engineering. For example, researchers have produced AlGaAs–GaAs quantum-dot lasers that have emission wavelengths that range from 950 to 1370 nm [16]. If the active region were able to be reduced to produce quantum-dots that are smaller than the exciton Bohr radius the density of states would result in a delta function [16]. This delta-function density of states would produce a near delta function in the emission spectrum as well, yielding an extremely narrow-linewidth optical output when compared to double heterostructure and quantum-well lasers. A true delta function density of states across the aggregate quantum-dot active region would require that all the dots be identical (homogeneous) in every way and arranged in a perfectly uniform pattern. Unfortunately, this homogeneity has proven unattainable using currently available fabrication technologies. Quantum-dot non-uniformity (heterogeneity) causes the emission spectrum of the laser to broaden [17]. A quantitative value that is assigned to this phenomenon is called the linewidth-enhancement factor.

The linewidth-enhancement factor can be used to characterize the effect variations of the carrier density have on the index of refraction of the active region. This is represented by α in the formula shown in Equation (7) [18].

$$\alpha = -\frac{4\pi}{\lambda}\frac{dn/dN}{dg/dN} \tag{7}$$

In this equation, n is the index of refraction, N is the carrier density, and g is the optical gain. The joint optical density of states approximates a delta function, therefore the differential optical gain term should be very high resulting in an overall smaller linewidth enhancement factor and improved optical spectrum. While a factor of zero may not be practical, as early as 1999 Newell *et al.* achieved an α of 0.1 [18].

The reduction of the density of states is not always the best option for all device applications. A side effect of this is a reduction in the overall peak gain. One way to increase the gain of a quantum-dot laser is by using multiple layers of dots that are self-assembled in multiple strained quantum wells [17]. Figure 11 shows the effect that straining the quantum wells has on the optical gain. The strained quantum well has over eight times the gain of an unstrained quantum well.

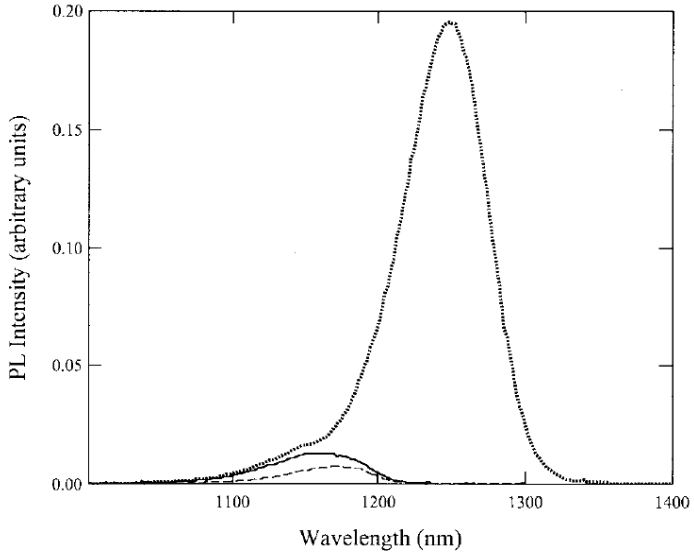

Figure 11: InAs quantum-dots grown on bulk GaAs (dashed line), InAs quantum-dots grown in a quantum-well (solid line), and InAs quantum-dots grown in a strained quantum-well [17].

An added effect of having a small active region is that it allows the device to be susceptible to gain saturation. This creates a more dramatic dynamic effect than that of the linewidth-enhancement factor alone. Initially, as bias current levels are increased the device begins lasing from the ground state of the quantum-dots. As this current is increased, further competition between the ground-state and excited-state transitions alters the optical spectrum [17]. Figure 12 shows that once the quantum dots are completely gain saturated, the laser begins emitting from the wetting layer. This excited-state emission happens more readily in lasers having short cavities and limits the linewidth-enhancement factor to values greater than one [19]. This is combined with the original quantum-dot emission wavelength being blueshifted [16].

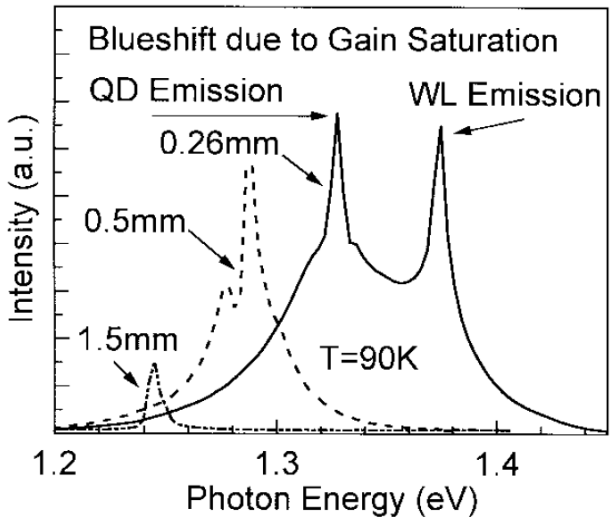

Figure 12: Blueshift of the quantum-dot emission due to state filling. Each spectrum is marked with the corresponding laser cavity length. For short cavity lasers the quantum-dot gain is completely saturated and the emission jumps to wetting layer states [16].

The optical spectrum may also be shifted by altering the cavity length of the device. Eight lasers with different lengths were tested uniformly by Lester *et al.* [17]. Various cavity lengths produced optical emissions ranging from 1050 to 1240 nm as

illustrated by Figure 13. The 1.5 mm length device illustrates the gain saturation phenomenon when it is biased at 6.7 times the threshold current. One revealing characteristic of the quantum-dot device is the trough in the spectrum between ground and excited emissions [17].

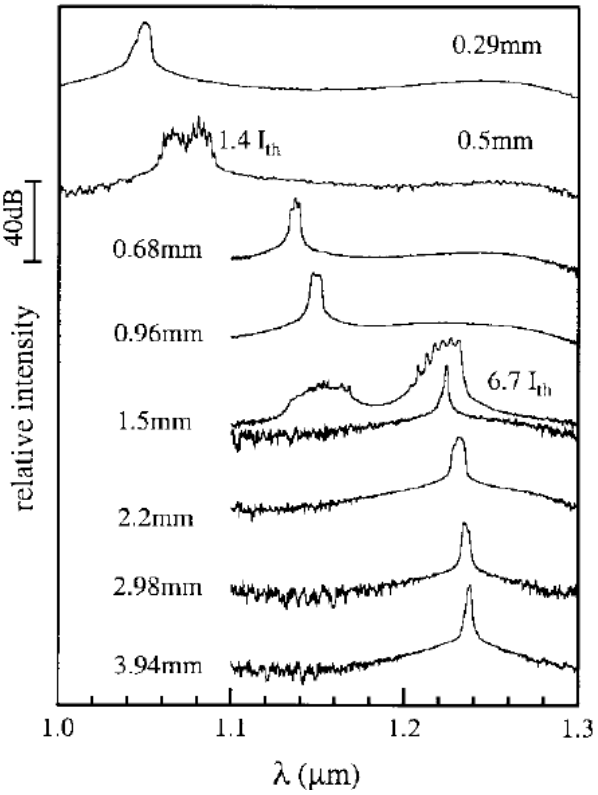

Figure 13: The measured lasing spectra of InAs QD lasers with eight different cavity lengths. The pump current level is 1.1 × threshold if not otherwise noted [17].

2.2.3 Mode Locking

Mode locking is a technique in which a laser is used to generate optical pulses. These pulses generally have short temporal widths, on the order of femtoseconds or picoseconds. The repetition rates of mode-locked semiconductor lasers can be used to create microwave sources with the potential for application in RF photonics [20]. One such application is master clock distribution where delays in RF circuitry are becoming

the limiting factor in high-speed digital circuits [21], [22]. For example, a 10-GHz oscillator was created from a monolithic two-section laser having an RF linewidth of 500 Hz [23]. This device was packaged, as shown in Figure 14, as a stand-alone component which allows easy integration as a component of a larger application. Mode locking has also been used to create optical pulse sources for studying ultrafast chemical phenomena [24], as well as in the construction of RF transmitters that utilize mode-locked quantum-dot lasers integrated with bowtie antennas [25]. There are three different types of mode locking discussed in literature: active, passive, hybrid mode locking. This section focuses on passive mode locking as a multi-section device with a reversed biased saturable absorber and passive mode locking with a single section device.

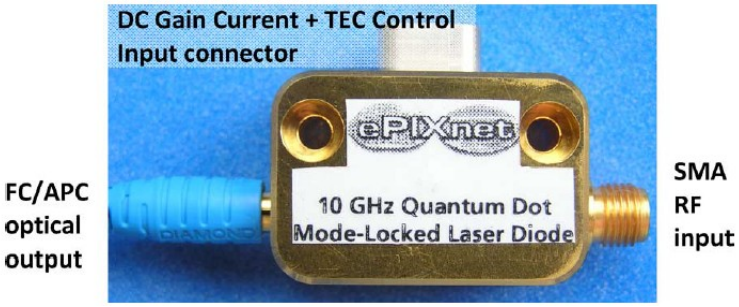

Figure 14: Packaged 10 GHz oscillator [23].

2.2.3.1 Passive Mode Locking in a Multi-Section Device

Passive mode locking is generally thought to be capable of creating the shortest pulses of the three types of mode-locking [24]. A typical laser cavity that is used for passive mode-locking is shown in Figure 15 (top). There is a gain medium, a saturable absorber, and two reflective ends which are either simply cleaved ends of the semiconductor or cleaved ends where a highly reflective coating has been applied [20]. As the optical pulse moves through the cavity it passes through the saturable absorber

which begins to absorb the lower power leading and/or trailing edges of the pulse, effectively shortening the pulse [26]. This creates a pulse train with a repetition rate that is approximately equal to the free-spectral range of the laser cavity and given by:

$$FSR = \frac{c}{2nd}, \tag{8}$$

where c, n, d are the speed of light in a vacuum, the index of refraction inside the laser cavity, and the length of the laser cavity. To increase the saturable absorption in a semiconductor device a reverse bias may be applied. This requires a two section laser that is optically coupled but electrically isolated. Passive mode locking has been successful in creating millimeter wave signals with low RF linewidth [27], [28].

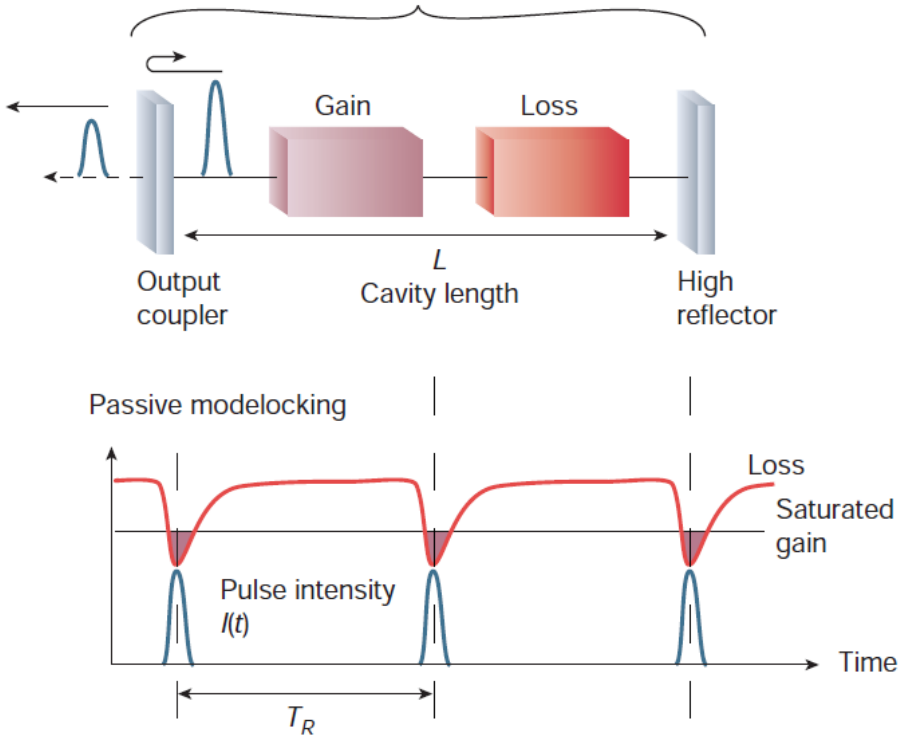

Figure 15: Illustration of laser cavity for use in passive mode-locking [20].

2.2.3.2 Passive Mode Locking in a Single-Section Device

Passive mode locking in a single-section device lacks a dedicated reverse biased saturable absorber. This type of passive mode locking exhibited in single-section devices has the advantage of being easier to fabricate, as well as eliminating vulnerabilities to bias current sensitivity since a single-section device is not susceptible to the bias current sensitivity that can cause chaotic operations in multi-section devices [29]. A single-section 1-mm long laser produced the 40.2-GHz tone observed in Figure 16 (inset) with a 3-dB linewidth of less than 1 MHz [29].

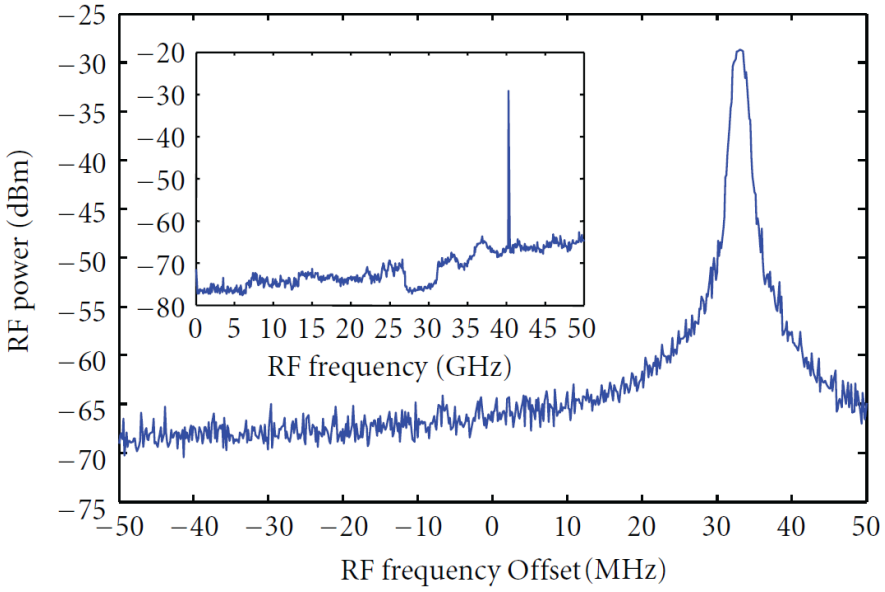

Figure 16: RF Spectrum of a single section mode-locked device [29].

Single-section passive mode locking is less prominent in the literature when compared to multi-section devices used in passive mode locking, possibly because this phenomenon requires more stringent device characteristics to exhibit self-pulsation. This was a factor in research on quantum-cascade lasers where only longer devices (> 3.5 mm) exhibited mode locking as a single-section device [30].

Other studies have focused on self-pulsation in multi-section distributed feedback lasers [31], [32]. The optical spectrum illustrated in Figure 17(a) is of a three-section laser that is biased above threshold with DC current that produces a single optical mode with greater than 50 dB side mode suppression [32]. Figure 17(b) illustrates that as current is increased in one of the sections the laser begins to "self-pulsate" with a repetition rate of 8 GHz. Figure 17(b) also shows that as the current in one section is increased the optical pulse is broadened, reduced in intensity, and an additional optical pulse is formed approximately 5 nm away from the fundamental mode [32].

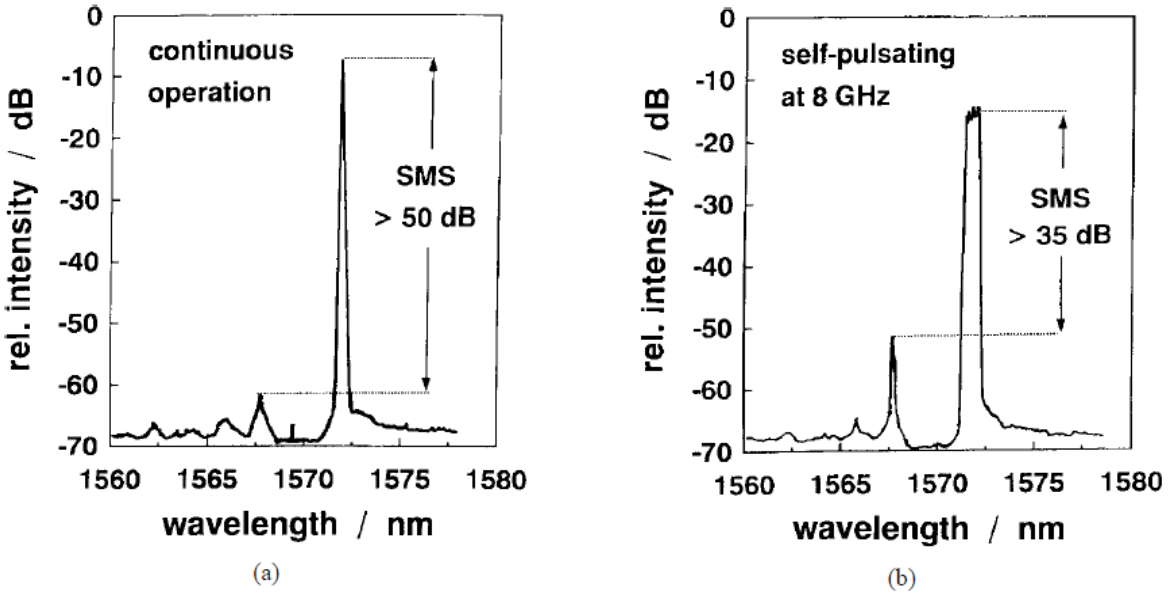

Figure 17: Optical spectrum of a three section DFB exhibiting self-pulsation [32].

The causes for this type of mode locking are not well understood and theories and models used to describe this behavior are still evolving. Current investigations have suggested the coupling of multiple spatial modes in the laser cavity [29], [33], self-focusing due to the Kerr effect [30], and dispersive Q-switching [31], [32] as some of the theories that may explain this behavior.

2.2.4 Modulation Response

Lasers that are designed to work in optical communication systems as transmitters require a modulation scheme to facilitate the transfer of information. There are different methods for encoding a signal onto a laser beam. Direct modulation is the simplest form, where a laser is biased into operation by a DC signal that is superimposed with an RF signal [34]. The other common modulation configuration requires an external modulator that modifies the output beam of the laser. As with most designs, each modulation configuration has its advantages and drawbacks.

Direct modulation is an ideal scheme for a laser that will be integrated into a small-scale device, such as a microprocessor where size is crucial. External modulation can be accomplished by an external device, such as a Mach-Zehnder modulator that varies the optical intensity of the beam once it is outside of the laser cavity. These modulators can be added as a separate component along the optical path of the fiber or implemented on-chip. This modulation technique has the benefit of reduced frequency chirp, but is incurred at the expense of additional equipment and a larger size [2]. The gain-lever effect investigated in this work is a sub-category of the direct modulation scheme.

Direct modulation is the easiest to integrate into a design since it requires no additional equipment. Also, the conversion of biasing current to modulated light output is linear over much of the laser's operating range. Direct modulation also allows high data rates to be accomplished due to the extremely short photon lifetime in a laser cavity [35]. However, frequency chirp from direct modulation causes a dispersion penalty which can affect the operation of long-haul high-bit rate communication systems [36]. Regardless of

this potential shortfall, direct modulation has been actively researched for the past 40 years [37]. Modern research using quantum-dot lasers has yielded direct modulation measurements of 25 Gbps [38], and directly modulated nanoscale lasers using exotic photonic crystal laser cavities, shown in Figure 18, are being employed for use in on-chip optical interconnects to create high-speed circuits [39].

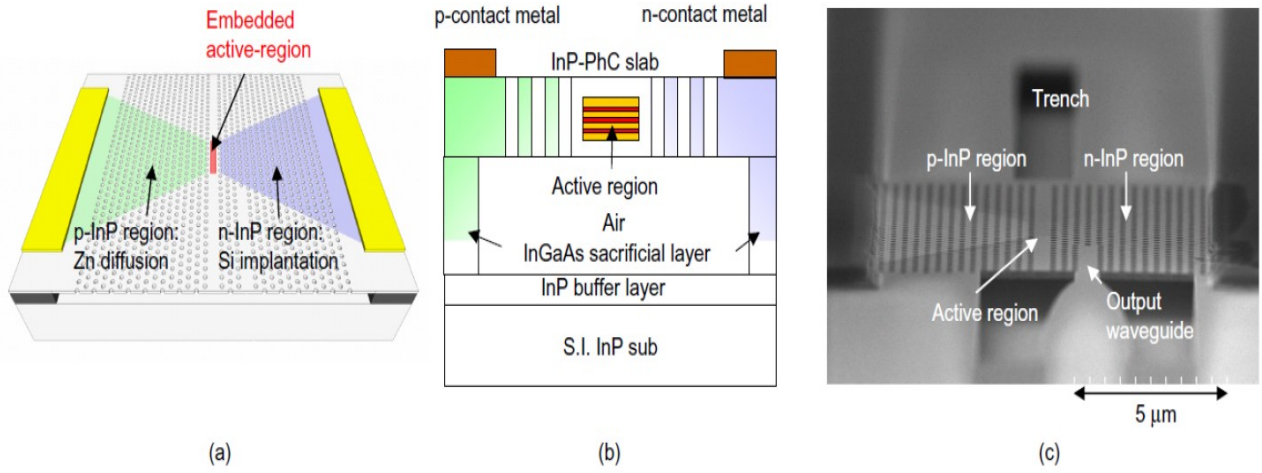

Figure 18: Schematic of laser: (a) top view (b) cross-section (c) scanning electron microscope image [39].

The frequency response bandwidth is one metric used to measure the performance of the laser. A higher bandwidth means more information can be transferred across an optical link in a shorter time period. An expression for the frequency response of the single-section laser is derived from the coupled rate equations and is shown in Equation (9) [40].

$$|R(f)|^2 \propto \frac{1}{1+(2\pi f\tau_c)^2}\frac{f_r^4}{\left[(f_r^2-f^2)+\left(\frac{\gamma}{2\pi}\right)^2 f^2\right]} \tag{9}$$

where γ is the relaxation rate which has a linear relationship with laser power, τ_c is part of the parasitic capacitance of the associated electrical interconnects. The resonant frequency term is denoted by f_r and is proportional to the square root of the laser output power and f is the operating frequency [41]. The relationship that the relaxation rate and the resonant frequency has with the output power shows that as power is increased the bandwidth of the laser will increase, as illustrated in Figure 19, until an over-damped situation occurs and further increases in bias current degrade the 3-dB bandwidth. Additionally, there are limitations to this relationship, as thermal effects, and facet damage could occur if the power was increased too much [41].

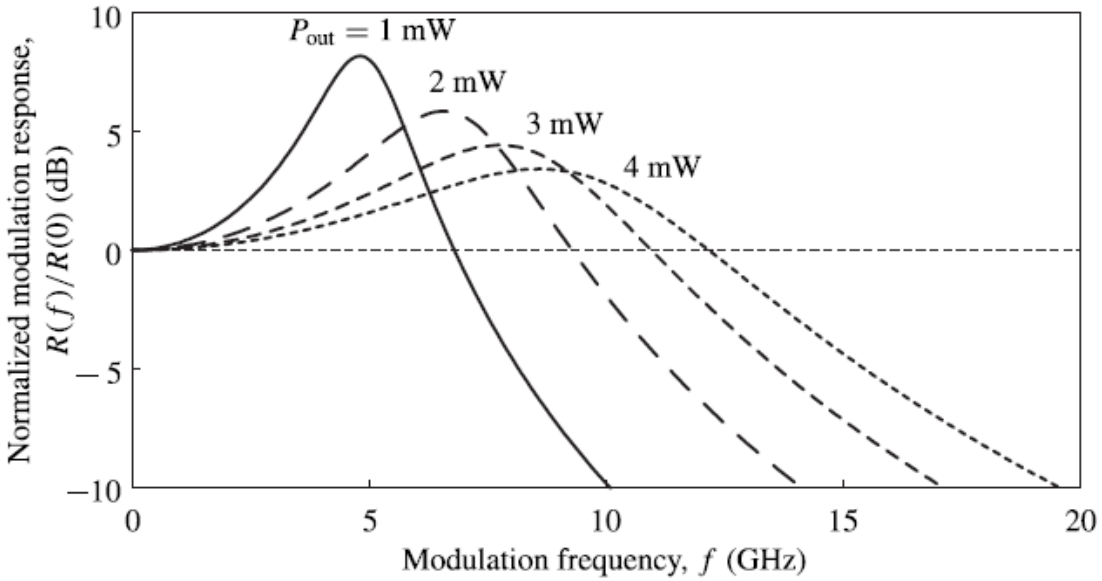

Figure 19: Normalized modulation frequency response of a semiconductor laser [41].

As the laser's output power is increased, via an elevated bias current, the modulation response begins to flatten out. If increased enough, the response will eventually drop below the 3-dB point as the system becomes over damped. Equation (10) is used to relate the 3-dB bandwidth and the relaxation frequency of a semiconductor

laser [40]. The 3-dB bandwidth is a common measure of performance for communication systems. Current proposed devices are predicting a record performance of 110 GHz for the 3-dB bandwidth [42].

$$f_{3dB} \approx f_R\sqrt{1+\sqrt{2}} \approx 1.55 f_R \tag{10}$$

The single-section transfer function, shown in Equation (9), adequately describes modulation response curves observed in Figure 19, but it does not accurately predict the behavior of all single section devices. The plot depicted in Figure 20 displays the frequency response of a single section Fabry–Perot device that exhibits the self mode-locking behavior discussed earlier. It is clearly evident that an accurate curve fit using Equation (9) would not be possible, and demonstrates that factors other than those captured by the laser rate equations affect the frequency response of the device.

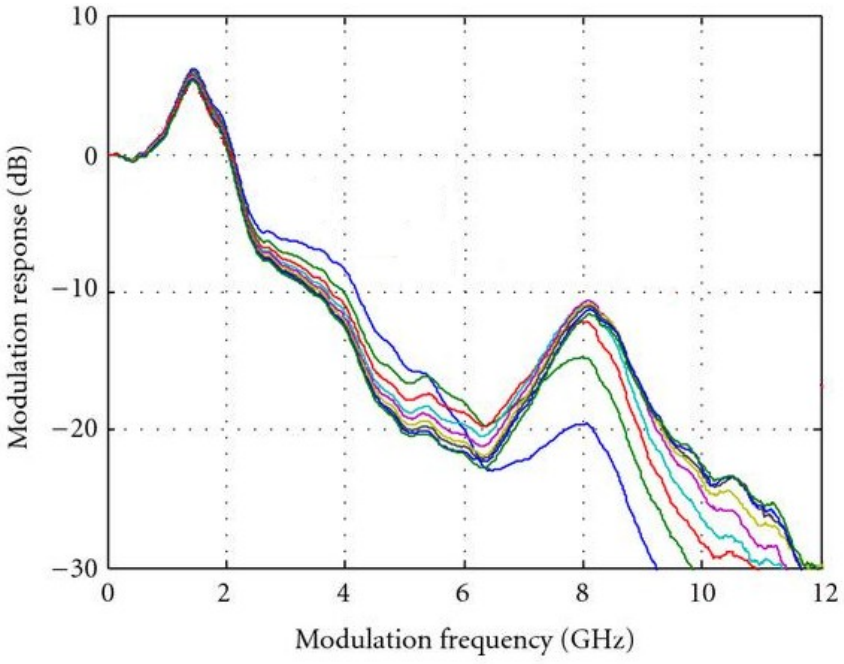

Figure 20: Single section mode-locked laser frequency response for various bias levels [29].

Quantum-dot lasers are being studied for their implementation in optical communication systems for the reasons stated in the previous sections, such as their potentially narrow linewidth and low threshold current density. However, there are some reported limitations to the frequency response of quantum-dot devices [43], [44]. The first limitation is the so-called phonon bottleneck. This is a predicted nonradiative process that is responsible for increasing the relaxation rates inside the quantum-dots [43]. This increase in carrier relaxation rates is detrimental to the frequency response of the device because fewer carriers will be available to contribute to stimulated emission. Figure 21 shows the degradation of frequency response when the recombination lifetime is reduced [45].

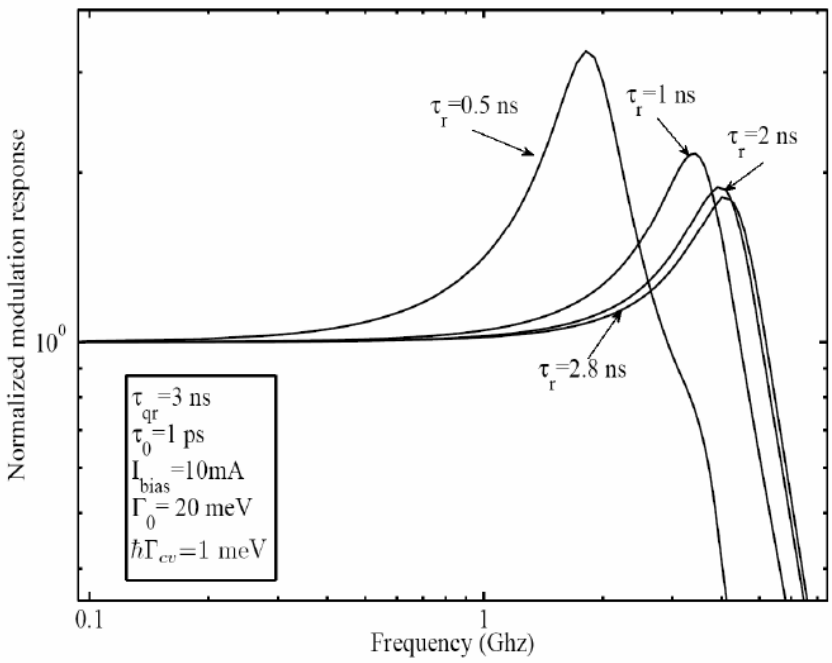

Figure 21: Modulation response of quantum-dot laser with various recombination times [45].

Another limitation to the 3-dB modulation response arises from the highly complex nonlinear carrier dynamics present in the quantum-dot active region. These

dynamics, which are not completely understood, cause enormously different responses when comparing small- and large-signal modulation [44]. This allows results, like the ones shown in Figure 22**,** where a quantum-dot laser, modulated with a pseudo-random-bit-sequence, generates a well-defined eye diagram at 15 Gbps. This contradicts the small-signal frequency response which presents a small-signal 3-dB bandwidth of only 5 GHz. A similar result was found by Ishida *et al.* where their quantum-dot device had a bandwidth of 11 GHz but was successfully modulated at 25 Gbps [38].

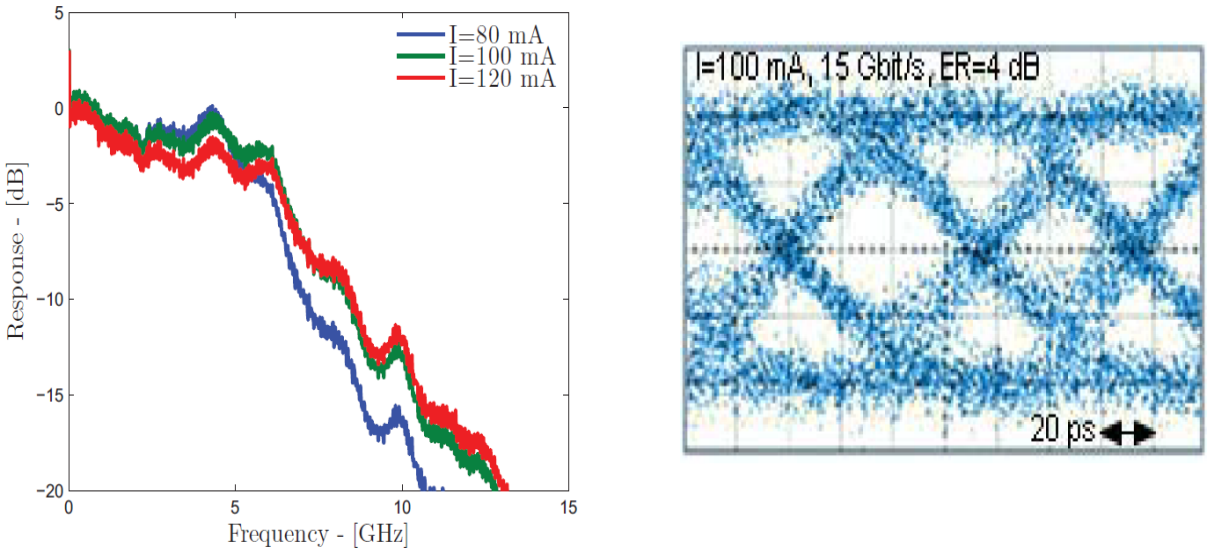

Figure 22: Small signal response on left, digital modulation on right for quantum-dot device [44].

This disparity between the small-signal bandwidth and the digital modulation (5 GHz 3-dB bandwidth vs. 15-Gbps bit rate) is intriguing because it defies what is expected in the laser. The small-signal modulation is varied by a sinusoidal signal while the digital modulation utilizes a square wave. In normal instances the small-signal bandwidth is required to exceed the digital modulation rate to allow for the multiple harmonics of the Fourier series square wave.

Copious research has been performed on directly modulated quantum-dot lasers that utilize various geometries and fabrication techniques in the laser cavity to tune the performance of the laser, while other research, such as the gain-lever effect, has focused on altering the laser's performance by adjusting levels of biasing along the length of the cavity.

2.2.5 Gain-Lever Effect

The gain-lever effect was first explored optically by Vahala *et al.* [7]. Since then research has been performed using the gain-lever effect with distributed feedback lasers [46]; comparisons have been made between bulk semiconductors and multiple quantum-well lasers [47], between optical and electrical gain-lever effect of quantum-well lasers [48], and various tests on the electrical gain-lever effect in quantum-dot lasers [8],[9] [34], [49], [50].

The gain-lever effect in its most prevalent form utilizes a two-section laser where the two sections are optically coupled but electrically isolated. They are optically coupled because they share the same optical cavity and electrically isolated during the manufacturing process; there is generally >1 MΩ between adjacent contacts. The device represented by Figure 23 (left) labels the electrically isolated sections as a and b; the section labeled a is commonly identified as the modulation section, while section b is referred to as the gain section.

The electrical isolation between the sections allows for different biasing to be applied to each section. The longer gain section is biased to provide the majority of the gain for the signal. This section is biased to the point of gain clamping at the threshold

value, which means that high amplification is provided to transmit the information, but there is low differential gain because of the clamping effect [34]. The modulation section is biased at a much lower current density and it is directly modulated by the RF signal that carries the desired information.

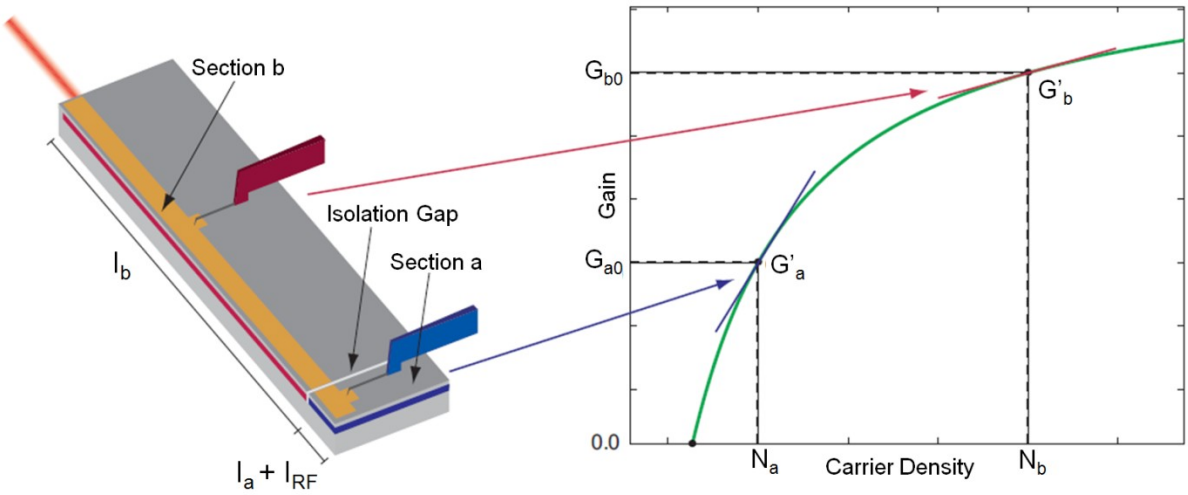

Figure 23: Typical layout for a two section laser (left), gain profile denoting common biasing points utilized in multi-section devices [51] (labels modified to match convention in this document).

Figure 23 (right) shows the approximate bias level of in each section. As stated previously, section b is biased at a high level and is responsible for providing the majority of the gain. To ensure section a has a very large differential gain, which is characterized by the tangential slope, this section is biased at a much lower level. This slope shows that a small change in carrier concentration, in this case a superimposed RF signal on the modulation section, will have a large effect on the overall gain of the device. This increase in response is caused by the ratio of differential gains between the sections and the clamping effect.

The laser must maintain clamping in steady state; as a result section b reduces the gain until the overall gain of the laser is again equal to the threshold gain. Section b of

the laser has a low differential gain and therefore the section must lower the overall gain much more dramatically to compensate for section a [9]. This difference in differential gain between the sections is the basis for modulation enhancement when utilizing the gain-lever effect and can be realized by analyzing the laser's rate equations. The rate equations for a two section laser are expressed as [34]:

$$\frac{dP}{dt} = P\left[\Gamma G_a(1-h) + \Gamma G_b h - \frac{1}{\tau_p}\right], \tag{11}$$

$$\frac{dN_a}{dt} = \frac{J_a}{ed} - \frac{N_a}{\tau_a} - G_a P, \tag{12}$$

$$\frac{dN_b}{dt} = \frac{J_b}{ed} - \frac{N_b}{\tau_b} - G_b P, \tag{13}$$

where P is the photon density, $J_{a,b}$, $N_{a,b}$, $\tau_{a,b}$, and $G_{a,b}$ are the current density, carrier density, carrier lifetime and unclamped gains in sections a and b, respectively. Γ is the optical confinement factor, h is the fractional length of the gain section, and d is the active region thickness [34]. In order to reduce these equations to a transfer function several approximations and assumptions are made. The first approximation is that we are only using one rate equation for the change in photon density with respect to time. Even though the laser may be biased on two different levels this assumption is reasonable because the two sections of the laser are optically coupled [34]. Assuming the spontaneous carrier lifetime is much larger than the stimulated lifetime and the fractional length is near unity, the rate equations can be solved using small signal analysis. The result is the modulation response equation that is shown in Equation (14) [34]:

$$|R(f)|^2 \propto \frac{\left(\frac{\gamma_a\gamma_b}{2\pi\gamma_{uni}}\right)^2\left(1+\left(\frac{2\pi f}{\gamma_b}\right)^2\right)}{\left[\frac{\gamma_a\gamma_b}{2\pi\gamma_{uni}}-(\gamma_a+\gamma_b)\frac{f^2}{2\pi}\right]^2+\left[\left[f_r^2+\frac{\gamma_a\gamma_b}{4\pi^2}\right]f-f^3\right]^2} \quad (14)$$

The $\gamma_{a,b}$ terms are the damping factors for sections a and b respectively. The damping factor γ_{uni} is determined by curve fitting the multi-section device while under uniform bias. The only other unknowns are the frequency term f and the resonant frequency term f_r [34]. Clearly the transfer function for the modulation response of the multi-section device is more complex than that of the single-section device, but additional analysis of the equation is required to determine what added benefits accompany this additional complexity. To make a valid comparison that is applicable to both devices, approximations are made to the multi-section transfer function.

In order to reach a comprehensible figure of merit for the modulation enhancement, the limiting cases for the modulation response equation are analyzed. This essentially compares a multi-section to a single-section laser. There are still further approximations that can be made including the device is operated at a high power and that the inverse carrier lifetime is small compared to the damping rate [34]. These approximations and Equations (15) and (16), reduce the ratio of the modulation response equations to a modulation enhancement factor, η, shown in Equation (17) [6].

$$\gamma_a = \frac{1}{\tau_a} + G'_{a0}P \quad (15)$$

$$\gamma_b = \frac{1}{\tau_b} + G'_{b0}P \quad (16)$$

$$\eta \approx \frac{\gamma_b G'_{a0}}{\gamma_a G'_{b0}} \tag{17}$$

This expression can be further simplified by stating that the laser is operating at a low bias, and therefore the spontaneous decay terms dominate Equations (15) and (16). Equation (17) is then reduced to Equation (18) where the enhancement factor is dependent on the differential gain and the carrier lifetime [6].

$$\eta \approx \frac{\tau_a G'_{a0}}{\tau_b G'_{b0}} \tag{18}$$

One final assumption can be made by saying that the laser is operating under a low photon density in which case $\tau_a = \tau_b$ [6]. This assumption leads to the most basic expression of the modulation enhancement factor displayed in Equation (19).

$$\eta \approx \frac{G'_{a0}}{G'_{b0}} \tag{19}$$

This equation analytically indicates that the two sections should be biased at points similar to those shown in Figure 23 (right). A very high differential gain in section a and a very low differential gain in section b will yield the highest modulation-enhancement factor. This figure of merit, while easily understood, has flaws stemming from the assumptions that led to this expression. Obviously there is no physical system that would allow a differential gain of near infinity in section a nor one near zero in section b.

Modulation enhancement tests have been reported using various biasing levels in two section quantum-dot lasers recently. An 8-dB modulation enhancement was achieved for a multi-section laser having a modulation section of 0.5 mm and a gain section of 1.0

mm and is shown in Figure 24 [8]. This device exhibits a flat frequency response up to 2 GHz and has a broad gain over the usable response range.

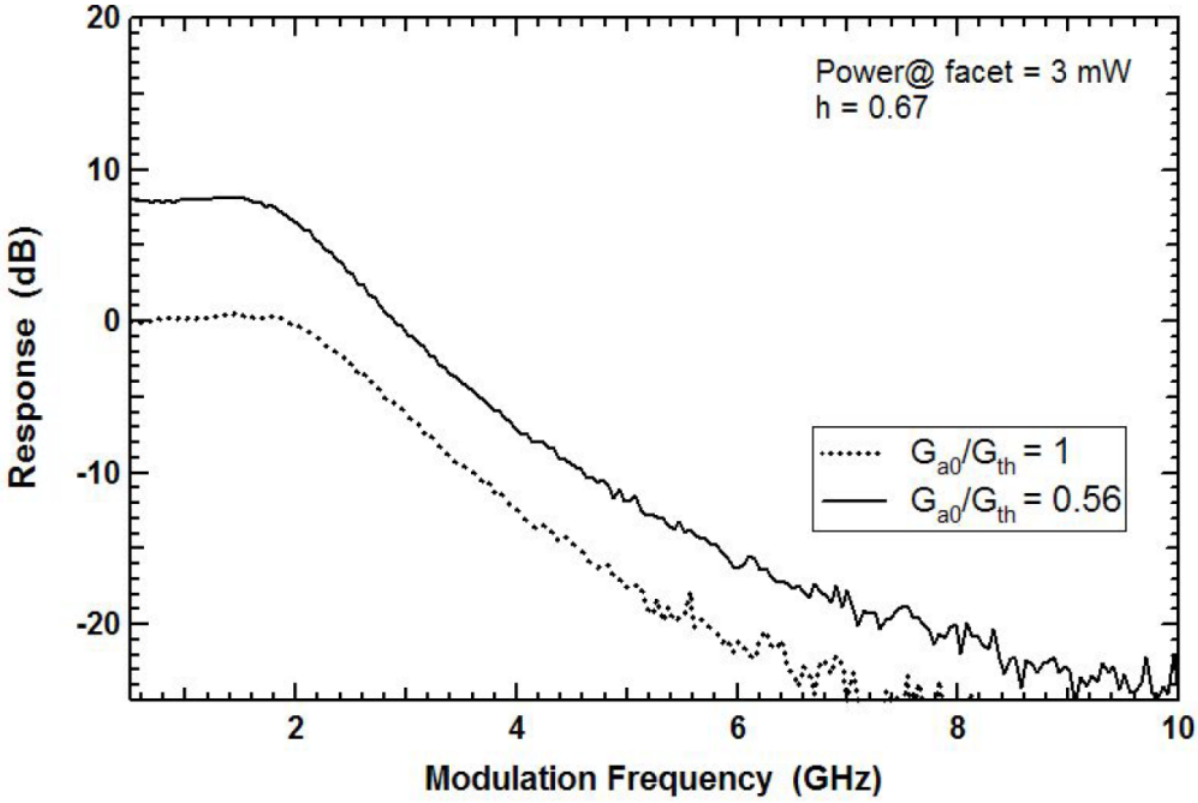

Figure 24: Modulation response of a multi-section device [8].

Another experiment performed by Li *et al.* improved upon previous results by reporting a 20-dB enhancement of the modulation response [50]. The results for a range of pumping values are shown in Figure 25. The 20-dB enhancement is shown in Figure 25 where sections *a* and *b* were biased at 0.6 and 84.7 mA, respectively; the 20-dB enhancement is measured in comparison to the laser under uniform bias conditions [34].

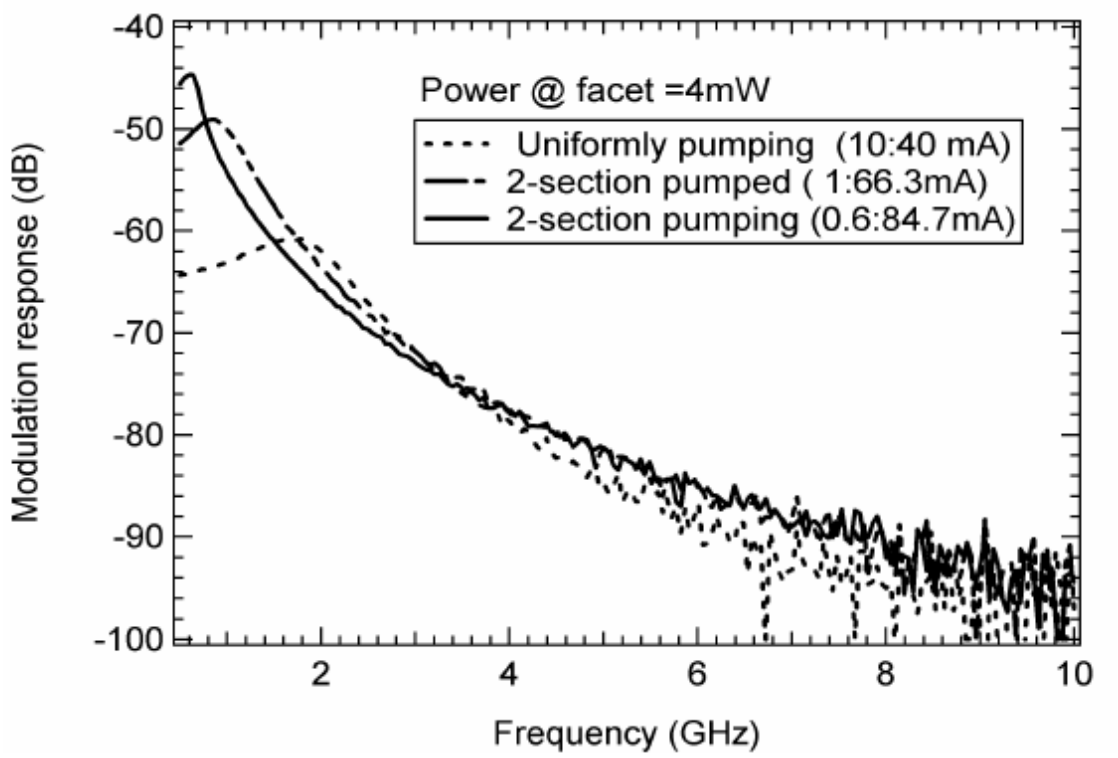

Figure 25: Modulation response for different pumping level in the two sections [34].

The uniform pumping case is used as a baseline for this measurement. The multi-section laser is biased at an equal current density in each section which allows the laser to act as a single section device.

The modulation response observed in Figure 25 shows a compromise between the 3-dB bandwidth and the modulation enhancement of the device. The uniform device has a much broader bandwidth than the asymmetrically pumped cases. If this laser were used as a transmitter in an optical communication system, it would have to be determined whether the extra gain was worth the loss of bandwidth. Perhaps a better tradeoff would be the uniform pumped case that is amplified 20 dB before transmission. There have been some advances in the bandwidth of the two-section lasers by utilizing different

architectures, such as varying the lengths of the two sections or using different biasing ratios. One research team showed an increase in the bandwidth of approximately 70% over the uniformly biased case [9]. A simple conclusion is that great care must be taken when deciding the fractional length h and the different biasing levels on the two sections when choosing a multi-section laser for an application.

2.2.5.1 Modulation Response of Long Cavity Lasers

There have been several research efforts aimed at capturing the modulation response in a transfer function that is derived from the rate equations [8], [9]. Unfortunately, these functions only hold for frequencies near the relaxation resonance frequency peak. No complete model exists that appropriately describes the physics of long-cavity laser devices where the free-spectral range of laser approaches the relaxation resonance frequency. The resonant peaks at the free-spectral range frequency in experimental data cannot be properly described by the familiar two-pole (single-section) or three-pole (multi-section) frequency response transfer function. The disadvantage of this convention is that it assumes fields to be uniform throughout the length of the laser cavity [52], [51], [53].

Early work on cavity effects of semiconductor lasers by Doerr utilized linearized differential equations to develop an analytical model that showed differing modulation response plots depending on whether the input or output side of the laser was modulated [52]. This phenomenon is illustrated along with his experimental results in Figure 26**.**

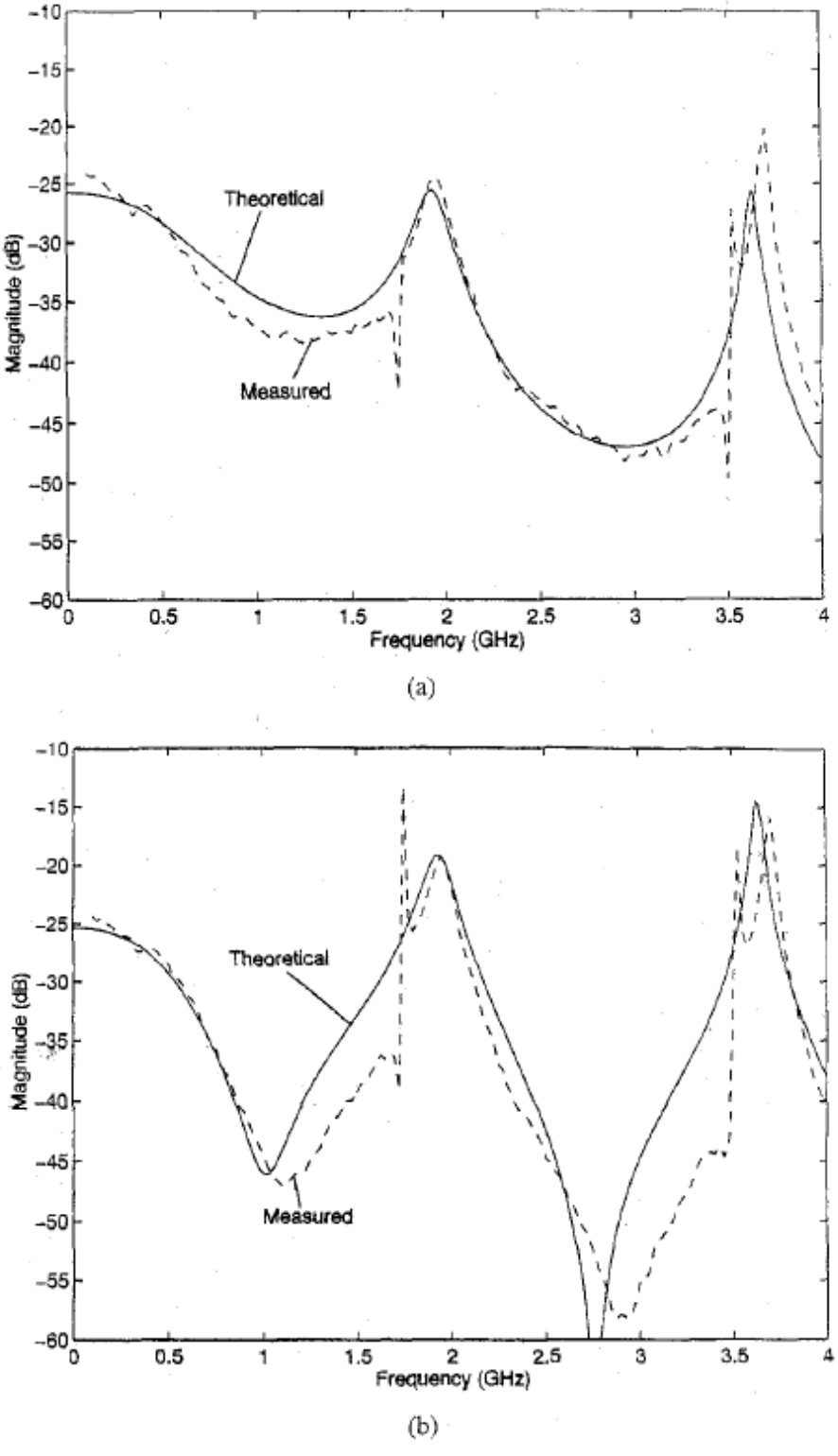

Figure 26: Comparison of the analytical and experimental modulation response for a long cavity laser [52].

The experimental and the analytical model shown in Figure 26 are matched rather well with one notable exception being the discontinuities that are near the resonant peaks. The author attributed this to coupling between the allowed modes of the laser and to the laser being in the mode-locked regime of operation [52]. Another prominent detail is the different responses obtained depending on whether the output side or input side of the laser is modulated. Specifically the nulls present in Figure 26(b) are related to the relationship between the modulation frequency and the cavity round-trip frequency. These nulls, that are not apparent in Figure 26(a), express a dependence on the placement of the modulation section within the system. If the cavity round-trip frequency is twice the modulation frequency, the modulation effect will "wash out" and the laser will not produce a modulated output at these frequencies. This is observed in Figure 26(b) at approximately 1 and 3 GHz [52].

This work was expanded upon, albeit using a more rigorous numerical model, by Usechak *et al.* [51]. This model utilizes the traveling intensity wave equations shown in Equations **(**20) and (21) that allow for the incorporation of spatial effects meaning that the intensity and carrier density of the device is allowed to vary in time, *t*, and position along the length of the cavity, *z* [51].

$$\pm\frac{\partial I^{\pm}(t,z)}{\partial z} = -\frac{1}{v}\frac{\partial I^{\pm}(t,z)}{\partial t} + \Gamma g(z)[N(t,z) - N(z)^{tr}]I^{\pm}(t,z) - \alpha(z)I^{\pm}(t,z) + \beta BN(t,z)^2 \quad (20)$$

$$\frac{\partial N(t,z)}{\partial t} = \frac{J(t,z)}{ed} - \frac{N(t,z)}{\tau(z)} - BN(t,z)^2 - vg(z)[N(t,z) - N(z)^{tr}][I^{+}(t,z) + I^{-}(t,z)] \quad (21)$$

These waves are allowed to travel in either direction along the length of the device ensuring that a self-consistent solution is found. This is particularly useful for

investigating multi-section devices with various geometries including the gain-lever effect, where sections differ in length and levels of biasing. In Figure 27 the modulation response of nine different configurations are shown.

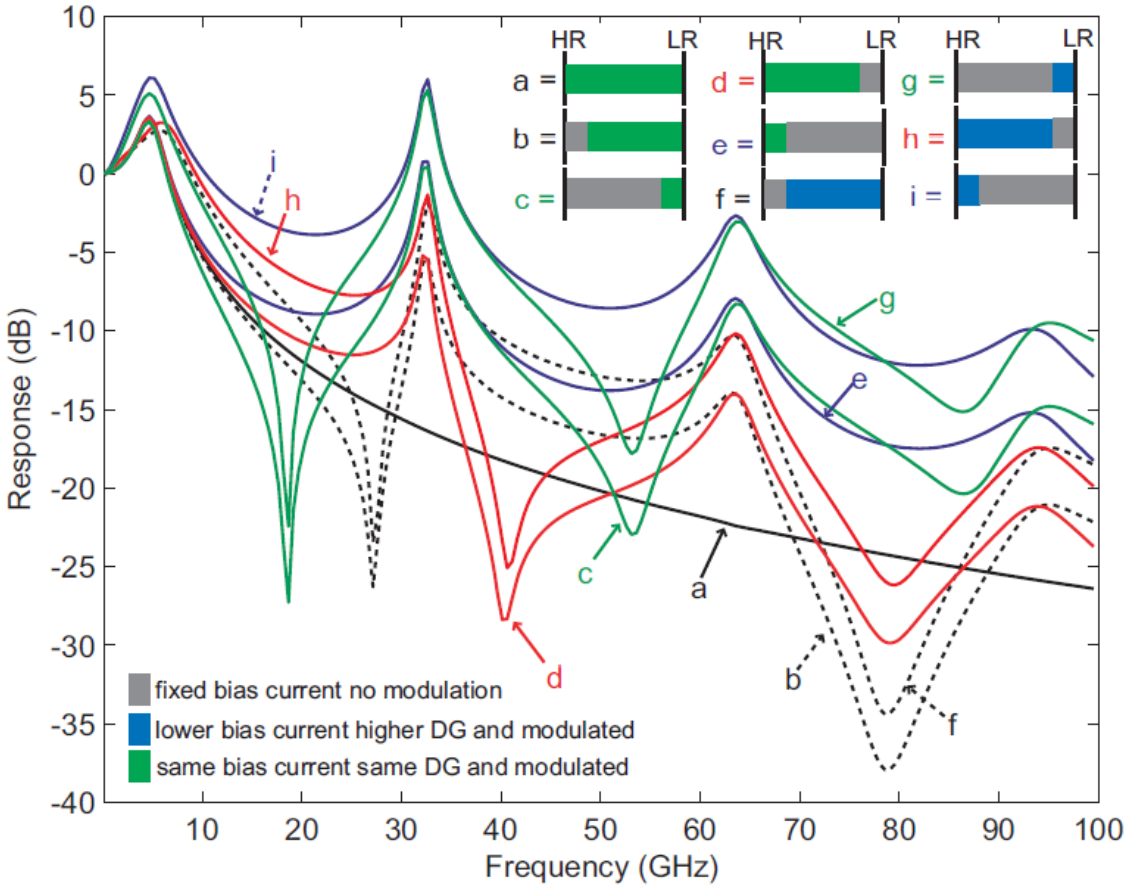

Figure 27: Device simulation of a two-section laser under various biasing and modulation schemes. HR and LR refer to high reflectivity and low reflectivity respectively, the exception to this convention is (a) where HR=LR (modified figure to include configuration information) [51].

The nine cases illustrated in Figure 27 are colored in grey, blue, and green. Grey represents DC bias only. Blue signifies a section that is modulated but is biased at a level lower than the unmodulated section (gain-lever effect). Finally, green sections are also modulated, but are biased at a current density equal to the unmodulated sections (uniform bias). All of the scenarios depicted, with the exception of (a), correlate to a multi-section

device. The configurations tested in (b, d, f, h) utilize a large modulation section, while (c, e, g, i) employs a small modulation section. The modulation sections are moved to different locations in the cavity and produce vastly different frequency responses. This figure provides an excellent representation of why the standard closed-form transfer functions are insufficient as they show no preference on the location of the modulation section.

These simulations show similar nulls in (c, g) to those reported by Doerr [52]. They were explained by Usechak *et al.* as a result of the photons traveling through the modulated section near the output while the section was modulated at a frequency equal to one half of the free-spectral range frequency [51]. The single section device illustrated in Figure 27(a) was the only simulation that did not display a peak at the free-spectral range of the laser. This was due to the laser having equal reflectivity on either side of the laser cavity and filtering out this effect [51]. It is important to note that in Figure 27, the modulation response is normalized and therefore the enhancement of the modulation efficiency is not observed.

The arctangent-like behavior that is observed by Doerr has also been reported to be present in the modulation response of external cavity lasers. This phenomenon is referred to as resonance-peak spectral splitting (RPSS) and takes place at the free-spectral range of the cavity and harmonic frequencies [54]. Premaratne *et al.* have developed models that demonstrate the interaction between current bias level and position/shape of the spectral splitting effect; these finding are illustrated in Figure 28. This behavior is thought to be due the coupling between the amplitude and phase in the active and passive resonant cavities in an external-cavity laser (ECL) [54]. While typical multi-section

devices and ECLs are different they share some commonalities. Both have active and passive sections. An ECL relies on a small active cavity and a large passive cavity while a multi-section laser may have several smaller passive sections between the active sections of the laser. It is plausible that the amplitude and phase dynamics that are responsible for the RPSS occurring in the external cavity are of similar origin to the complex response viewed by Doerr.

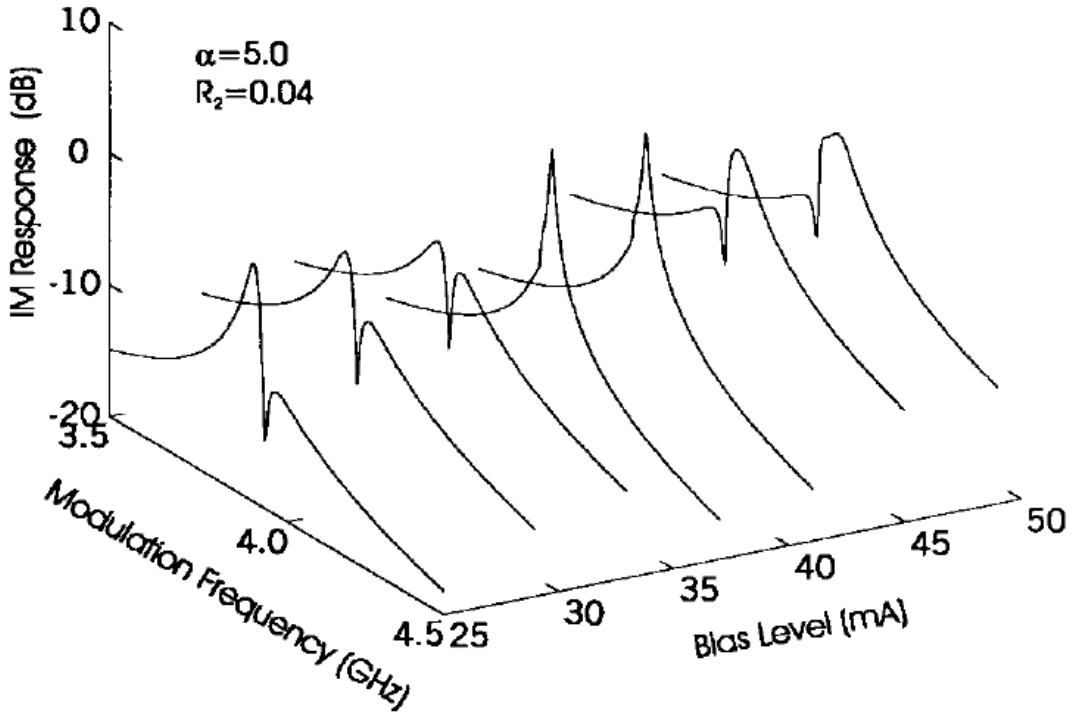

Figure 28: Variation in the resonant peak spectral splitting in a 4 GHz cavity over various bias levels [54].

2.3 Conclusion

Quantum-dot lasers show promise for use in optical communication systems because of their narrow gain profile and low threshold current. These attractive characteristics have motivated research to increase the modulation response of such devices. Characteristics such as mode locking have also been investigated with the intent

of creating laser-based frequency standards. Current research of the gain-lever effect has shown the potential for an increase in the bandwidth of the devices, while long-cavity lasers have been scrutinized to be able to better describe the physics taking place in the optical cavities. Laboratory experiments that are designed to characterize the laser's operating parameters, frequency response, and the gain-lever effect will be the focus of the methodology outlined in Chapter 3.

3. Methodology

This chapter outlines the procedures required to characterize the quantum-dot lasers under investigation in this work. Experiments were performed to determine various operational characteristics and how the gain-lever effect changes the overall modulation response of the device. This chapter begins by describing the quantum-dot laser being tested and then briefly discusses the relevant laboratory equipment used in our characterization/measurements. Preliminary preparation steps are presented before describing the tests performed. Finally, a modulation response simulation is introduced that will be utilized to process the acquired frequency response.

3.1 Multi-Section Quantum-Dot Laser

The device that is central to this research is a multi-section quantum-dot laser that was fabricated by Zia Laser at the University of New Mexico Center for High Technology Materials (UNM/CHTM) and later delivered to AFRL/RYDP for research studies. The laser was grown on an n-type GaAs substrate. The active region consists of six layers of self-assembled InAs quantum dots in InGaAs quantum wells. This constitutes a so-called DWELL, or dots-in-a-well, structure. Each of the six quantum well layers are separated by a 16-nm GaAs barrier. The active region is enclosed in a 20-nm GaAs layer. The upper and lower clad regions are 2.5-μm thick, and made of doped AlGaAs which was strained to improve the performance of the quantum-dot device. The device is capped with a 60-nm layer of GaAs. A four-micron-wide ridge waveguide was fabricated having a cavity length of 8.3 mm. The cavity length is divided into 17 separate sections, with 16 sections having a length of 0.5 mm, and the section nearest the output

having a length of 0.3 mm. These 17 sections are optically coupled, but electrically isolated. An illustration of the aforementioned layers is shown in Figure 29.

GaAs	Cap Layer	60 nm
$Al_{0.2\rightarrow0.0}GaAs$	Graded p-AlGaAs Layer	40 nm
$Al_{0.2}Ga_{0.8}As$	Upper Clad, Heavily p-Doped	1500 nm
$Al_{0.2}Ga_{0.8}As$	Upper Clad, Lightly p-Doped	1000 nm
$Al_{0.0\rightarrow0.2}GaAs$	Graded u-AlGaAs Layer	37 nm
GaAs	Upper Part of Waveguide	20 nm
GaAs	Barriers	16 nm 5X
InAs/InGaAs	DWELL Layers	7.6 nm 6X
GaAs	Lower Part of Waveguide	20 nm
$Al_{0.2\rightarrow0.0}GaAs$	Graded u-AlGaAs Layer	37 nm
$Al_{0.2}Ga_{0.8}As$	Lower Clad, Lightly n-Doped	1000 nm
$Al_{0.2}Ga_{0.8}As$	Lower Clad, Heavily n-Doped	1500 nm
$Al_{0.0\rightarrow0.2}GaAs$	Graded n-AlGaAs Layer	40 nm
GaAs	n-type Buffer	300 nm
GaAs	Substrate	

Figure 29: Layer structure of quantum-dot laser.

The 17 electrically isolated sections (depicted pictorially in Figure 30) allow for great flexibility in the configuration of the laser. Of the sections, only the one nearest the output lacks a contact pad for wire bonding. This is problematic for applying a DC bias to this 0.3-mm section which can only be accomplished by placing a DC probe directly on the laser. The repetitive nature of the rigorous laboratory testing and repeated probing could cause serious degradation and possibly even permanently damage the laser. Therefore, there were only select points during data collection that were used to determine how this section affected the output power, optical spectrum, mode-locking ability, and frequency response. Any appreciable dependence on the 0.3-mm section is

reported in Chapter 4. The majority of testing involved ignoring this non-wire bonded section by leaving it unbiased; the discussion of the 0.3-mm section is omitted when describing the wire bonding configurations used during testing.

Wire bonds can be added or removed to electrically connect or disconnect each of the electrically isolated sections, permitting the creation of multi-section lasers of varying lengths. The initial configuration consists of the 16 sections divided into three groups of contacts by wire bonding. The group nearest the output of the laser consists of five sections wire bonded together. The middle group has nine sections combined, while the remaining group has two sections. This configuration is depicted in Figure 30. The two front groups are shorted together using the DC probes shown. The device is then biased with the front 14 sections accounting for the majority of the gain of the device, while the last two sections are biased near transparency producing a large differential gain when modulation is applied.

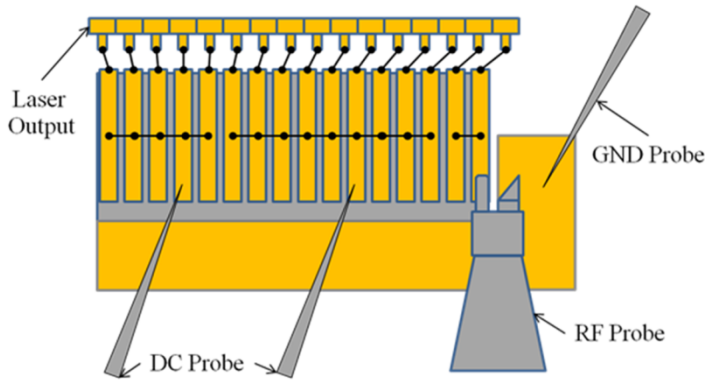

Figure 30: Initial configuration of multi-section quantum-dot device.

This configuration is altered in subsequent tests. The first alteration utilized two additional wire bonds to connect all 16 segments of the laser together, in essence creating a single section laser. In this configuration the RF probe provides both the DC bias and

the modulating signal. This structure was created to act as a baseline for frequency response measurements to verify quantitatively the improvement that a multi-section gain-levered laser produces. This contact arrangement is illustrated by Figure 31.

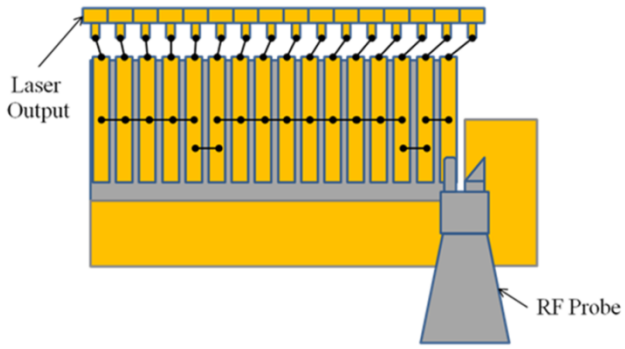

Figure 31: Multi-section device wire bonded as a single section laser.

Once comprehensive testing on the single-section configuration is completed, the wire bond connecting the section furthest from the output is removed. This creates an alternate configuration where 15 of the sections remain wire bonded together, leaving one section separated. This extreme gain-to-modulation section ratio is illustrated in Figure 32.

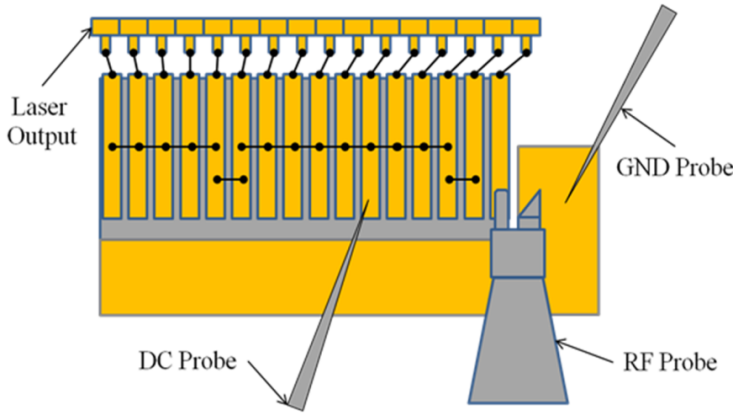

Figure 32: Multi-section laser having a gain section of 7.5 mm and a modulation section of 0.5 mm.

3.2 Laboratory Equipment Introduction

There are several pieces of equipment that are utilized during laboratory testing. Each item serves a specific purpose in the characterization of the quantum-dot laser and they are introduced below.

3.2.1 Laser Diode Controller

The DC biasing of the laser's sections is controlled by using Stanford Research Systems model LDC501 laser diode controllers. In addition, the laser diode controller monitors and adjusts the temperature of the laser using a thermistor and thermoelectric cooler, respectively.

3.2.2 Bias Tee

The bias tee acts as an isolator between the network analyzer and the laser diode controller. Different models were used in this work depending on the frequency range under test. This device blocks any DC component that may be present from entering the network analyzer and passes the AC component only. Indeed, the AC component is combined with the DC biasing from the laser diode controller to create the modulation signal.

3.2.3 Photodetector

The photodetector is a device that converts the optical laser signal to an electrical signal. The specific photodetector used in this work was a New Focus model 1414 having a 3-dB bandwidth of 25 GHz. The photodetector has the ability to measure a modulated

optical signal that is below the 25-GHz limit; the oscillations of the optical carrier are ignored because the frequency of approximately 200 THz is far too high to be detected.

3.2.4 Network Analyzer

The Agilent E8361C PNA microwave network analyzer was used as both a receiver and a transmitter in these experiments and was the primary means of collecting frequency response data. The network analyzer generates an AC signal that is output through port 1, combined with the DC biasing at the bias tee, and applied to the modulation section of the laser. The signal is fed back to port 2 through the photodetector. At port 2, the network analyzer compares the returned signal to the originating one to determine the modulation response of the laser. These comparisons generate the modulation response plots displayed on the screen known as "S_{21} curves."

To ensure accurate data are being obtained, the network analyzer must be calibrated. Calibration was performed by using the Agilent N4694 E-Cal module and following the on-screen prompts. The calibration minimizes measurement errors by remedying accuracy drift caused by changing environmental factors. Additionally, the calibration corrects for the frequency response of any associated connectors and additional cables that are used to perform the calibration. To achieve the most accurate calibration, the network analyzer is calibrated using the same setup as when actual measurements are made. This negates any of the unintended and unwanted effects that the setup may have on the data collection.

3.2.5 Electrical Spectrum Analyzer

The Agilent E4448A electrical spectrum analyzer was used to measure harmonics and resonant frequencies that are present in the laser cavity. A photodectector must be used to convert the optical signal to an electrical one before analyzing the electrical spectrum. This piece of equipment is primarily used to measure power level, frequencies, and harmonics of mode-locked pulses.

3.2.6 Optical Spectrum Analyzer

The Yokogawa AQ6370 optical spectrum analyzer provides a visual representation of the fundamental optical frequency of the quantum-dot device. This enables straightforward analysis of the power level, wavelength, and shaping of the optical spectra.

3.2.7 Optical Power Meter

The Newport model 1830-C optical power meter measures the average power present in an optical fiber. The power meter is used extensively in the aligning of the laser with the lensed fiber and determining operating characteristics of the device.

3.2.8 DC Power Supply

The Hewlett Packard E3620A DC power supply is used to apply a leveled reverse bias when performing mode-locking experiments. The power supply is capable of producing ±25 V with 1 A driving current.

3.3 Preparation for Testing

Laser output parameters are temperature dependent, therefore stable operation of the laser can only be guaranteed by monitoring and controlling the temperature of the device. To accomplish this, the laser is mounted to a copper block that contains a sensor called a thermistor. This thermistor changes resistance based on the temperature of the copper block as it rises and falls during laser operation. A thermoelectric cooler is used to maintain a constant temperature. An external piece of laboratory equipment, the laser diode controller, monitors the thermistor measurements and adjusts the thermoelectric cooler accordingly.

The quantum-dot device under test is an unpackaged laser bar, which requires several steps first be taken in order to operate the laser. First the probes must be connected with the aid of a bench-mounted microscope. Both DC and small-pitch high-frequency RF probes are used to apply signals to the laser. Next, a laser diode controller is used to control the temperature of the device and provide the DC to the laser sections. At this point the laser is operating, but the output is not connected to the fiber optics. A lensed fiber is mounted on a micrometer-operated stand that is carefully moved into position in front of the laser; this can be viewed in Figure 33.

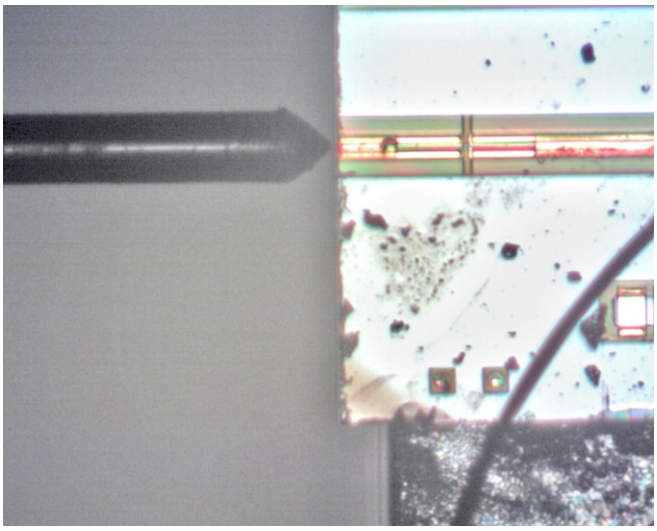

Figure 33: View of the laser output properly coupled into the lensed fiber.

The proper alignment of the fiber is fine tuned by connecting the other end of the fiber to an optical power meter and monitoring the power. Optimal alignment is achieved when the power coupled into the fiber is maximized. Therefore, the fiber is moved in all three dimensions to maximize the power as displayed on the power meter.

3.4 Laboratory Testing

Various tests are performed to properly characterize the multi-section quantum-dot laser. To determine general operating parameters the device's power output and the optical spectrum are first measured. Next the laser's optical output is passed into a high-speed photodetector and the output electrical signal is monitored on an electrical spectrum analyzer; this allows for the determination and characterization of, the mode-locking properties of the device if applicable. The modulation response testing is the final test performed. The results gained from this modulation response test show how the laser responds to modulation.

3.4.1 Optical Power Output

When characterizing a laser diode, one of the first steps is to determine how the device operates in response to an applied direct current. Figure 34 illustrates how the laser diode controller and an optical power meter are connected to perform this test. The laser diode controller is used to regulate the temperature of the laser since laser output power is directly related to the temperature. Furthermore the laser diode controller is connected to the quantum-dot laser through the use of DC probes. A uniform direct current is applied across the length of the device; this results in the laser producing an output that is coupled through a lensed fiber that is connected to the optical power meter. The power meter uses a photodetector to determine the power output of the laser. The measurements are used to create a curve that is useful in determining operating characteristics such as the threshold current.

Three parameters directly affect the measured power output: how well the laser is coupled to the fiber (coupling efficiency), the level of bias current applied to the laser, and laser temperature. The DC bias current parameter is the only parameter varied during this test. The coupling of the laser to the fiber needs to be consistent so the measured power is the same during subsequent tests. A known output power for a correlated input current is used as a reference to minimize this effect. The position of the lensed fiber is adjusted until the power meter indicates the known output value for the corresponding input current thereby allowing repeatable power measurements.

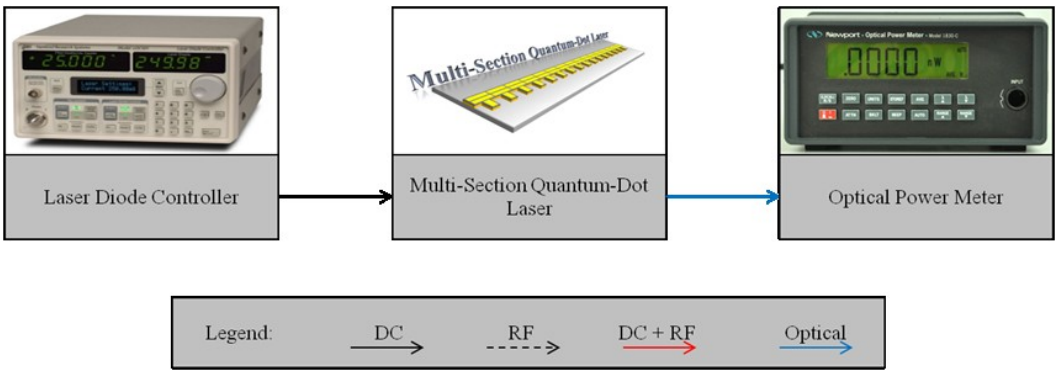

Figure 34: Test setup for measuring the output power versus input current.

3.4.2 Optical Spectrum Analysis

The optical spectrum of the quantum-dot device under test must be investigated to gain insight on the physical characteristics of the dots that are grown in the quantum wells. The setup for this experiment is shown in Figure 35. The laser diode controller is connected to the laser through the use of DC probes and set to apply various levels of current to the laser. The laser output is coupled to the lensed fiber and is connected directly to the optical spectrum analyzer. The operating wavelength and the supported modes of the laser can be viewed directly.

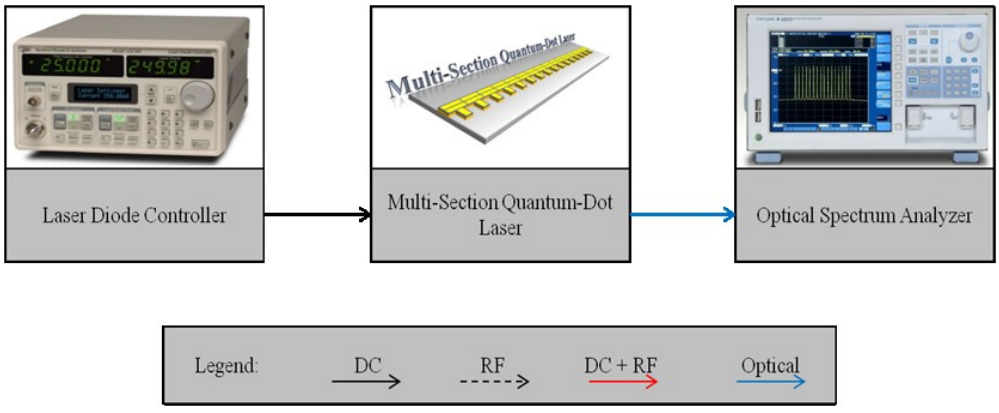

Figure 35: Setup to measure the optical spectrum of the quantum-dot laser.

3.4.3 Mode Locking

Lasers of certain construction have the ability to mode-lock under particular conditions. To examine the laser's mode-locking capability the laser was tested as presented in Figure 36. There are several variations of mode-locking that have been investigated in literature. This experiment focuses on two modes of passive mode-locking.

3.4.3.1 Passive Mode Locking as a Multi-Section Device

To test the passive mode-locking characteristics, the laser was connected exactly as shown in Figure 36. The laser diode controller was connected through DC probes to the first 15 of the 16 sections of the device. The power supply was connected to provide a negative voltage to the remaining electrically isolated section of the device. The laser diode controller was set to a constant DC bias while the power supply applied a reverse bias voltage. The optical spectrum analyzer connects to the output of the laser through a lensed fiber. The output was also coupled into a photodetector which converts the optical pulses into an electrical signal whose spectrum can then be viewed on the electrical spectrum analyzer.

3.4.3.2 Passive Mode Locking as a Single-Section Device

The laser was also tested to ascertain if mode-locking as a single-section device was possible. The equipment was setup as in Figure 36 except that the power supply was eliminated. All sections of the laser were connected to the laser diode controller through DC probes. The sections were biased with equal current density, therefore the laser is assumed to act as a single-section device. The optical spectrum and electrical spectrum were viewed on their respective analyzers at various biasing levels.

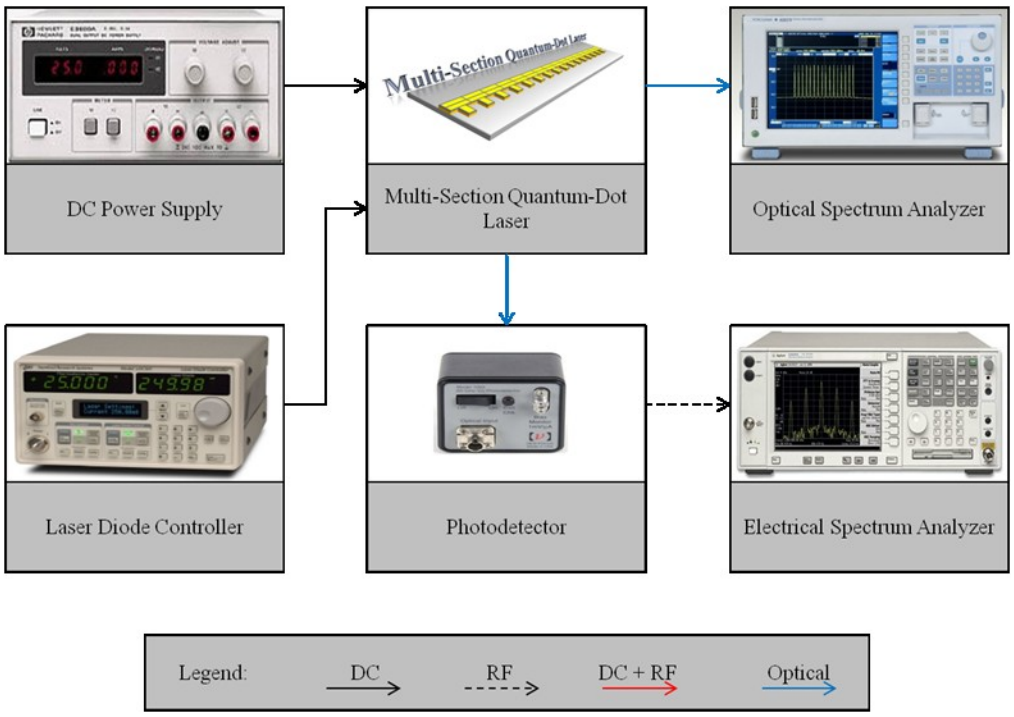

Figure 36: Laboratory setup for testing mode-locking.

3.4.4 Modulation Response

Another important characteristic of a laser is its modulation response. This experiment was performed with three different arrangements of the laser: first as multi-section devices (as pictorially represented in Figure 30 and Figure 32) then later as a single-section laser (as in Figure 31).

3.4.4.1 Multi-Section Modulation Response

The modulation response of the multi-section quantum-dot laser was tested using the equipment configuration shown in Figure 37. There are two laser diode controllers that are used during this experiment. One was connected directly to the laser through DC probes and applies a bias to the gain section of the laser. The second laser diode controller applies a small DC current to the bias tee where it was combined with the RF signal from port 1 of the network analyzer. This combined DC + RF signal was applied to

the modulation section of the laser through an RF probe. The output was optically coupled into the photodectector before reaching port 2 and the network analyzer generating a S_{21} plot.

The gain-lever effect was tested by varying the DC biasing levels of the two sections of the laser while the network analyzer swept the frequency from the designated starting and stopping points. The frequency response was dependent on the biasing levels that were chosen for each section. To approach this problem systematically, the span of the frequency response, the network analyzer power level, and the biasing of the gain section of the laser were held at a constant level. The biasing of the gain section was set to a level well above the current threshold value for the device. The biasing of the modulation section of the laser was slowly incremented from zero to a value that equals the current density of the gain section. For each increment an S_{21} curve was recorded and saved as raw data for later processing.

3.4.4.2 Single Section Modulation Response

In order to make a determination as to what improvement was gained in the frequency response by the gain-lever effect the laser was configured as a single-section device by wire bonding all of the sections together. This experiment uses the same equipment as the gain-lever test with the exception that there was only one laser diode controller needed. A uniform bias was applied to all the sections of the device through the bias tee and RF probe. Numerous biasing levels were tested and their S_{21} plots were recorded on the network analyzer.

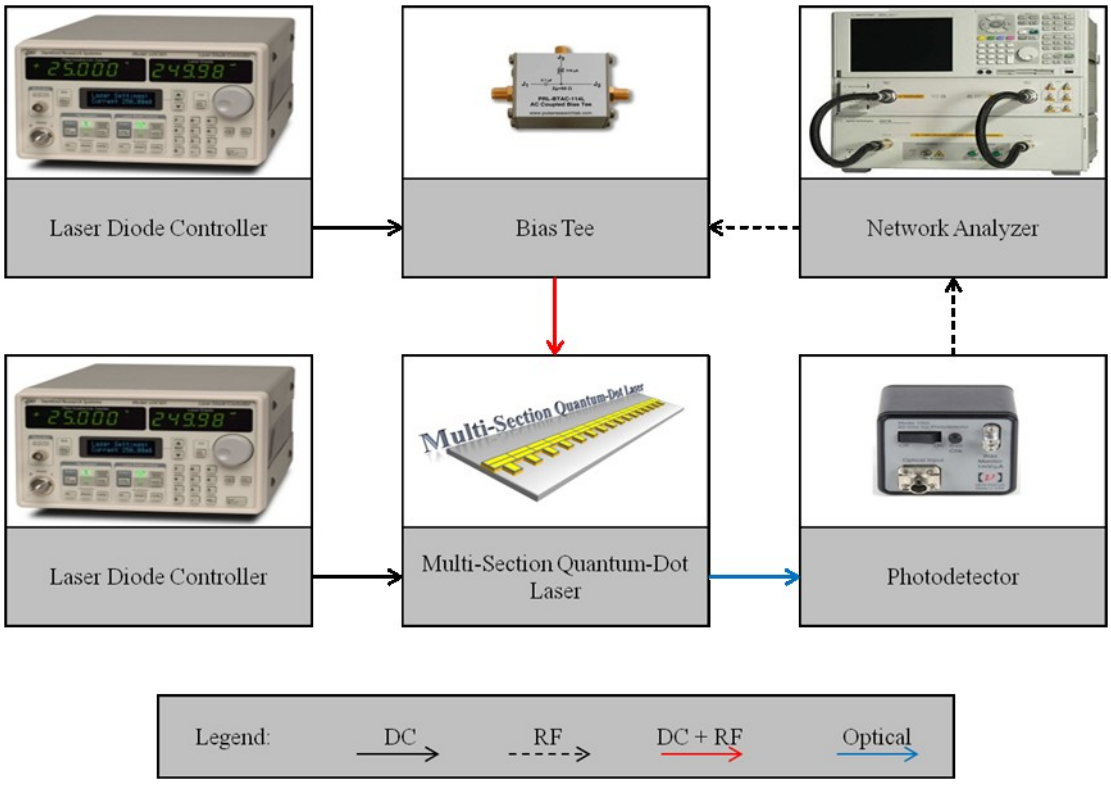

Figure 37: Modulation response equipment setup.

3.5 Modulation Response Simulation

The raw data were imported into the program and plotted as a frequency response. This process was repeated for several data files and showed the impact of the biasing level of the modulation section on the overall frequency response of the laser.

The experimentally recorded data was also compared to the analytical modulation response equation. The correlation between the two demonstrates the validity of the experiments and permits fine tuning of the parameters in the analytical modulation response model. Curve fitting was used to determine various lifetimes and rates that were unknown for this laser. The parameters that were extracted from the experimental data aided in the characterization of this unique quantum-dot device.

3.6 Conclusion

Using the aforementioned experimental processes and laboratory equipment, this chapter focused on the method of characterizing the unique long-cavity multi-section quantum-dot laser. The objective of this was to gain insight into the physics that governs the output properties of the laser cavity. Various operating parameters were measured and the data obtained are analyzed in the proceeding chapter. Data acquired from these experiments is utilized in Chapter 4 to achieve an improved understanding of the behavior of the device.

4. Analysis and Results

This chapter presents the results and analysis of the laboratory experiments described in Chapter 3. It begins by reporting the operating parameters, such as the optical power output of the laser, and the operating wavelength. This chapter then proceeds by analyzing how the optical spectrum behaves under various operating conditions. Next the dynamic response of the laser is analyzed by reporting the results of the mode-locking experiments, before presenting the results of the modulation response and the gain-lever effect tests.

4.1 Results of Optical Power Output Experiment

The first step to determining the operating parameters for a laser is to ascertain the threshold current and operating wavelength of the device. The results in Figure 38 were obtained by utilizing the equipment configurations shown in Figure 34 for threshold current, and Figure 35 to determine the wavelength of the device. The laser diode controller was swept from 0 to 300 mA.

The operating wavelength was determined to be 1234 nm from the optical spectrum plot shown in the inset of Figure 38. To determine the current threshold a linear fit (blue line) is applied to the data and the x-intercept is found. The current threshold for this 8.3-mm quantum-dot device when 16 sections were biased was 52 mA (162 A/cm^2) and 46 mA (138.6 A/cm^2) when all 17 sections were equally biased. This result is used to determine the proper biasing points for the laser which is an important parameter in subsequent tests. Additionally, this graph allows the laser to be coupled to the lensed fiber at a known point each time the laser is configured for a new test. This device

exhibits the expected behavior for a laser diode. This near-linear trend would continue until the ground state saturated, at this point a kink would be formed in the data which is an indication that the excited state begins lasing as the dominant mode. At very high current bias levels the output power would begin to decline due to thermal effects.

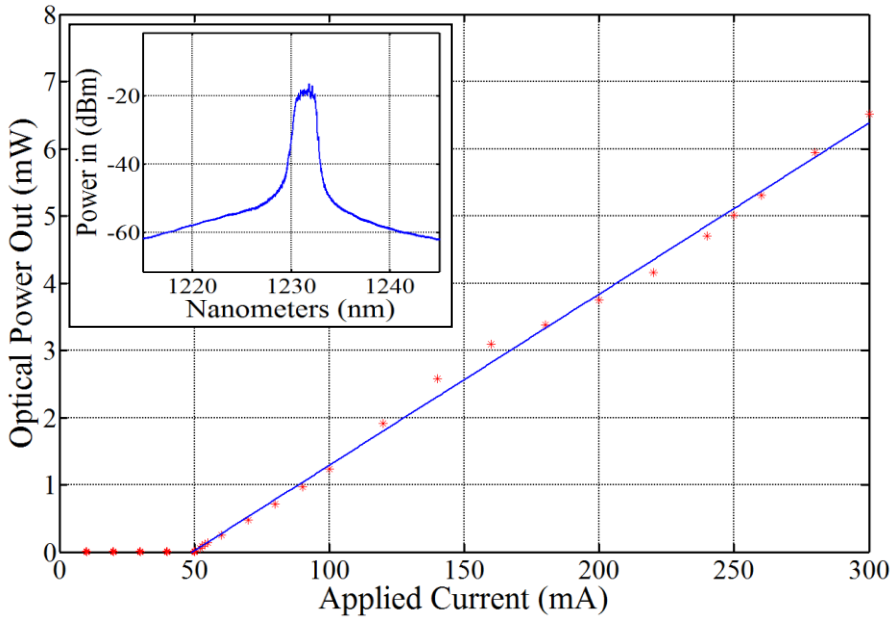

Figure 38: Optical power measurements (red data points) and associated linear fit (blue line); the optical spectrum is also shown (inset).

The external differential quantum efficiency (η_d) is derived from the slope of the optical power output above threshold. It is a measure of how efficient the laser is in transferring injected current into output power and is shown in Equation (22), where $\frac{\Delta P}{\Delta I}$ is the slope of the linear fit and q, λ, h, c are the fundamental charge, the operating wavelength of the laser, Planck's constant, and the speed of light respectively. The factor of 2 is added because of the symmetry of the cleaved cavity reflectivity.

$$\eta_d = 2\frac{\Delta P}{\Delta I}\left[\frac{q\lambda}{hc}\right] \tag{22}$$

When discussing efficiency, the highest possible value is the most desired, but in this case it is rather low. Performing the calculation results in an η_d of 4.966%. A comparable 2-mm quantum-dot device yielded an η_d of 30% [55]. This low value of 4.966% is presumably because this measurement is highly dependent on the coupling of the fiber to the laser and the confinement factor of the laser. The use of an integrating sphere would improve the coupling efficiency and improved this value. Moreover, the efficiency is generally reduced as cavity length is increased [17].

4.2 Results of the Optical Spectrum Analysis

The optical spectrum of the laser was measured using the configuration shown in Figure 35. The laser diode controller was swept in 5 mA increments from 50 to 500 mA. The results from the 91 optical spectra were appended together to create the surface plot shown in Figure 39. This figure utilizes a color map that corresponds to the optical power of the signal. Once above threshold the laser produces a single peak until the input current reaches approximately 140 mA. Above this point another peak begins to rise out of the noise floor as the laser begins to lase from another state. Initially this was thought to be an emission from an excited state, but after further inspection it was noted that the distance between the optical pulses ($\Delta\lambda$) is too narrow for that to be the case. An excited state should be expected at a location ~200 nm lower than the fundamental mode corresponding to the bandgap of either the wetting layer or quantum well, while these pulses are ~15 nm lower. As the bias current is increased further, the optical pulse centered at 1234 nm begins to form a dip that increases in depth until there is complete separation creating a third peak at a biasing of 425 mA. The separation continues to

increase until the culmination of the experiment where three well-defined spectral features remain at an input current level of 500 mA. One possible explanation for these features is that the laser is passively mode locked. This deduction is made because the optical spectrum is similar to Figure 17 where pulses are formed near the fundamental wavelength of the laser when dual frequency mode locking occurs. As the laser begins to mode lock the original optical pulse is widened; this behavior is observed in the experimental data collected during the course of this work and is illustrated in Figure 39.

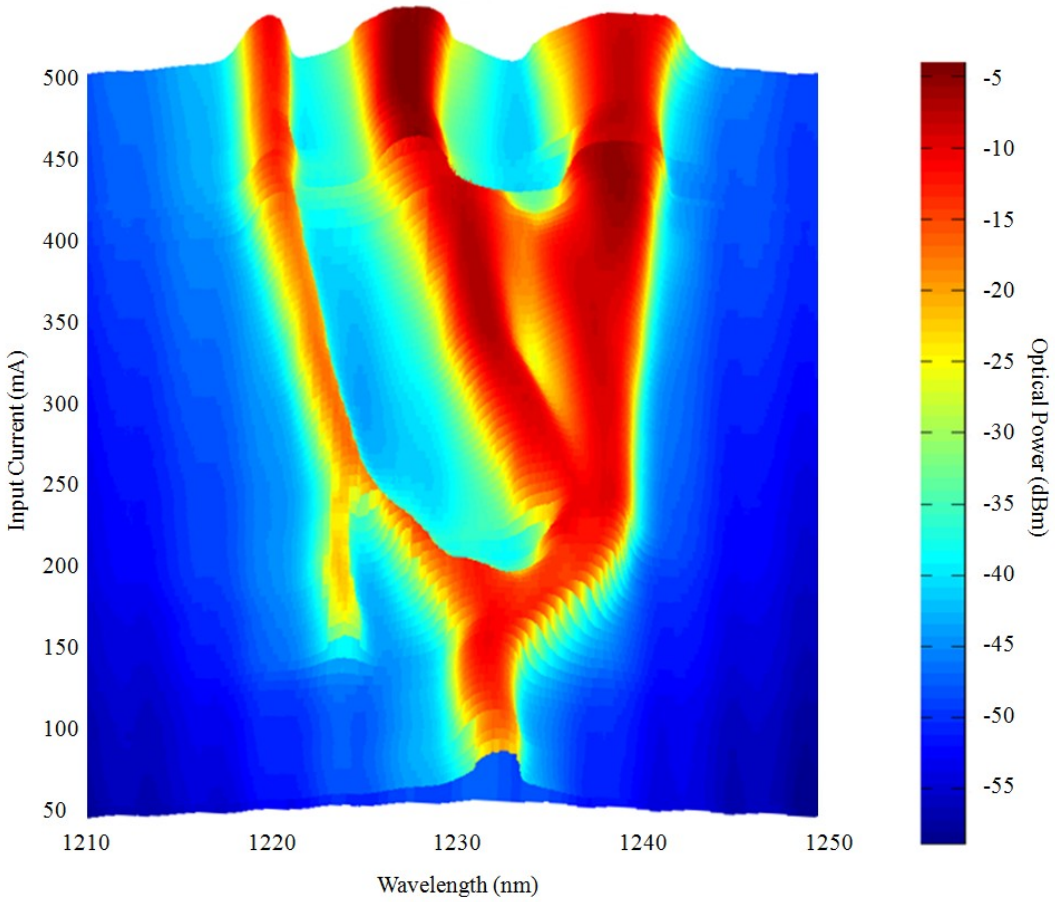

Figure 39: Optical spectrum surface plot over a range of bias currents.

A more familiar view of the optical spectrum results are shown in Figure 40. This plot shows a cross section of Figure 39 at key points in the biasing sweep. At 100 mA

there is a well-defined single pulse present. At a bias current of 150 mA there is a distinct second peak near 1222 nm. This spectral feature continues to blueshift as biasing is increased to 500 mA. The fundamental spectral feature widens at bias levels above 150 mA until a dip forms to create the third individual feature that is observed. As stated earlier, this separation continues throughout the remainder of the sweep.

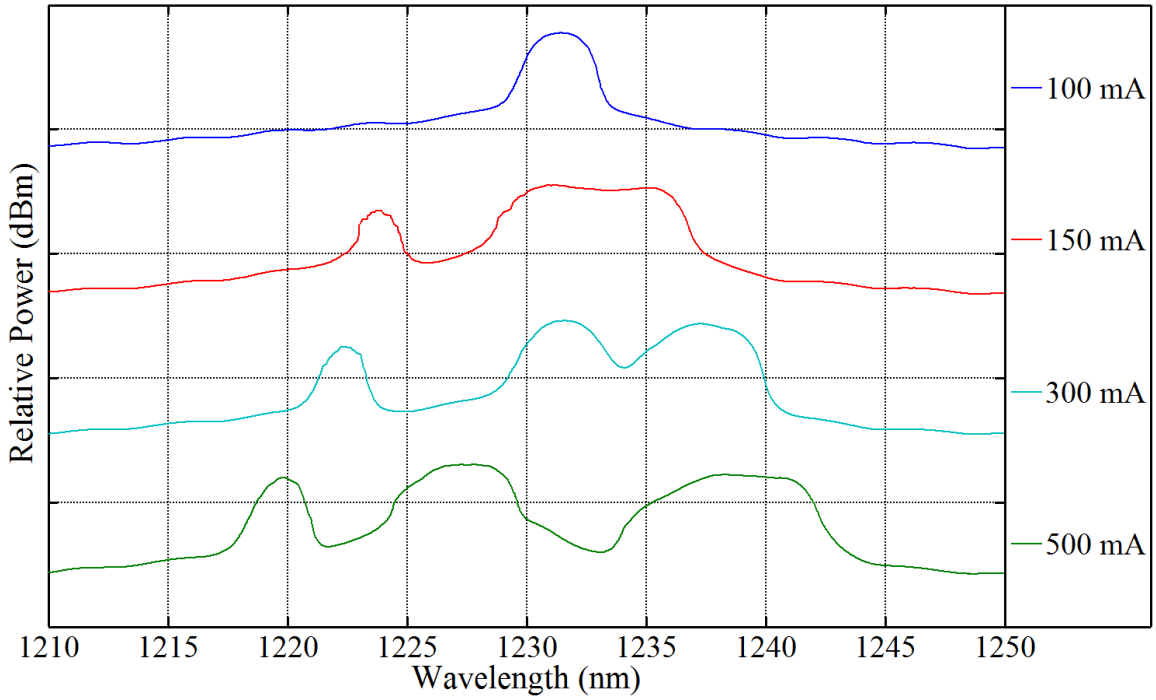

Figure 40: Optical spectrum at key points in the sweep of the bias current.

The span was increased on the optical spectrum analyzer to include lower wavelengths as shown in Figure 41 which illustrates the spectrum with bias currents of 100 and 200 mA applied. This plot displays the presence of an additional spectral feature near 1020 nm which is blueshifted by approximately 210 nm from the fundamental mode. This is most likely attributed to gain saturation where the laser emits from an excited state, and is similar to the results reported by Lester *et al.* that are illustrated in Figure 13 [17].

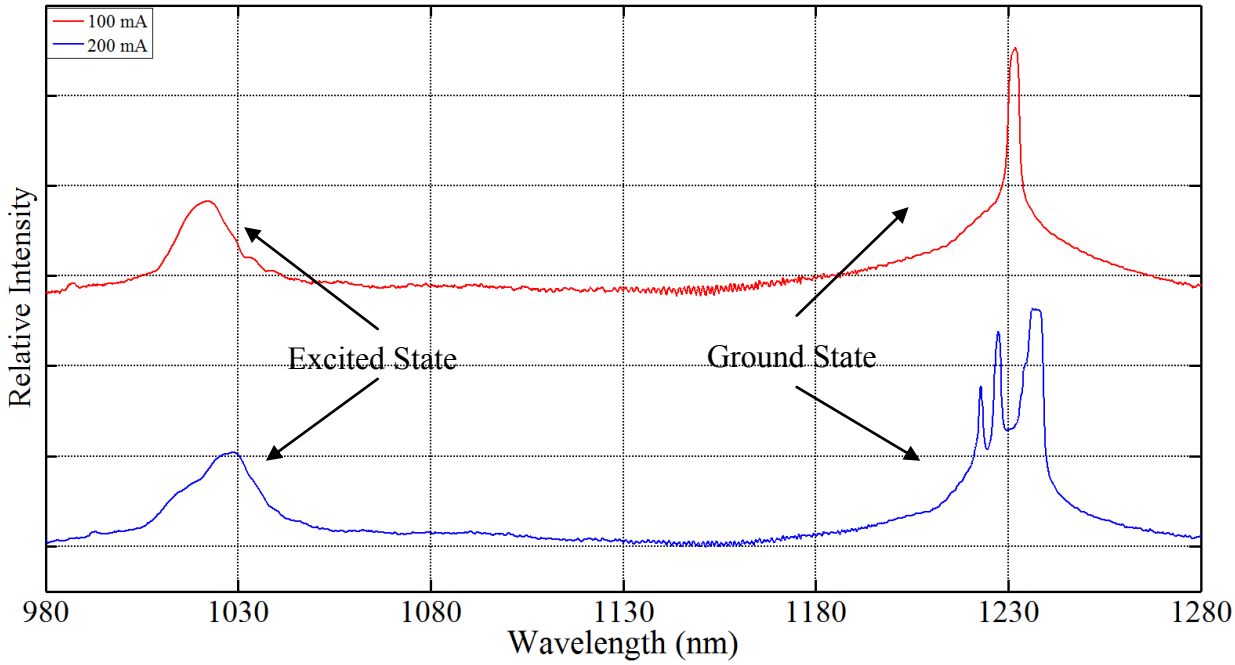

Figure 41: Broad optical spectrum measurement.

4.3 Results of Mode-Locking Experiments

The next phase of testing was directed at examining the laser's mode-locking characteristics. Both passive mode-locking mechanisms were systematically explored.

4.3.1 Passive Mode Locking as a Multi-Section Device

The laser and supporting test equipment was connected in accordance with Figure 36. The laser was in the configuration illustrated in Figure 32 with 15 sections wire bonded together while the last section remained independent. A DC voltage source was configured to reverse bias the last section to create an appropriate saturable absorber. The experiment was completed by adjusting the power supply in 37 increments from 0 to -4.5 volts and recording the electrical spectrum centered about the free-spectral range. Immediately it was clear by examining the recorded data that the laser possessed the ability to produce an RF signal at the predicted free-spectral range frequency. Figure 42

was created by combining all of the information in a single plot and illustrates how the saturable absorber enhances the 5 GHz signal.

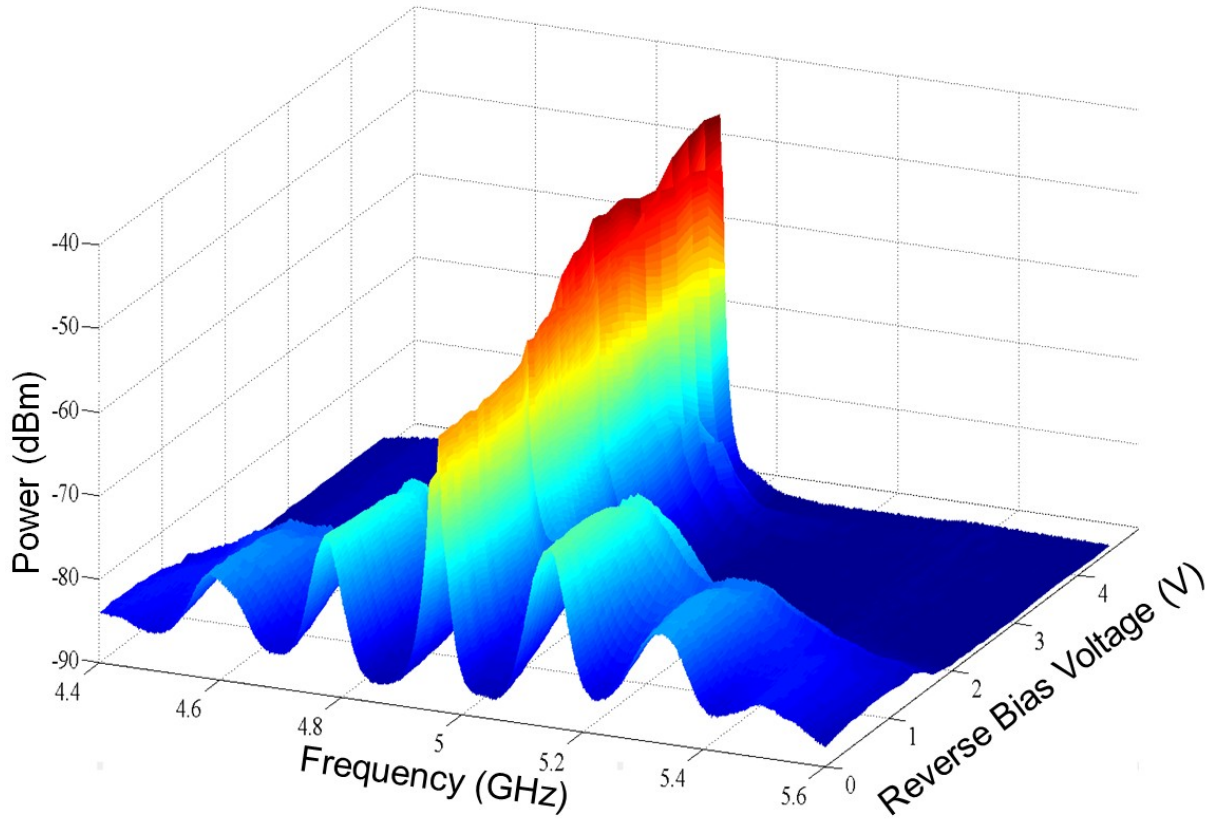

Figure 42: Variation in the electrical spectrum as the reverse bias voltage is increased.

A common figure of merit for how well a mode-locked laser is performing is the RF linewidth measured 3-dB below the peak of the spectrum. The trend in Figure 42 shows that the RF spectrum narrows as the reverse bias is applied. The highest reverse bias tested (-4.5 volts) was used to determine the best achievable linewidth for the passive mode-locking scenario. Reverse bias levels below -4.5 volts were not tested to prevent possible damage to the device. With -4.5 volts applied to the last section of the laser the electrical spectrum analyzer was monitored while applying increasing levels of

DC bias to the 15 sections that provide the gain in the mode-locking configuration. The input current was swept from 100 – 200 mA in 10-mA steps. The lineshape and linewidth varied during the test, with no discernible pattern. The lowest linewidth was measured with an applied bias of 110 mA. The spectrum for that configuration is illustrated in Figure 43. The linewidth was measured by calculating the width of the spectrum at -3 dBc. The linewidth for this particular stimulus was 34.4 kHz. It is theorized that a longer saturable absorber section or increased reverse bias could have aided in the further reduction of this parameter.

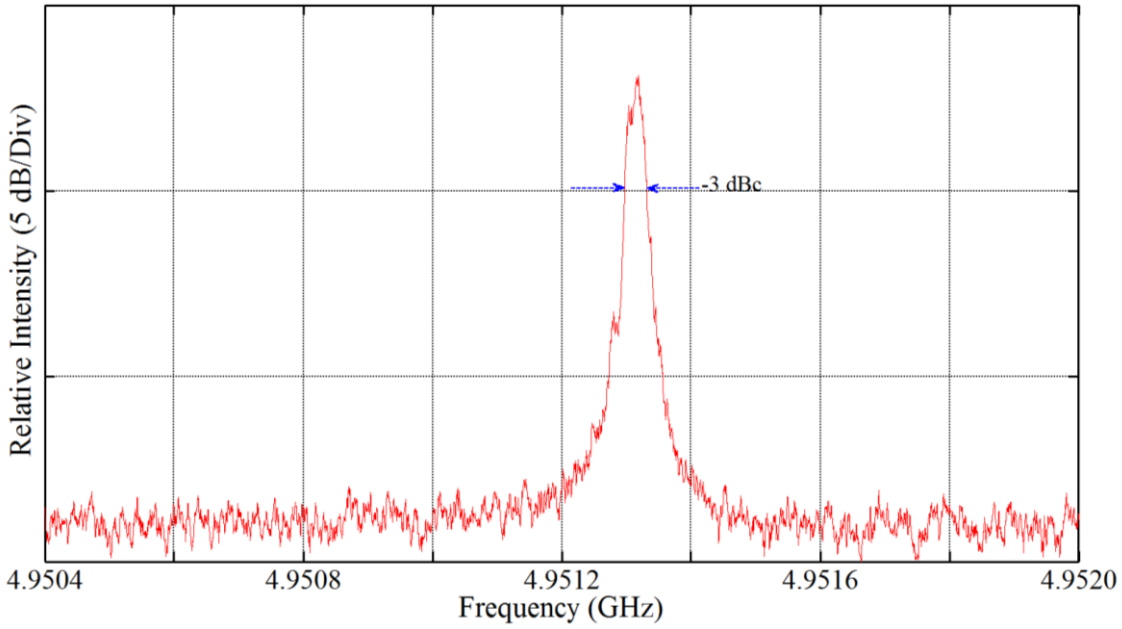

Figure 43: Passive mode-locked RF spectrum exhibiting a 34.4 kHz linewidth with -4.5 volts applied to the saturable absorber and 110 mA applied to the gain section.

4.3.2 Passive Mode Locking as a Single-Section Device

Due to observations made while measuring the modulation response of the laser in the single-section configuration, the laser was studied in more detail. This was performed while all 16 sections of the laser were biased, as shown in Figure 31. In this

configuration there is not a reverse biased section to act as a saturable absorber and therefore promote passive mode-locking. The test equipment required to perform this experiment is shown in Figure 36, minus the power supply. Interest in this anomalous mode-locking is warranted due to its simple configuration, given that only a stable DC bias current is necessary to produce a microwave frequency tone. The laser was biased from its current threshold in increments of 5 mA to a maximum of 500 mA. The linewidth was measured as described previously at the -3 dBc point. A minimum linewidth of 56.28 kHz occurred at a bias level of 110 mA. The spectrum for this measurement is illustrated in Figure 44.

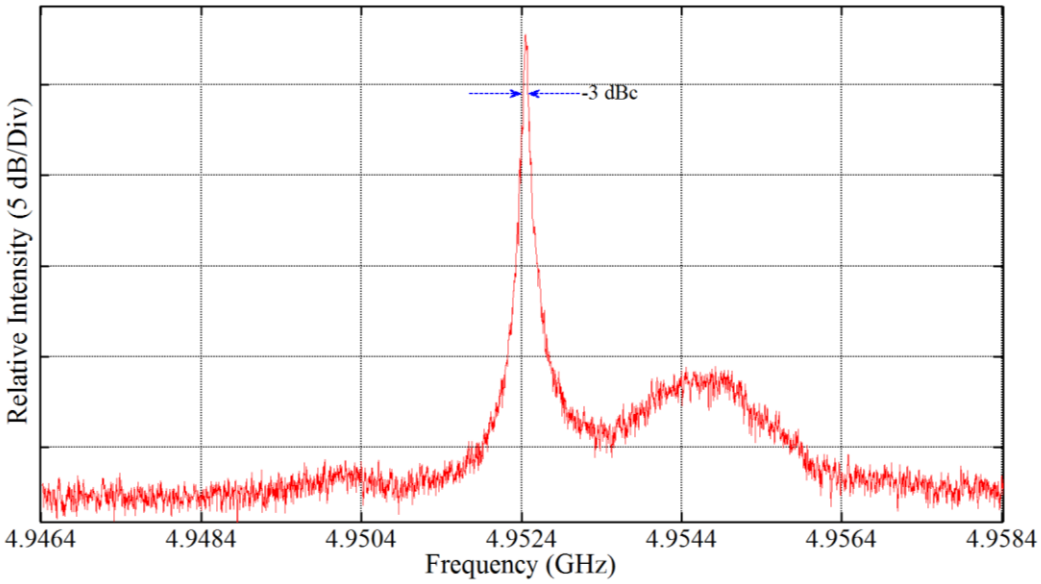

Figure 44: RF spectrum for the single section configuration exhibiting self mode-locking with a bias of 110 mA.

This measured linewidth is almost twice what was observed for the multi-section mode-locking scenario which employed the reverse biased section. This is expected as passive mode-locking with a reverse biased saturable absorber has typically exhibited very low linewidths. Another item worth noting is the shape of the spectrum. The multi-

section mode-locked device displayed a RF spectrum that could be accurately curve fit with a Lorentzian function while this spectrum displayed a pronounced 5-dB swelling near 4.9544 GHz. Moreover, this was not an isolated irregularity. The RF spectrum varied wildly throughout the current sweep. The lack of stability in the produced RF spectrum suggests that there is a chaotic nature to the formation of the pulses inside of the laser cavity. Figure 45 emphasizes this point by displaying how the spectrum shifts and changes shape as a function of bias current. Numerically a fluctuation of ± 2.67 MHz in the frequency peaks, and ± 6 dBm changes in intensity are observed when adjusting the bias by 60 mA.

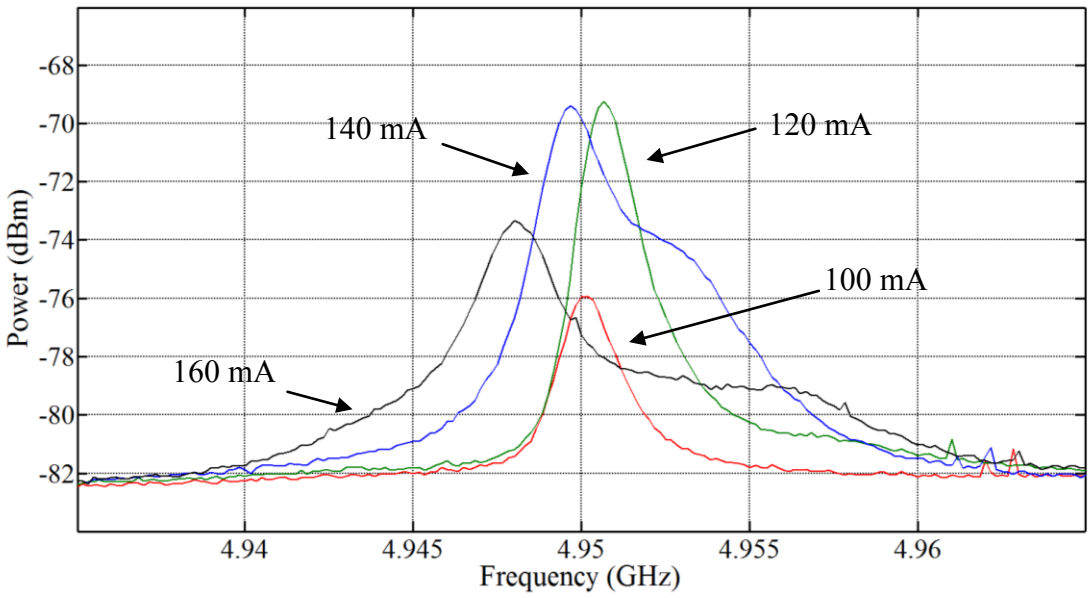

Figure 45: RF spectrum of a single section self mode-locked laser under various biasing levels.

To investigate this further an additional input current bias sweep was performed from 160–500 mA and the peaks of the spectrum were recorded. The result of this experiment is displayed in Figure 46.

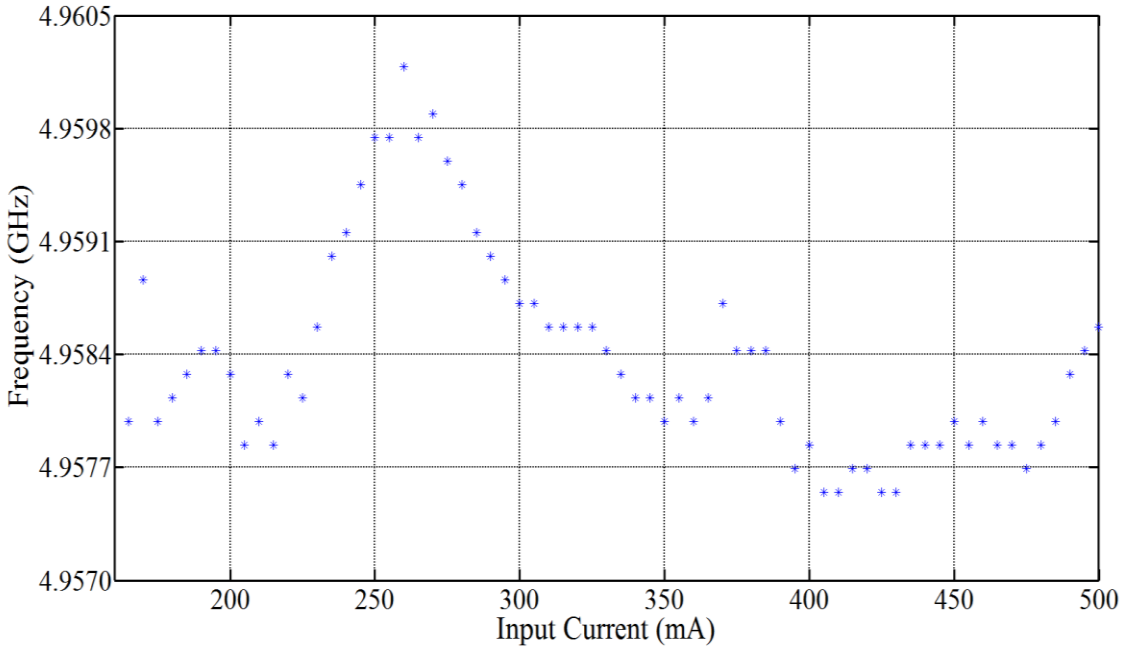

Figure 46: Fundamental frequency variance as operating current is altered.

This figure confirms the initial suspicions that the main mode-locked carrier frequency does indeed continue to shift with various currents applied. One item to note is that over different ranges (310–325 mA and 435–445 mA) the laser appears to produce a constant RF tone. After additional inspection of the data, some of the adjacent points had identical frequency values (exact to 1 μHz). This anomaly is most likely an artifact of the measurements made in the laboratory. Had the spectrum analyzer been set to a lower resolution bandwidth, the points would show a difference between them. This is only a minute observation that does not invalidate the general trend observed in Figure 46.

As stated earlier, the data collection process included carefully biasing the 0.3 mm section periodically to determine the effect it had on the experiments. It was concluded that having this section unbiased only altered the threshold current and the spectrum. Previously it was presented how the change in current bias affected the RF spectrum;

Figure 47 illustrates that the RF spectrum does change with the additional section, even though it is biased with the same current density. Before the experiment took place it was expected that the unbiased 0.3 mm section in the cavity would act as a saturable absorber and create a narrower RF spectrum; however, after performing the test the opposite was found. This leads one to conclude that the 0.3-mm section is not responsible for causing the mode-locking to occur.

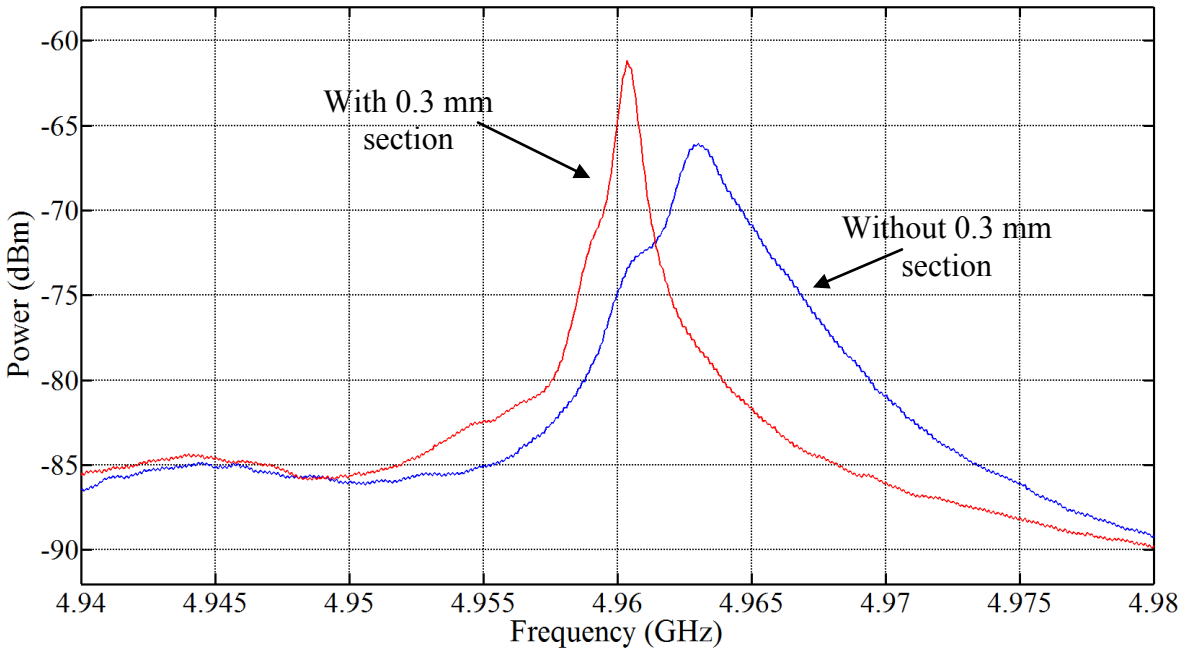

Figure 47: Self mode-locking with 0.3 mm section biased (red), and without biasing (blue).

4.4 Frequency Response

The gain-lever effect was tested in two different configurations, first the 14:2 gain-to-modulation ratio illustrated in Figure 30, and then the device was reconfigured with a 15:1 ratio, as shown in Figure 32, and the process was repeated. Additionally, the laser was wire bonded as a single-section device, Figure 31, and the frequency response was measured as a baseline performance parameter. The two main metrics that were

studied when analyzing the frequency response were the 3-dB bandwidth and the modulation enhancement. Additionally, there were other effects observed in testing that were unique to this device and a discussion on this is presented at the end of this chapter.

4.4.1 3-dB Bandwidth

The results in Figure 48 illustrate the gain-lever effect and how it has the potential to increase the 3-dB bandwidth. The 14:2 configuration has a 3-dB bandwidth of 6.3 GHz, while the 15:1 and single-section configurations have bandwidths of 3.3 GHz and 2.2 GHz respectively. The modulation response data for each configuration was normalized to 0 dB in order to make accurate comparisons between each S_{21} curve.

It is worth noting that the long-cavity of this laser plays an important role on the achieved 6.3 GHz bandwidth. The peak of the free-spectral range frequency located near 5 GHz effectively revitalizes the fading frequency response by way of the cavity resonance allowing higher bandwidths to be realized. One observation made from this data is that the modulation section of 0.5 mm performed worse than the 1.0 mm modulation section. There are two possible explanations for this behavior. One conclusion is that the 0.5-mm section is too short to have enough modulation strength to affect the entirety of the laser cavity effectively. Another feasible explanation is that the RF signal power is saturating the small section even though the DC bias is very low, just above threshold current density. Regardless of the true cause of the behavior, it suggests that there is an ideal/optimal modulation section length for the gain-lever effect. It also implies that some of the approximations used in deriving multi-section transfer functions

(e.g. that the modulation section can be considered infinitely small) do not hold for this quantum-dot device.

At this point it is necessary to discuss behavior of this device at frequencies that extend past the 3-dB bandwidth. This S_{21} curve varies considerably from most gain-levered multi-section quantum-dot lasers that are reported in literature [8], [9], [50] that exhibit typical low pass filter type behavior. The long cavity and associated spatial effects within the cavity, and the numerical proximity of the resonance frequency and free-spectral range of the laser are probable explanations of this deviation from conventional modulation response curves.

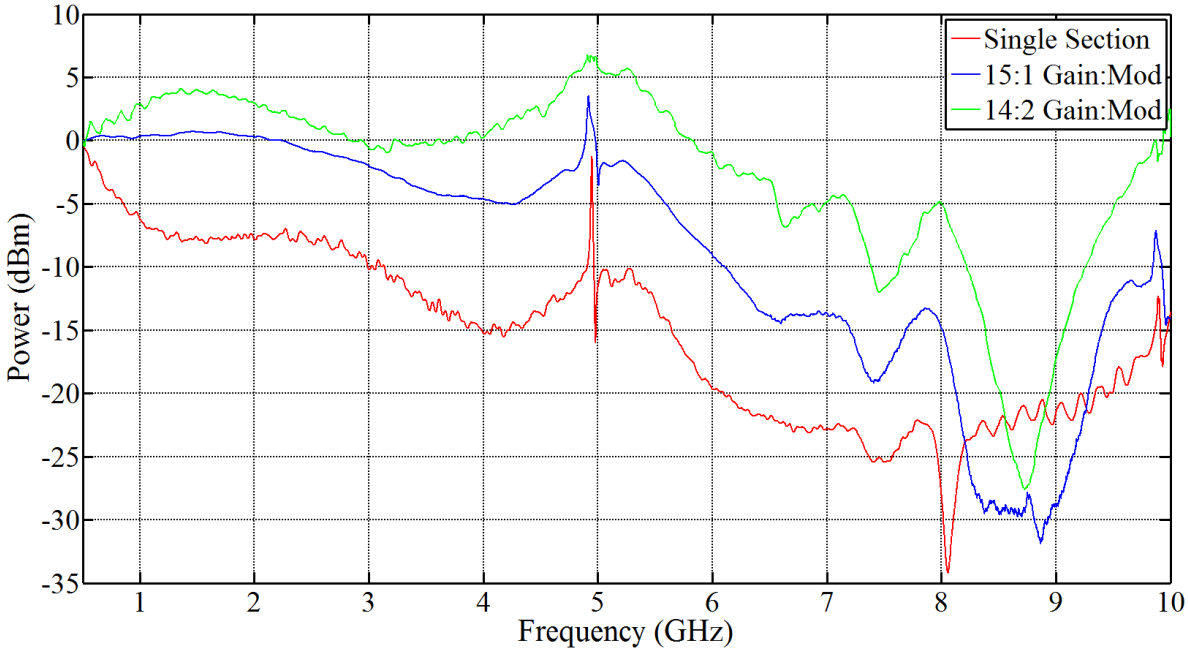

Figure 48: The gain-lever effect on the 3-dB bandwidth of the modulation response.

4.4.2 Modulation Enhancement

The modulation enhancement measurements were performed utilizing the 15:1 gain-to-modulation section configuration (Figure 32). The intent of this laboratory test

was to determine the modulation response for varied gain-to-modulation section bias current ratio. The results, in the form of S_{21} curves, are plotted in Figure 49. As expected, the least responsive (lowest modulation efficiency) case was observed under uniform bias conditions. This case describes all 16 sections of the device being biased at the same current density, 500 A/cm^2, while only one section was RF modulated.

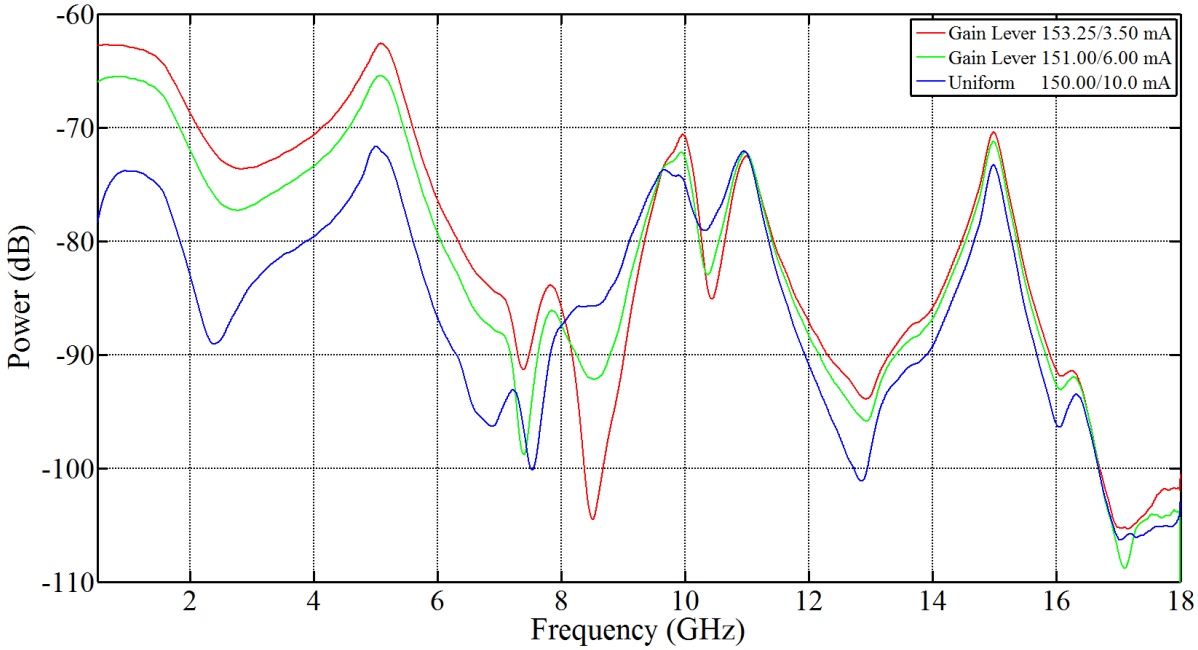

Figure 49: The gain-lever effect and its influences on modulation enhancement.

As predicted by the gain curve for a multi-section quantum-dot active region, shown in Figure 23, the uniform bias configuration is not the most efficient way to modulate a quantum-dot laser. The laser produces 3.2 mW of output power while being biased uniformly. In subsequent current bias configurations, the DC bias of the modulation section was reduced to increase the differential gain of the section, while the gain section DC bias was increased to keep the output power at a constant 3.2 mW. The most dramatic increase was near 500 MHz for the case where the gain section is biased at

153.23 mA and the modulation section is biased at 3.50 mA where a modulation enhancement of greater than 16 dB was measured. This level of enhancement is not constant throughout the frequency range, but there is an appreciable increase in the modulation response from 500 MHz to ~8 GHz. The results tabulated in Table 1 show that as the ratio of the current densities between the gain and modulation sections is increased, the modulation enhancement also increases.

Table 1: Current density ratio vs. modulation enhancement in gain-lever effect.

$Power\ (dBm)$	I_{gain} (mA)	J_{gain} $(\mathrm{A/cm^2})$	I_{mod} (mA)	J_{mod} $(\mathrm{A/cm^2})$	$Modulation\ Enhancement$	$\frac{J_{gain}}{J_{mod}}$
-78.44	150.00	500.00	10.00	500.00	0.00 dB	1.00
-65.99	151.00	503.33	6.00	300.00	12.45 dB	1.68
-62.79	153.25	510.83	3.50	175.00	15.65 dB	2.92

The general trend shown in Figure 49, and Table 1, leads one to assume that by continuing to reduce the DC bias in the modulation section that this increase in efficiency will continue to grow, but this is not the case. As the bias in the modulation section is reduced to below the transparency current density the overall amplitude of the modulation response begins to drop substantially, this is displayed in Figure 50 where the modulation section current was reduced from 9 mA to 0 mA. The efficiency is increased in the reduction from 9 mA to 3 mA, near the transparency current for the modulation section. As the bias is reduced further the efficiency suffers as in Figure 50(c, d). The results illustrated in Figure 49 represent the best case scenario in utilizing the gain-lever effect to increase modulation enhancement.

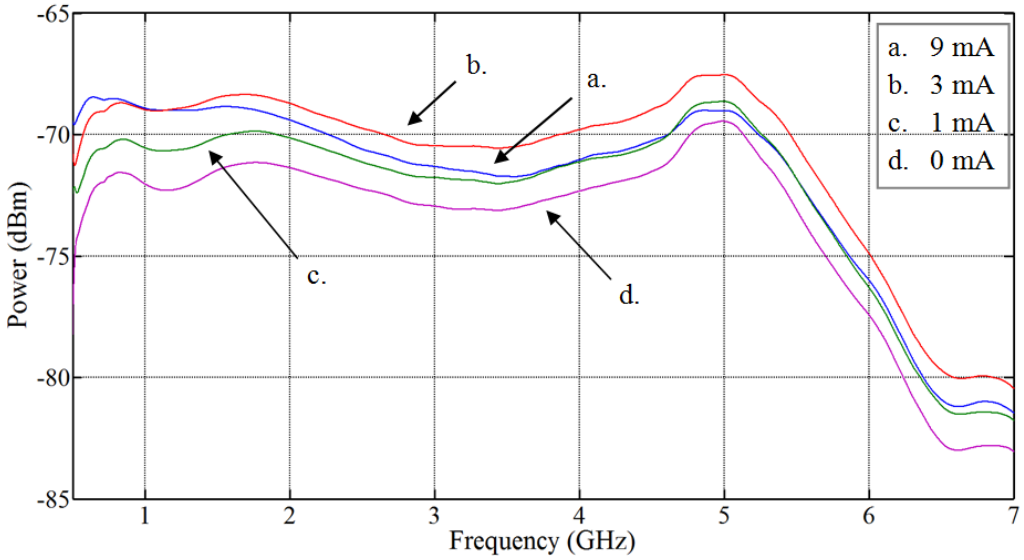

Figure 50: Modulation efficiency as bias in the modulation section is varied.

These results would be significant if this laser were implemented in an optical communication system where the enhanced modulation efficiency would increase the modulation depth of the amplitude modulated optical carrier and therefore simplify the detection/demodulation of the received signal. The most compelling conclusion from this experimental investigation is an improvement to the modulation response is achieved by varying the DC bias points on a single device. In essence, the modulation transfer characteristics of a given laser are enhanced by biasing it in a two-section fashion. From an integration perspective, it would take little more than the addition of a current divider to provide separate bias points for the sections. This integration could be easily integrated into laser packaging to create a better performing device.

4.4.3 Extracting Operational Parameters

The acquired frequency response is used to extract key laser operating parameters. One common method that is employed when experimenting with multi-section lasers is to

apply a uniform bias and curve-fit the response data to the single-section modulation response transfer function, shown in Equation (9). This device was wire bonded as a single section laser and biased from 100 mA to 300 mA in 50 mA increments and the frequency response was recorded. This data was curve-fit to the modulation response transfer function by utilizing a least-squares algorithm to determine the laser's resonance frequency and relaxation rate. These extracted parameters values are illustrated in Figure 51. A linear fit is applied to the parameters to determine the inverse carrier lifetime, the y-intercept of the linear fit.

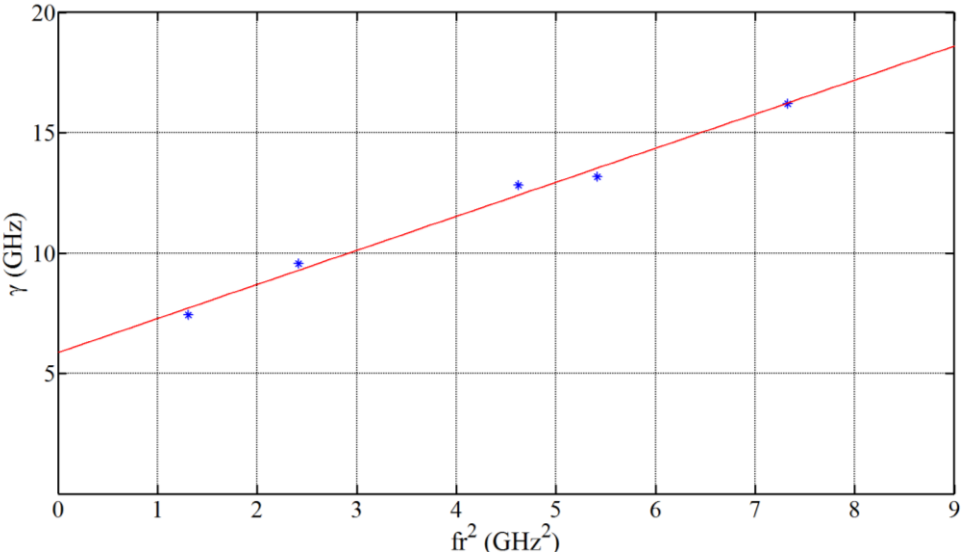

Figure 51: Resonant frequencies and relaxation rate determined by curve-fitting.

When dealing with a short-cavity laser the natural progression would be to use these discovered parameters in a two-section modulation response transfer function such as Equation (14) to create a simulation to determine optimum bias points. In a long-cavity device however, this approach does not to capture the spatial effects imparted on the frequency response data. Moreover, when this device was wire bonded as a single-section

laser, it was still not accurately modeled by Equation (9). This is demonstrated by Figure 52 which compares the measured response (red) and the approximated curve-fit (blue).

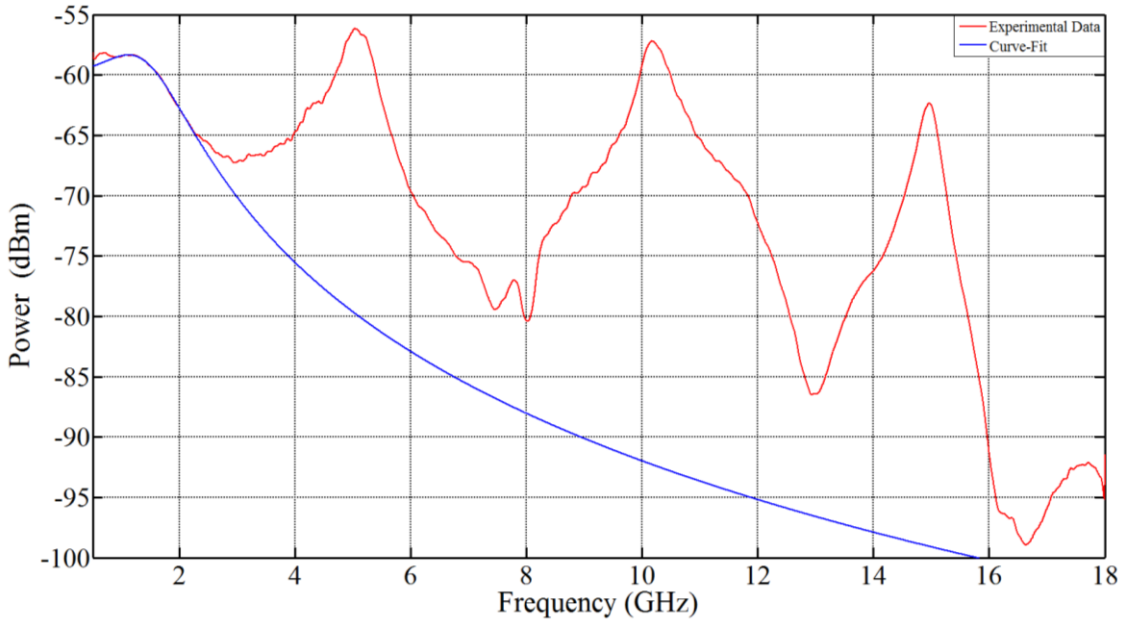

Figure 52: The disparity between the conventional modulation transfer function for the single section laser and acquired laboratory data.

The curve-fit is valid for a very select portion of the response, while the actual data has substantial peaks and nulls that highlight the additional dynamic behavior that is taking place inside the laser cavity. It is clear that the simplistic transfer function is inadequately equipped to handle this behavior. As discussed earlier, the simulation presented by Usechak *et al.* has the ability to account for some of the observed cavity effects, such as the resonant peaks observed in the multi-section frequency response plots [51]; however, the resonant peaks were observed in both the single-section and multi-section device. It is evident that this phenomenon was not demonstrated in their work by examining Figure 27(a). This realization led to an investigation to determine the root cause of this behavior.

4.5 Deviation from Expected Response

This section intends to rationalize the irregularities in the frequency response data obtained during laboratory experiments. Figure 53 illustrates two biasing schemes employed during the testing of the multi-section device: uniform biasing (blue), and asymmetric biasing (red) to investigate the gain-lever effect. The figure has a number of different letters that correspond to different proposed mechanisms for the behavior in the laser.

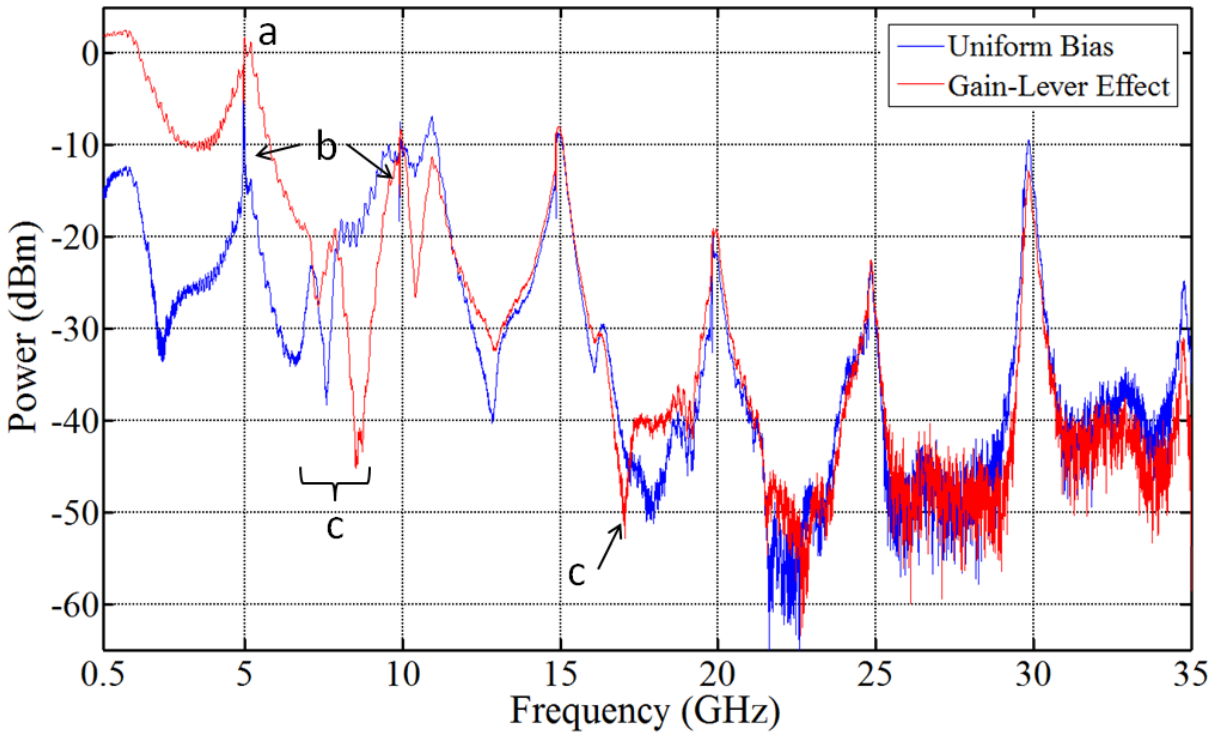

Figure 53: Frequency response data for the multi-section device biased in two different configurations. Labels indicate areas that deviate from expected norms.

4.5.1 Resonant Peaks

Figure 53(a) calls attention to the resonant peaks observed in the frequency response data. These are expected in long-cavity multi-section device. However, they are

rarely reported since the majority of multi-section devices are short enough that the free-spectral range frequency is outside the dynamic range of the network analyzer. It is highly unexpected to have these peaks appear in single-section devices, which is precisely what is occurring and is illustrated in Figure 52. One possible explanation is that the device demonstrated the ability to mode-lock in the absence of a reversed biased section when wire bonded as a single section or a multi-section device and biased uniformly. It is possible that this generation of pulses is being fueled by intra-cavity reflections due to the isolation gaps between the electrically isolated sections. These pulses could be building up on successive round-trips through the laser cavity and coupling to the dominant free-spectral range frequency.

Another possibility is that the sections are not biased uniformly even though they are all wire bonded together. Placement of the wire bonds and the irregularities in the printed circuit board contacts that interface with probes could both be the culprit. Subsequent frequency response tests were performed while biasing the laser uniformly and moving the DC probe to various locations about the gain section and observing the effects. There was no discernible difference between measurements. This finding eliminates the possibility that probe locations are causing asymmetric biasing conditions. The best method to examine this further is to remove all wire bonds and bias each section independently to ensure a uniform bias is applied.

The free-spectral range of this device is approximately 5 GHz; with the network analyzer set to view 0.5 – 35 GHz seven harmonics should be observed, this is nearly the case. The 3rd through the 6th harmonics display strong resonant peaks whereas the 7th is quite attenuated. This attenuation is likely due to the limitation of the electrical

components used. The 2nd harmonic should be located at 10 GHz. Instead there is a null that seems to be cancelling the resonant peak out. A possible cause for that is that there are phase effects taking place inside the cavity.

4.5.2 Arctangent Spectrum Shape

Figure 48 reveals arctangent shaped peaks/nulls near the free-spectral range frequency and harmonics of it. These anomalies have been reported by Doerr who attributed t hem to active mode-locking [52]. While this is a plausible explanation, it lacks a mathematical construct that describes this behavior and that can be added to existing theories and simulation programs. Premaratne *et al.* related this to the coupling and amplitude and phase effects. Figure 54 is an enhanced illustration of the arctangent-like function located near the free-spectral range frequency (5 GHz).

4.5.3 Atypical Nulls

Figure 53(c) highlights nulls in the frequency response that are unexpected. Nulls similar to these have been reported in experiments [52], and simulations [51], but not for the modulation configurations experimentally explored in this work. The frequency response data can be qualitatively compared to the simulations in Figure 27(a, e, i) for the single section, uniform biased multi-section, and gain-lever configurations. Immediately one notices that there are no nulls present in this simulation data for these configurations, and that the only appearance of nulls is when the section nearest the output of the laser is modulated.

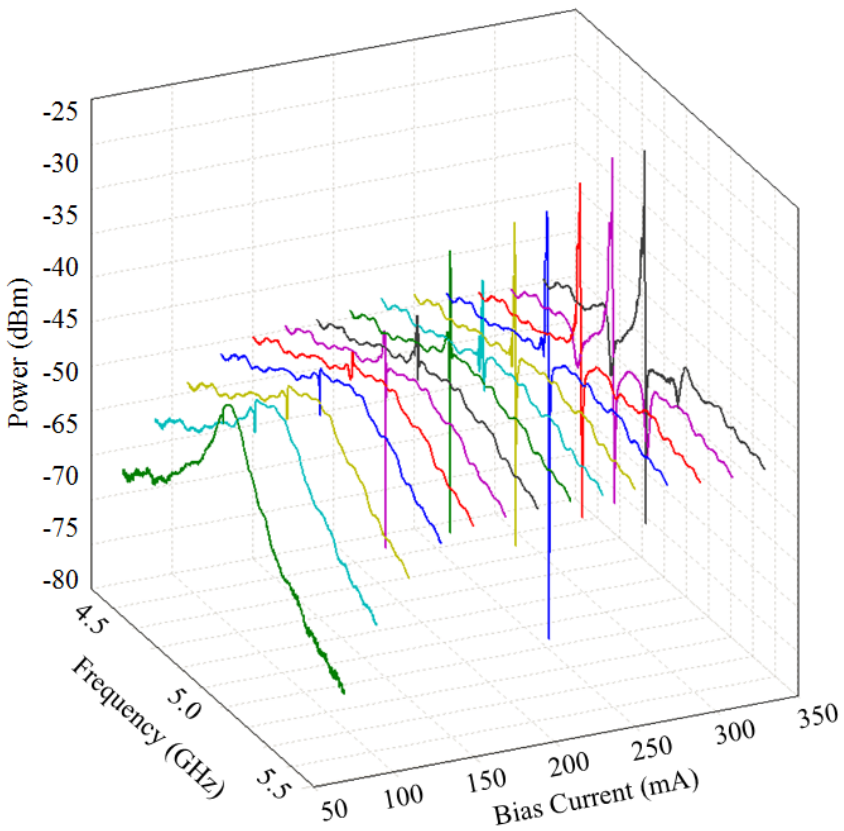

Figure 54: Arctangent-like spectrum that appears at the free-spectral range frequency and its harmonics over various bias currents.

Another item of interest is that the null that appears near 8 GHz in Figure 53 shifts in frequency based on how the modulation section is biased. Even when these nulls are expected, as illustrated in Figure 27, when changing the differential gain of the modulation section it only alters the depth of the null, but does not shift its frequency. This leads one to believe that this effect is not solely based on the geometry of the device configuration.

Several postulations for this behavior were explored. One idea was that there was harmonic or interharmonic mixing of frequencies inside the laser cavity and at certain frequencies, they interfere destructively and cancel out creating a null. These frequencies would be based on the free-spectral range frequencies of different clusters of sections in

the multi-section device. This possibility was investigated by mathematically determining how several combinations of free-spectral range frequencies for different lengths would mix and interact. Although there was some correlation observed it was not considered a good agreement. Also it did little to explain the reason for null to vary frequencies based on differential gain, a phenomenon that was not reported by Usechak *et al*.

The unbiased 0.3-mm section was also examined to determine its effect on these nulls. A DC probe was connected to the 0.3-mm section with a switch in series with the laser diode controller. Data was recorded with the switch both connecting, and disconnecting the section and holding the current density constant for each measurement. The results showed there was no discernible difference between the two measurements.

Finally it was proposed that the wire bonds may be contributing to the unexplained performance in the frequency response. To reiterate from Chapter 3, there are numerous wire bonds, illustrated in Figure 55, that connect both the individual contacts to each other (red) on the printed circuit board and from the board to the laser sections (black).

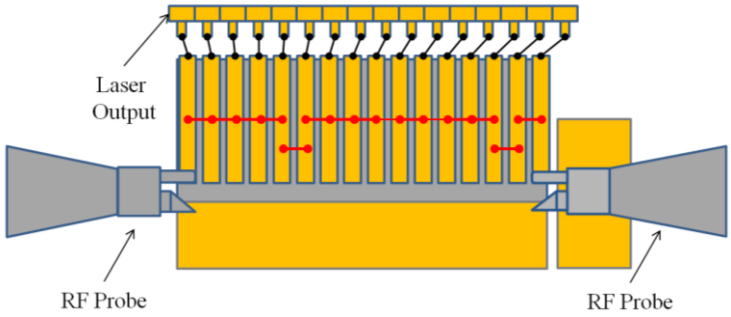

Figure 55: Testing configuration to analyze a select portion of the wire bonds.

Due to the nature of the connections, only the frequency response data of the wire bonds between the contacts (red wire bonds in Figure 55) was able to be measured. The

wire bonds shown in black remained connected while the measurement took place. The data obtained by the network analyzer is depicted in Figure 56. It shows nulls that are present in the 7–8.5 GHz range, and again near 16 GHz. These are precisely the areas of concern in the frequency response data of the laser. There is not a direct comparison between the nulls from the wire bonds and the nulls from the overall response. This is most likely because of two factors: changes in the differential gain of the modulation section and additional wire bond effects. As was shown earlier the nulls in the frequency response data are dependent on the biasing of the modulation section; therefore, finding a single value for the location of the nulls is impossible. The wire bonds that have shown this poor response are only half of the total wire bonds used; additional wire bonds connect the contact pads on the printed circuit board to the contacts directly on top of the laser bar's ridge waveguide. It is logical to assume that the additional wire bonds will have an added deleterious effect on the frequency response as they are longer in length than the bonds that were measured.

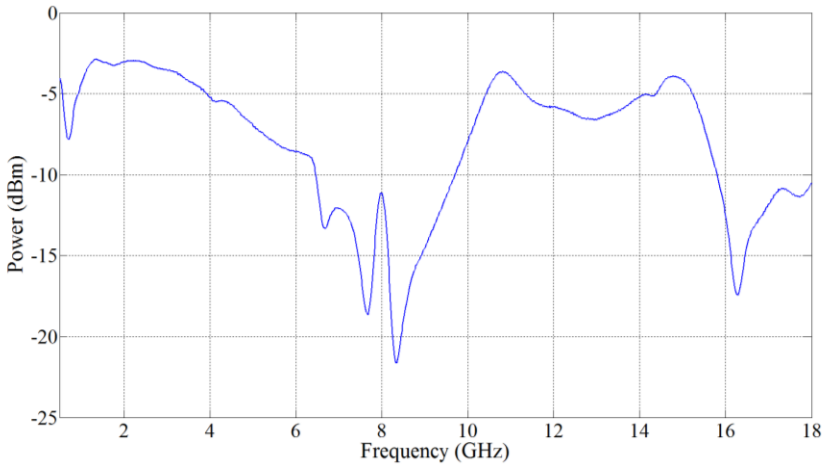

Figure 56: S_{21} response plots of the wire bonds between contacts.

4.6 Summary of Findings

This chapter reported the laboratory experimental results of the experiments outlined in Chapter 3. Additionally the data was analyzed to explain and justify possible causes for any results that differed from what was expected. The output power test revealed that the laser had a threshold current of 52 mA without the 0.3-mm section biased and 46 mA with the section biased. The laser was found to operate at 1230 nm but additional modes appeared when the biasing was increased. Passive mode-locking was observed which produced RF signals of approximately 5 GHz with RF linewidths of 34.4 kHz with a reverse biased section, and 56.28 kHz without a reversed biased section. The frequency response was measured for different configurations and resulted in a maximum modulation enhancement of 16 dB and a maximum 3-dB bandwidth of 6.3 GHz. Additionally, anomalies in the frequency response measurements were presented and speculations as to their origins were addressed.

5. Conclusions and Recommendations

This chapter summarizes the investigation into the characterization and analysis of long-cavity multi-section gain-levered quantum-dot lasers. The conclusions of the research are presented before delving into specific contributions that are gained from this study. Finally, possibilities for advancements to this body of work are discussed.

5.1 Conclusions of Research

The objective of this research focused on a novel 8.3-mm multi-section quantum-dot laser. The device allowed modulation-to-gain section contact ratios as high as 15:1, a configuration that has not previously been reported in literature. This allowed the gain-lever effect to be investigated along with a host of other dynamic behavior that came into fruition while gathering laboratory experimental data.

After constructing the necessary supporting equipment and apparatuses for the experiments outlined in Chapter 3, ample data collection took place. The threshold current and operating wavelength were first discovered. Numerous optical spectrum measurements were recorded to create an optical spectrum map for the quantum-dot device. Mode-locking experiments investigated the viability of utilizing a laser as a microwave reference oscillator, although the variability of the reference frequency with input current bias is apt to limit this device's functionality in such a system. The frequency response of the laser was analyzed by collecting an abundant amount of data for the three different configurations discussed in Chapter 3. The maximum bandwidth and modulation enhancement were determined and reported from the acquired data. Analysis of this experimental work also revealed irregularities in the modulation

response. Considerable time was devoted to understanding the dynamics that were exhibited by this laser and appropriate conclusions were drawn to explain said behavior. This dynamic behavior also limited the ability of the frequency response to be curve-fit by the traveling-wave equations.

5.2 Contributions of Research

- Assembled unique laboratory workstation to allow testing and characterization of bare lasers.
- Experimentally determined a threshold current of 52 mA and an operating wavelength of 1230 nm.
- Analyzed passive mode-locking capability in two separate configurations; measuring optical pulses with a repetition rate of approximately 5 GHz with linewidths of 34.4 kHz and 56.28 kHz for the multi- and single-section configurations respectively.
- Experimentally demonstrated the benefits of the gain-lever effect on modulation enhancement (increase of 16 dB) and the 3-dB bandwidth (6.3 GHz achieved).
- Analyzed and experimentally verified some possible causes for the anomalies, such as packaging issues like wire bonding.

5.3 Recommendations for Future Research

This research illustrated that this multi-section quantum-dot device has the ability to benefit the frequency response by utilizing the gain-lever effect. It also brought forth a multitude of other possible avenues for research. This section contains a few possible areas which could benefit from additional research.

The mode-locking ability of this laser is one area that was explored in this document as it was part of the characterization process. There is already a wealth of published knowledge on the subject of passive mode-locking with purpose built devices routinely reporting RF linewidths of less than 1 kHz. The passive mode-locking tested presented here were only using a single 0.5-mm section as the saturable absorber. One possibility would be to determine the correlation between saturable absorber length and RF optical pulse generation in terms of stability and linewidth.

Another mode-locking topic that needs to be addressed is the discovery of the laser's ability to mode-lock in the absence of a saturable absorber. There is very little literature that discusses the mechanism driving this phenomenon. Possible theories presented in this thesis suggest that intra-cavity reflections or asymmetric biasing of the laser's sections may be the root cause. To examine whether asymmetric biasing is the cause one could remove all of the wire bonds and bias each section individually and observe the results. If the device no longer mode-locks without a saturable absorber, or the generated optical pulses vary based on pump current, conclusions could be drawn about packaging effects and how wire bonds alter the perceived behavior of the laser.

As stated earlier in this document, it was intended to model this long-cavity device with the assistance of Dr. Usechak and the software that was developed by him.

The frequency response that was recorded in the laboratory had additional atypical factors that could not be properly modeled because the mathematical construct causing the behavior was not known at the time. Additional testing could be performed to either discover the source of the behavior and develop a mathematical representation of it, or find a regime of operation that does not exhibit this abnormality.

6. References

[1] H. Altug, D. Englund and J. Vuckovic, "Ultrafast photonic crystal nanocavity laser," *Nature Physics,* vol. 2, pp. 484-488, 2006.

[2] G. P. Agrawal, Fiber-Optic Communication Systems, New York: John Wiley & Sons, 2002.

[3] A. Blum, "Mapping the Internet: Undersea Cables," *Fortune,* 23 Jul. 2012.

[4] R. A. Linke, "Transient chirping in single-frequency lasers: lightwave systems consequences," *Electronics Letters,* vol. 20, no. 11, pp. 472-474, 1984.

[5] L. Billia, J. Zhu, T. Ranganath, D. P. Bour, S. W. Corzine and G. E. Hofler, "40-Gb/s EA Modulators With Wide Temperature Operation and Negative Chirp," *IEEE Photonics Technology Letters,* vol. 17, no. 1, pp. 49-51, 2005.

[6] Y. Li, "Techniques for High-Speed Modulation of Quantum Dot Lasers," Ph.D. dissertation, Electrical Engineering, University of New Mexico, Albuqurque, NM, 2008. [Online].

[7] K. J. Vahala, M. A. Newkirk and T. R. Chen, "The optical gain lever: A novel gain mechanism in the direct modulation of quantum well semiconductor lasers," *Applied Physics Letters,* vol. 54, no. 25, pp. 2506-2508, 1989.

[8] N. A. Naderi, Y. Li, C. Dziak, Y. C. Xin, V. Kovanis and L. F. Lester, "Quantum Dot Gain-Lever Laser Diode," in *Lasers and Electro-Optics Society*, Montreal, 2006.

[9] Y. Li, N. A. Naderi, V. Kovanis and L. F. Lester, "Enhancing the 3-dB Bandwidth via the Gain-Lever Effect in Quantum-Dot Lasers," *IEEE Photonics Journal,* vol. 2, no. 3, pp. 321-329, 2010.

[10] "Fiber Optic 101," Nov 2010. [Online]. Available: http://fiberoptic101.blogspot.com/. [Accessed 20 Jul. 2012].

[11] Thorlabs, "Laser Diode Tutorial," [Online]. Available: http://www.thorlabs.com/tutorials.cfm?tabID=26065. [Accessed 2 Jun. 2012].

[12] B. E. A. Saleh and M. C. Teich, Fundamentals of Photonics, Hoboken: John Wiley & Sons, 2007.

[13] E. Hulicius, P. Hazdra, J. Voves, J. Oswald, J. Pangrac, K. Melichar, M. Vancura, O. Petricek and T. Simecek, "Quantum size InAs/GaAs lasers-preparation and properties," in *Advanced Semiconductor Devices and Microsystems*, Smolenice, 2000.

[14] M. Asada, Y. Mitamoto and Y. Suematsu, "Gain and the threshold of three-dimensional quantum-box lasers," *IEEE Journal of Quantum of Electronic,* vol. 22, no. 9, pp. 1915-1921, 1986.

[15] B. Ellis, M. A. Mayer, G. Shambat, T. Sarmiento, J. Harris, E. E. Haller and J. Vuckovic, "Ultra-low Threshold Electrically Pumped Quantum Dot Photonic Crystal Nanocavity Laser," in *Conference on Lasers and Electro-Optics*, Baltimore, 2011.

[16] D. Bimberg, N. Kirstaedter, N. N. Ledentsov, Z. I. Alferov, P. S. Kop'ev and V. M. Ustinov, "InGaAs-GaAs Quantum-Dot Lasers," *IEEE Journal of Selected Topics in Quantum Electronics,* vol. 3, no. 2, pp. 196-205, 1997.

[17] L. F. Lester, A. Stintz, H. Li, T. C. Newell, E. A. Pease, B. A. Fuchs and K. J. Malloy, "Optical Characteristics of 1.24-um InAs Quantum-Dot Laser Diodes," *IEEE Photonics Technology Letters,* vol. 11, no. 8, pp. 931-933, 1999.

[18] T. C. Newell, D. J. Bossert, A. Stintz, B. Fuchs, K. J. Malloy and L. F. Lester, "Gain and Linewidth Enhancement Factor in InAs Quantum-Dot Laser Diodes," *IEEE Photonics Technology Letters,* vol. 11, no. 12, pp. 1527-1529, 1999.

[19] J. M. Vazquez, H. H. Nilsson, J. -Z. Zhang and I. Galbraith, "Linewidth Enhancement Factor of Quantum-Dot Optical Amplifiers," *IEEE Journal of Quantum Electronics,* vol. 42, no. 10, pp. 986-993, 2006.

[20] U. Keller, "Recent developments in compact ultrafast lasers," *Nature,* vol. 424, pp. 831-838, 2003.

[21] P. J. Delfyett, D. H. Hartman and S. Z. Ahmad, "Optical Clock Distribution Using a Mode-Locked Semiconductor Laser Diode System," *Journal of Lightwave Technology,* vol. 9, no. 12, pp. 1646-1649, 1991.

[22] Y. -C. Xin, L. F. Lester, A. L. Gray and L. Zhang, "Characterization of the Static and Dynamic Parameter in a 1.3 -um Quantum Dot Mode-locked Laser," in *Conference on Lasers and Electro-Optics*, Baltimore, 2007.

[23] G. Carpintero, M. G. Thompson, R. V. Penty and I. H. White, "Low Noise Performance of Passively Mode-Locked 10-GHz Quantum-Dot Laser Diode," *IEEE Photonics Technology Letters,* vol. 21, no. 6, pp. 389-391, 2009.

[24] K. Y. Lau, "Short-Pulse and High-Frequency Signal Generation in Semiconductor Lasers," *Journal of Lightwave Technology,* vol. 7, no. 2, pp. 400-419, 1989.

[25] J. H. Kim, C. G. Christodoulou, Z. Ku, N. A. Naderi and L. F. Lester, "Quantum-Dot Laser Coupled Bowtie Antenna," in *Antennas and Propagation Society International Symposium*, San Diego, 2008.

[26] K. Y. Lau, "Narrow-band modulation of semiconductor laser at millimeter wave frequencies (>100 GHz) by mode locking," *IEEE Journal of Quantum Electronics,* vol. 26, no. 2, pp. 250-261, 1990.

[27] F. van Dijk, A. Enard, G. -H. Duan, A. Accard, F. Lelarge, A. Shen, O. Parillaud, A. Akrout, G. D. Valicourt, S. Ginestar and A. Ramdane, "Laser Diodes for Microwave and Millimeter Wave Photonics," in *Mediterrannean Microwave Symposium*, Tangiers, 2009.

[28] Y. -C. Xin, L. F. Lester, S. R. Bank, H. P. Bae, H. B. Yuen, M. A. Wistey and J. S. Harris, "Monolithic 1.55 um GaInNAsSb Quantum Well Passively Mode-Locked Lasers," *Electronics Letters,* vol. 44, no. 9, p. 581, 2008.

[29] W. Yang, "Single-Section Fabry-Perot Mode-Locked Semiconductor Lasers," *Advances in OptoElectronics,* vol. 2011, pp. 1-11, 2011.

[30] R. Paiella, F. Capasso, C. Gmachl, D. L. Sivco, J. N. Baillargeon, A. L. Hutchinson and A. Y. Cho, "Self-mode-locking in quantum cascade lasers," in *Conference on Lasers and Electro-Optics*, 2000.

[31] P. Phelan, D. McDonald, A. Egan, J. Hegarty, R. O'Dowd, G. Farrell and S. Lindgren, "Comparison of self-pulsation in multisection lasers with distributed feedback and intracavity saturable absorbers," *IEE Proceedings - Optoelectronics,* vol. 141, no. 2, pp. 114-118, 1994.

[32] B. Sartorius, M. Mohrle, S. Reichenbacher, H. Preier, H. -J. Wunsche and U. Bandelow, "Dispersive Self-Q-Switching in Self-Pulsating DFB Lasers," *IEEE Journal of Quantum Electronics,* vol. 33, no. 2, pp. 211-218, 1997.

[33] A. Soibel, F. Capasso, C. Gmachl, M. L. Peabody, A. M. Sergent, R. Paiella, D. L. Sivco, A. Y. Cho and H. C. Liu, "Stability of Pulse Emission and Enhancement of Intracavity Second-Harmonic Generation in Self-Mode-Locked Quantum Cascade Lasers," *IEEE Journal of Quantum Electronics,* vol. 40, no. 3, pp. 197-204, 2004.

[34] Y. Li, N. A. Naderi, Y. -C. Xin, C. Dziak and L. F. Lester, "Multi-section gain-lever quantum dot lasers," in *Physics and Simulation of Optoelectronic Devices*, San Jose, 2007.

[35] T. L. Paoli and J. E. Ripper, "Direct Modulation of Semiconductor Lasers," *Proceedings of the IEEE,* vol. 58, no. 10, pp. 1457-1465, 1970.

[36] R. S. Tucker, "High-Speed Modulation of Semiconductor Lasers," *Journal of Lightwave Technology,* vol. 3, no. 6, pp. 1180-1192, 1985.

[37] K. Y. Lau and A. Yariv, "Ultra-High Speed Semiconductor Lasers," *IEEE Journal of Quantum Electronics,* vol. 21, no. 2, pp. 121-138, 1985.

[38] M. Ishida, M. Matsuda, Y. Tanaka, K. Takada, M. Ekawa, T. Yamamoto, T. Kageyama, M. Yamaguchi, K. Nishi, M. Sugawara and Y. Arakawa, "Temperature-Stable 25-Gbps Direct-Modulation in 1.3 um InAs/GaAs Quantum Dot Lasers," in *Conference on Lasers and Electro-Optics*, San Jose, 2012.

[39] S. Matsuo, K. Takeda, T. Sato, M. Notomi, A. Shinya, K. Nozaki, H. Taniyama, K. Hasebe and T. Kakitsuka, "10-Gbit/s Direct Modulation of Electrically Driven Photonic Crystal Nanocavity Laser," in *Optical Fiber Communication Conference and Exposition*, Los Angeles, 2012.

[40] L. A. Coldren and S. W. Corzine, Diode Lasers and Photonic Integrated Circuits,

New York: John Wiley & Sons Inc, 1995.

[41] J. -M. Liu, Photonic Devices, New York: Cambridge University Press, 2005.

[42] G. A. Smolyakov and M. Osinski, "Modulation Bandwidth Enhancement Beyond 100 GHz in Strongly Injection-Locked Cascaded Semiconductor Ring Lasers," in *Opto-Electronics and Communications Conference*, Busan, 2012.

[43] V. I. Pipa, V. V. Mitin and M. Stroscio, "Acoustic phono bottleneck in quantum dots: role of deformation variation of electron effective mass," *Solid State Communications,* vol. 117, no. 12, pp. 713-717, 2001.

[44] D. Gready, G. Eisenstein, C. Gilfert, V. Ivanov and J. P. Reithmaier, "High-Speed Low-Noise InAs/InAlGaAs/InP 1.55-um Quantum-Dot Lasers," *IEEE Photonics Technology Letters,* vol. 24, no. 10, pp. 809-811, 2012.

[45] M. H. Yavari and V. Ahmadi, "Effects of Carrier Relaxation and Homogeneous Broadening on Dynamic and Modulation Behavior of Self-Assembled Quantum-Dot Laser," *IEEE Journal of Selected Topics in Quantum Electronics,* vol. 17, no. 5, pp. 1153-1157, 2011.

[46] G. Griffel and C. -H. Chen, "Static and Dynamic Analysis of Tunable Two-Section High-Speed Distributed Feedback Laser Utilizing the Gain Lever Effect," *IEEE Journal of Quantum Electronics,* vol. 32, no. 1, pp. 61-68, 1996.

[47] C. P. Seltzer, L. D. Westbrook and H. J. Wickes, "The "Gain-Lever" Effect in InGaAsP/InP Multiple Quantum Well Lasers," *Journal of Lightwave Technology,* vol. 13, no. 2, pp. 283-289, 1995.

[48] M. D. Pocha, L. L. Goddard, T. C. Bond, R. J. Nikolic, S. P. Vernon, J. S. Kallman and E. M. Behymer, "Electrical and Optical Gain Lever Effects in InGaAs Double Quantum-Well Diode Lasers," *IEEE Journal of Quantum Electronics,* vol. 43, no. 10, pp. 860-868, 2007.

[49] N. G. Usechak, M. Grupen, V. Kovanis, N. Naderi, Y. Li and L. F. Lester, "Cavity-Enhanced Modulation in Gain-Lever Semiconductor Lasers," in *2010 23rd Annual Meeting of the IEEE Photonics Society*, Denver, 2011.

[50] Y. Li, N. A. Naderi, Y. -C. Xin, V. Kovanis and L. F. Lester, "Two-section quantum dot lasers with 20-dB modulation efficiency improvement," in *Conference on Lasers and Electro-Optics*, Baltimore, 2007.

[51] N. G. Usechak, M. Grupen, N. Naderi, Y. Li, L. F. Lester and V. Kovanis, "Modualtion effects in mult-section semiconductor lasers," in *Physics and Simulation of Optoelectronic Devices XIX*, San Francisco, 2011.

[52] C. R. Doerr, "Direct Modulation of Long-Cavity Semiconductor Lasers," *Journal of Lightwave Technology,* vol. 14, no. 9, pp. 2052-2061, 1996.

[53] L. Ramunno and J. E. Sipe, "Dynamical Model of Directly Modulated Semiconductor Laser Diodes," *IEEE Journal of Quantum Electronics,* vol. 35, no. 4, pp. 624-634, 1999.

[54] M. Premaratne, A. J. Lowery, Z. Ahmed and D. Novak, "Modeling Noise and Modulation Performance of Fiber Grating External Cavity Lasers," *IEEE Journal of Selected Topics in Quantum Electronics,* vol. 3, no. 2, pp. 290-303, 1997.

[55] G. T. Edwards and P. M. Smowton, "The Differential Efficiency of InP Quantum Dot Lasers," in *Conference on Quantum Electronics and Laser Science*, Baltimore, 2009.

[56] M. -H. Mao, F. Heinrichsdorff, A. Krost and D. Bimberg, "Study of high frequency response of self organised stacked quantum dot lasers at room temperature," *Electronics Letters,* vol. 33, no. 19, pp. 1641-1642, 1997.

[57] N. Moore and K. Y. Lau, "Ultrahigh efficiency microwave signal transmission using tandem-contact single quantum well GaAlAs lasers," *Applied Physics Letters,* vol. 55, no. 10, pp. 936-938, 1989.

REPORT DOCUMENTATION PAGE

Form Approved
OMB No. 074-0188

1. REPORT DATE *(DD-MM-YYYY)*	2. REPORT TYPE	3. DATES COVERED *(From – To)*
21 Mar 2013	Master's Thesis	08 Sep 2011 – 21 Mar 2013

4. TITLE AND SUBTITLE
Characterization and Dynamic Analysis of Long-Cavity Multi-Section Gain-Levered Quantum-Dot Lasers

5a. CONTRACT NUMBER
5b. GRANT NUMBER
5c. PROGRAM ELEMENT NUMBER

6. AUTHOR(S)
Schmidt, John R., Second Lieutenant, USAF

5d. PROJECT NUMBER
5e. TASK NUMBER
5f. WORK UNIT NUMBER

7. PERFORMING ORGANIZATION NAMES(S) AND ADDRESS(S)
Air Force Institute of Technology
Graduate School of Engineering and Management (AFIT/EN)
2950 Hobson Way
WPAFB OH 45433-7765

8. PERFORMING ORGANIZATION REPORT NUMBER
AFIT-ENG-13-M-45

9. SPONSORING/MONITORING AGENCY NAME(S) AND ADDRESS(ES)
Air Force Research Laboratory Sensors Directorate (AFRL/RYDH)
Dr. Nicholas G Usechak, Research Engineer
2241 Avionics Circle, Area B Bldg 620
WPAFB OH 45433

10. SPONSOR/MONITOR'S ACRONYM(S)
AFRL/RYDH

11. SPONSOR/MONITOR'S REPORT NUMBER(S)

12. DISTRIBUTION/AVAILABILITY STATEMENT
DISTRIBUTION STATEMENT A. APPROVED FOR PUBLIC RELEASE; DISTRIBUTION UNLIMITED.

13. SUPPLEMENTARY NOTES

14. ABSTRACT

This research investigates the impact of different device architectures on the frequency response of long-cavity multi-section quantum-dot lasers. This work focused on a novel 8.3-mm multi-section quantum-dot device which possessed the flexibility to be configured either as a single- or multi-section device having gain-to-modulation section ratios of 14:2 and 15:1. The long-cavity device design facilitated the testing of increased gain-to-modulation section length ratios previously unexplored in the context of the gain-lever effect. The investigation of the gain-lever effect showed improvements to both the modulation efficiency and modulation bandwidth of the device under test. The modulation efficiency and modulation bandwidth were found to vary as the modulation section length was increased, leading to the conclusion of an ideal gain-to-modulation section ratio. In addition to providing a means to investigate the gain-lever effect, the long-cavity quantum-dot device exhibited passive mode locking both with and without a saturable absorber present. While the predictable gain-lever effects were observed, long-cavity and mode-locking effects were also present in the response; these effects presented unexpected characteristics that are not captured by current published models.

15. SUBJECT TERMS
quantum-dot; multi-section laser; gain-lever effect; mode-locking

16. SECURITY CLASSIFICATION OF:			17. LIMITATION OF ABSTRACT	18. NUMBER OF PAGES	19a. NAME OF RESPONSIBLE PERSON
a. REPORT	b. ABSTRACT	c. THIS PAGE			Michael C. Pochet, Maj, USAF
U	U	U	UU	111	19b. TELEPHONE NUMBER *(Include area code)* (937) 255-6565, x 4393 (Michael.pochet@afit.edu)